Approaches to improving thermal performance of inductors with a view to improving power density

A thesis submitted by

David Andrew Hewitt

in partial fulfilment of the requirements for the degree of

Doctor of Philosophy

in

The Department of Electronic and Electrical Engineering at The University of Sheffield

Supervised by

Prof. David Andrew Stone and Dr Martin Paul Foster

September 2015

Summary

This thesis considers a range of methods for improving the power density of inductors. This is motivated by the desire to reduce the size of power electronic systems. Within said systems, a large proportion of the size/weight is provided by the passive components; therefore, any size reductions influence the overall system considerably. Two factors are considered which limit inductor size reductions. These are the losses within the inductor and the ease of thermal conduction within the component.

The inductor losses are investigated by considering the winding material choice. Here aluminium is considered as a replacement for copper. This decision is influenced by the fact that when frequency effects are considered, the electrical performance of aluminium doesn't compare as poorly to copper as would be predicted based solely on the resistivities of the material. In fact, in some winding topologies, aluminium actually exhibits a lower ac resistance than copper for a range of frequencies. This combined with the other advantages of aluminium (cost, weight) make a potential case for its use in place of copper in some designs.

Thermal transfer within the component is considered in two ways. Firstly, the use of aluminium oxide as an insulation material is explored by producing a planar inductor which uses this insulation material. It is found that considerable thermal improvements are achieved when the oxide is used, especially if it is combined with a heat sink compound between the layers.

Additionally the influence of using encapsulants combined with thermally conductive fillers is examined. This work considers the modelling of the resultant composite for use within design tools. It is found that predictions with an accuracy of 10 % can be achieved when a thermal conductivity value (from an analytical model) which contains up to a 30 % error is used.

Publications

Parts of this work have been presented by the author at conferences:

[1] D.A. Hewitt, D.A. Stone, M.P. Foster; "*An investigation into the feasibility of using aluminium oxide to insulate aluminium planar windings*"; iPower^2; Warwick, November 2012

[2] D.A. Hewitt, D.A. Stone, M.P. Foster; "*Design of thermally integrated planar inductors utilising aluminium oxide as a winding insulation material*"; Power Control and Intelligent Motion (PCIM) Europe 2013; Nuremberg, May 2013; pp 223-230

[3] D.A. Hewitt, D.A. Stone, M.P. Foster; "*An experimental evaluation of thermally conductive filler loaded encapsulant composites*"; 7th IET international conference on Power Electronics, Machines and Drives (PEMD), Manchester, April 2014

[4] D.A. Hewitt, D.A. Stone, M.P. Foster; "*Modelling the enhancement to the thermal performance of encapsulants using thermally conductive filler materials*"; Power Control and Intelligent Motion (PCIM) Asia 2015; Shanghai, June 2015

Additionally a paper is currently in preparation to be submitted to an internationally recognised journal:

D.A. Hewitt, D.A. Stone, M.P. Foster; "*A method for identifying inductor topologies which exhibit lower ac resistive losses using aluminium windings than copper"*

Acknowledgements

Over the course of my PhD there have been many people who have been a great help to me and provided support over the last four years. I would like to take this opportunity to thank them here.

Firstly I would like to thank my supervisors Dave Stone and Martin Foster for their guidance throughout the course of this work. Your help and advice has been invaluable throughout this whole process.

Secondly I would like to thank my parents, Ann and Andrew, whose continued love and support throughout this process has been a source of great comfort and encouragement. I would also like to acknowledge my wider family, especially my brother Chris for their support.

Next I would like to thank 'Free to a good home' (Alex Duke, Mark Sweet, Dave Growney) for providing me with a space to unwind and relax.

For his assistance in all things coding related I would like to thank Jonathan Davidson.

I would also like to thank Rui Zhao for his highly enjoyable company during the PCIM Asia conference.

There are many people who I have had the pleasure of sharing an office with over the course of this work; I would like to thank Dan Schofield; Chi Tsang; Dan Rogers; Glynn Cooke; Harry Harrison; Sami Abuzed; Katharine Fewings; Jonathan Gomez; Huw Price and Dalil Benchebra for their interesting discussions and providing an enjoyable environment in which to work.

I would like to acknowledge the support of EPSRC in providing the funding for this work as part of the VESI project.

Finally I would like to offer my thanks to all of the administrative and technical staff who have helped with the smooth running of this project, especially the workshop staff who have been tasked with bringing my CAD drawings to life.

Contents

List of Figures

List of Tables

Chapter 1

Introduction

1.1 Background

In the electronics industry, the continuing trend is towards the miniaturisation of electrical systems. This in turn influences the development of the components within the system in that they must be smaller but still capable of handling the same amount of power (requiring an increased power density). Within a typical power electronics system, the passive components make up a large proportion of the overall system size and weight (55 % - 74 % of the convertor mass [5, 6]). Therefore, any improvements which can be made in this area will have a considerable effect on the overall system. With this in mind this thesis focuses on increasing the power density of inductors. Decreasing the size of an inductor has the effect of reducing the available surface area from which heat can be extracted. Consequently, assuming that the losses within the component remain constant its operating temperature is inversely proportional to the component size. This can be problematic as the increased temperature may be above the ratings of some of the constituent parts of the component. Techniques for reducing the operating temperature can be divided into two categories:

- Reducing the losses within the inductor
- Improving the thermal transfer within the inductor structure

When discussing power density it is important to consider the fact that there are two different measures of power density:

- Volumetric power density (kW/m^3)
- Mass power density (kW/kg)

Depending on the final application of the inductor, it may be the case that only one of these is a priority. In the case of automotive applications both are of importance:

- The size of the components should be kept to a minimum as any space occupied by electronics cannot be used for passengers/luggage;
- The weight is also a consideration however as it is necessary for the vehicle to carry the component around for the entire lifetime of the vehicle.

While the inductors designed within this work were not targeted for a specific convertor topology, some of the designs are better suited to certain types of convertors. The most pertinent example of this relates to the aluminium wound inductors investigated in chapter 3. Here it is concluded that under operating conditions which include a large dc current the advantages of aluminium are reduced. Consequently, this type of inductor is particularly suited to resonant convertors, in which the inductor is not subjected to a large dc current. That being said, this does not necessarily limit the use of the inductors exclusively to this type of convertor as it may be appropriate for other topologies, depending on the desired optimisation objectives.

1.2 Novelty

This thesis considers a range of different tools available to an inductor designer for the purpose of increasing the power density of inductors. The novelty within this thesis can be divided into three major areas:

1. An exploration into cases in which aluminium exhibits lower winding resistance than copper within inductor windings

   The use of aluminium as a winding material is explored with consideration given to the influence of frequency effects on the winding resistance. In this analysis, it is found that in some cases aluminium will exhibit a lower ac resistance than copper for a range of frequencies. Based on this, the influences of different winding parameters are explored with respect to this effect. Additionally a method of identifying whether or not aluminium will outperform copper in a given topology is explained.

   Further to this effect it is also observed that in cases which do not exhibit behaviour in which aluminium outperforms copper, the deficit in the performance of aluminium is not as great as would be predicted if only the material resistivity values were considered as a result of the frequency effects.

2. The use of aluminium oxide as a winding insulation material for planar windings

   Aluminium oxide has a thermal conductivity value which is considerably larger than that of conventionally used insulation materials. A layer of suitable thickness for insulation purposes can be grown on the surface of aluminium by anodisation. Due to the brittleness of the material it is best employed in topologies which do not require the anodised aluminium to be bent after anodisation, as this can lead to cracks forming in the oxide layer. With this in mind, a planar winding topology is considered as part of this work.

3. The modelling of composite materials for the purpose of encapsulating components

   Encapsulants can be employed in the manufacture of passive components for both thermal and mechanical purposes. Considering the thermal aspect, it is possible to increase the thermal conductivity of the encapsulant through the addition of thermally conductive filler materials. To design components which employ these composites it is necessary to be able to model their bulk performance. This work considers methods of determining the bulk properties of the composite, in addition to determining how accurately it is necessary to know the bulk values to achieve an acceptable level of accuracy when modelling the composite using design tools (*e.g.* Finite Element Analysis).

1.3 Thesis Structure

The work in this thesis is structured into seven chapters. A brief summary of the contents of these chapters is provided here:

Chapter 1 introduces the thesis and establishes the motivation for the work performed herein. Additionally the novelty and structure of the remaining thesis is set out here.

Chapter 2 provides an overview into the considerations which can be made during the design of an inductor. This serves to give an insight into the design decisions which must be made by an inductor designer in addition to reviewing a range of available techniques employed for the purpose of controlling losses; improving the thermal management of the component and increasing inductor power density.

Chapter 3 considers the use of aluminium as a winding material in place of copper. Owing to aluminium's lower density when compared to copper, exchanging the winding material in this way can reduce the weight of an inductor. This is particularly attractive in cases in which (due to the frequency effects on the windings) aluminium exhibits a lower winding resistance than copper at some frequencies. This work addresses the novelty point highlighted in the previous section as point 1.

In **Chapter 4** the use of aluminium oxide as an insulation material for planar windings is explored. Such an exchange is desirable owing to aluminium oxides superior thermal performance when compared to that of conventional insulation materials such as plastics. Analysis is performed comparing the thermal performance of aluminium oxide grown on aluminium windings by anodisation to that of kapton film. Next a prototype is constructed and evaluated which incorporates the proposed aluminium oxide insulation. This work addresses point 2 in the novelty list and was disseminated in [1] (iPower^2,2012) and [2](PCIM Europe, 2013)

Chapter 5 introduces the concept of encapsulant materials made from composites and considers a range of methods by which they can be modelled. In this chapter the performance of analytical models from literature is compared against that of numerical models and experimental evaluation of composite samples. Conclusions are formed regarding the effectiveness of said models, in addition to the effect which different mixing methods have on the composite performance. This forms the groundwork for addressing novelty point 3 and was published in [3] (PEMD, 2014). This work is built upon in **Chapter 6**. Here inductors are constructed which are encapsulated using the composites discussed in the previous chapter. The performance of the composite encapsulant is compared to an inductor encapsulated with standard epoxy. Additionally the performance of the component is predicted by using selected analytical models within finite element analysis (FEA). This also addresses novelty point 3 and was published in [4] (PCIM Asia 2015).

Finally, in **Chapter 7** the work presented in this thesis is drawn together and conclusions are drawn from the work as a whole. Additionally, a future direction for the work is proposed so as to further advance the findings of this work.

Chapter 2

Review of considerations in inductor design

In the previous chapter, the motivation for this work and the aims of this thesis were laid out. This Chapter will now discuss some of the considerations which must be made when designing inductors. The design of inductors can be considered as a complex multifaceted optimisation process which considers a wide range of variables with the goal of achieving the most suitable design for a given application. It is worth observing at this point that the optimisation objectives specified for an inductor will be highly dependent upon its specification, and may vary considerably from application to application. The final inductor design which is selected will generally be a compromise between the following parameters:

- Power Density (kW/kg)
- Volumetric Power Density (kW/m^3)
- Efficiency (%) / Power Loss (kW)
- Cost (£/kW)
- Reliability (Statistically predicted component lifetime)

The importance placed on each category is dependent on the end use of the component. To achieve the optimum design an assortment of design and construction techniques are at the disposal of the designer; these will be outlined in the remainder of this chapter.

2.1 Design of Power Inductors

A power inductor differs from a signal inductor in one key aspect, the level of current which is designed to carry. Due to these high current levels (> 10 A) saturation of the magnetic core is a real possibility unless steps are taken during the design process to avoid this. This means, that in the case of a power inductor the design must consider not only the required inductance, but also the maximum current for which this inductance is achievable. To prevent core saturation, some designs contain an airgap; this increases the total reluctance of the magnetic circuit, reducing the flux for a given current and allowing the inductor to operate at a higher current than if the airgap was not present. The increase in reluctance is not without penalty however, as it also leads to a reduction in inductance. For a given core, the designer must select an appropriate airgap length and number of winding turns, such that both the desired inductance and maximum saturation current are satisfied.

One side effect of the inclusion of an airgap is that the relative permeability of the magnetic core becomes less important than would be the case if designing a signal inductor, as usually the majority of the magnetic reluctance is contributed by the airgap, and not the core. Consequently, this value is usually not as critical as would be the case in an un-gapped inductor. An exception to this statement would be for materials which employ distributed airgaps. In these cases a discreet airgap is not included, instead the magnetic material of the core is combined with a non-magnetic material, reducing the overall permeability (typically to a value of 20 - 80); here a lack of a physical airgap means that the core properties have a larger influence on the resultant inductor performance.

2.2 Magnetic Considerations

The design of an inductor in the magnetic domain requires several key design decisions to be taken. These decisions can broadly be divided into two major categories: those concerning the 'magnetic core’ and the ones concerning the ‘windings’. Magnetic core choices include material selection and core shape; while winding choices include decisions on the winding material; insulation; and actual winding configuration.

2.2.1 Core Loss Mechanisms

A magnetic core is employed within the construction of an inductor to provide a low reluctance path through which the magnetic flux can pass. It can be manufactured in a range of shapes and from a variety of materials, the most suitable of which will be dependent on the operating conditions of the inductor. One parameter which influences the choice of core material is the core losses; these losses can be divided into two distinct categories which are the result of different physical phenomena:

- Eddy current losses
- Hysteresis losses

2.2.1.1 Eddy Current Losses

Eddy currents are generated when a conductive material is placed within a time-varying magnetic field. This placement results in an electrical current being generated within the conductor resulting in losses due to the current flow. The function of a magnetic core is to control the position of a magnetic field, and so inherently it will carry the changing field resulting in the generation of eddy currents within the core. If the magnetic core is produced from a material with a low electrical resistivity, the magnitude of these eddy currents can be substantial and lead to considerable losses within the core. The methods used to address this loss vary, and are dependent on the core material being used. These techniques will be discussed later in this chapter, alongside the materials which they pertain to.

2.2.1.2 Hysteresis Losses

Magnetic materials are made up of many magnetic domains; when a magnetic field is applied to these materials the domains align themselves to the external field. This realignment causes energy to be dissipated within the material, resulting in the production of heat. If the magnetic field in question is an alternating field it is necessary for the domains to realign at the same rate as the field is alternating. Consequently, it should be apparent that the losses in a material will be higher when the material is operated at higher frequency. Again the actual loss is dependent on the material in question.

2.2.2 Determining Core Losses

To accurately predict the operating temperature of a wound component it is necessary to know the core losses. Several approaches have been proposed which allow the estimation of core losses, an overview of these techniques will be considered now.

In the simplest cases it is possible to obtain the core losses from the core material data sheet. This can give acceptable results if the losses have been evaluated under the desired operating conditions (flux swing, frequency and dc bias). An example core loss diagram which may be provided by a core manufacturer is shown in Figure 2.1; in this case, this figure shows the data for 3F3 ferrite material manufactured by Ferroxcube. It can be seen from this figure that the data is only presented for a discreet number of frequencies and flux swings; consequently, in some cases it is necessary to extrapolate the core losses using the data from the core loss diagram. This may potentially be inaccurate if the material behaves in a non-linear manner.

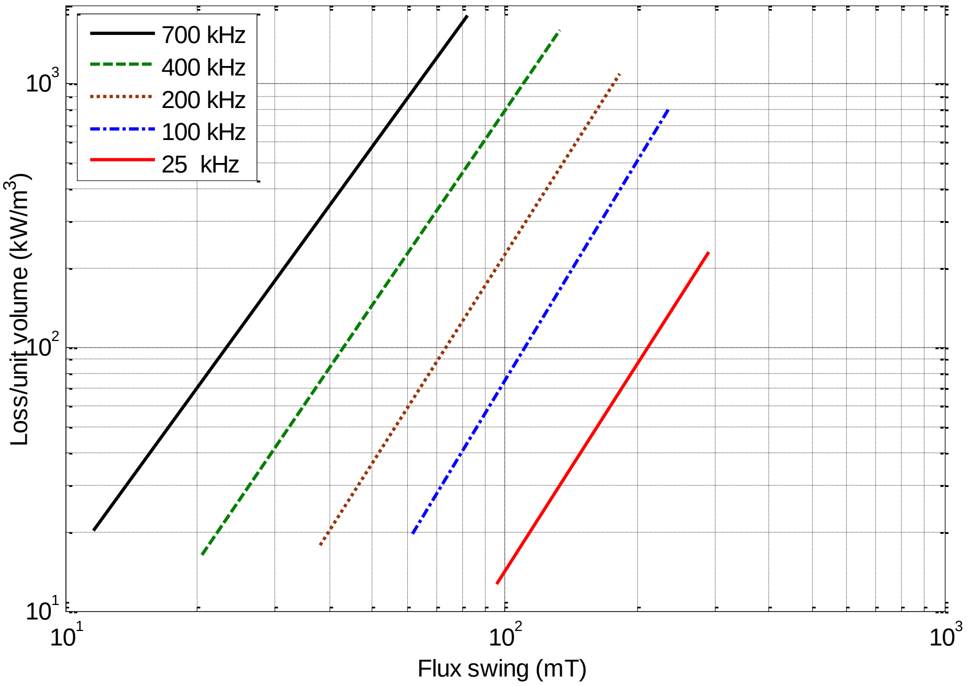

Figure 2.1 – Core loss diagram with respect to flux swing and frequency for 3F3 ferrite material at 100 °C (adapted from [7])

An alternative approach is to use the Steinmetz approximation presented here as equation (2.1) [8].

$$P = kB^{\beta} f^{\alpha} \tag{2.1}$$

Where:

P	Is the loss/unit volume of the material (kW/m^3)
k, α, β	are material constants found by curve fitting to the material properties
B	is the flux swing (T)
f	is the operating frequency (Hz)

To use this equation the material constants are calibrated empirically such that the calculated core losses correspond with those from the material datasheet. This model has limitations as it does not have the capacity to include effects such as the influence of temperature; consequently a variety of modifications to the model have been proposed in literature. Each variation was proposed to address a specific drawback of an assumption made in the original equation. One such assumption is that the core losses will be equal for all temperatures. One method of adding temperature dependency to the Steinmetz equation is presented in [9], this adds an additional polynomial $(C_{t2}T^2 - C_{t1}T + C_{t0})$ to the equation, allowing temperature dependency to be included within the model. This is presented here as equation (2.2)

$$P = kB^{\beta}f^{\alpha}(C_{t2}T^2 - C_{t1}T + C_{t0}) \tag{2.2}$$

Where:

T is the operating temperature of the component (°C)

C_{t2}, C_{t1}, C_{t0} are temperature dependant material co-efficients.

A further limitation of the Steinmetz equation is that the core losses specified by the manufacturer are determined for sinusoidal excitation; in modern applications such as switched mode power supplies it is not unusual for the excitation current to be a more complex shape. It is possible to derive equations which predict the core losses for a non-sinusoidal excitation based on the core loss data for a sinusoidal excitation. Several authors have proposed possible solutions to address this; these solutions can be found in [9, 10, 11, 12]. Additionally, for reference, a historical overview of the evolution and development of the various versions of the Steinmetz equation can be found in [13].

Equations derived from equation (2.1) are most suited for use with core materials which produce losses primarily through hysteresis. For materials for which this is not the case it is not unusual to employ equations based on the Steinmetz equation which employ additional parameters for eddy current losses; examples of this can be found in [14, 15].

An alternative to calculating the core losses is to determine them experimentally; a summary of methods which can be used to accomplish this can be found in [16]. Several of these methods employ thermal measurements to determine the core losses. These methods revolve around calorimetry and work by placing the component in a thermally isolated environment and operating it under the desired test conditions. Based on the temperature increase within the environment it is possible to determine the dissipated power within the component. One drawback to this approach is that losses measured will be provided by both the core and windings and it is not possible to separate them using only this data.

An alternative method is the two winding method. For this method an additional sense winding is added to the core [16] which is connected as shown in Figure 2.2. The method works by driving the main winding with the test waveform and measuring the current through it, simultaneously the voltage on the open circuit sense winding is also measured. Using Equation (2.3) the core loss can be determined from these measurements.

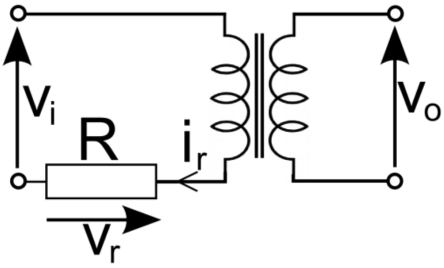

Figure 2.2 - Experimental configuration for core loss measurement

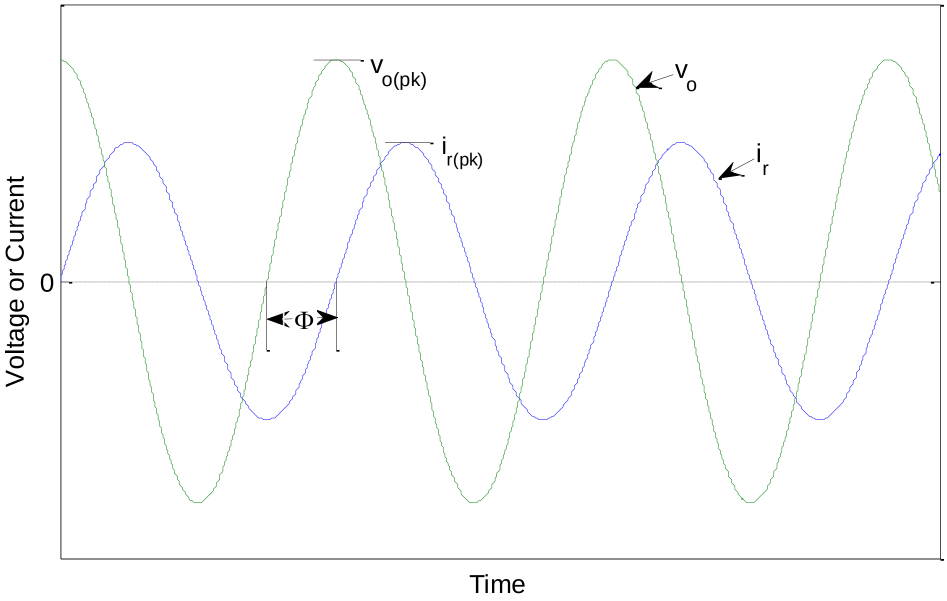

Figure 2.3 – Sample expected waveforms from configuration shown in Figure 2.2

$$P_{Core} = \frac{1}{T}\int_0^T V_o i_r \; dt = \frac{1}{TR}\int_0^T V_o V_r \; dt \tag{2.3}$$

An important property which needs to be considered during this measurement is the synchronisation between the sampling of the two waveforms, as this may introduce a slight additional phase shift between the two measured waveforms. This is particularly an issue in cases in which the core exhibits low losses, as in this case the phase angle between the two waveforms (labelled ϕ in Figure 2.3) will be close to 90°. Therefore, any error in the measurement of the angle has the potential to have a large effect on the calculated core losses. A discussion of this measurement method and an alternative method which alleviates this problem are considered in [16].

2.2.3 Core Materials

In the design of an inductor there are a range of core materials available for the designer to choose from. Generally speaking, the choice of core material is a trade-off between:

- Material saturation flux density;
- Relative permeability;
- Core losses generated by the material under the desired operating conditions;
- Cost.

The inductance of an inductor can be calculated using equation (2.4) [17]; in terms of core material choice, the parameter which directly influences inductance is μ_r. However, other parameters will also indirectly influence the inductance. (For example: if a core is being operated above its saturation level, its permeability will fall, resulting in a reduction in inductance.) An overview of available core materials will now be provided.

$$L = \frac{N^2 \mu_0 \mu_r A}{l} \tag{2.4}$$

Where:

L is the inductance of the component (H)
N is the number of turns within the winding
μ_0 is the permeability of free space ($4\pi x 10^{-7}$) (H/m)
μ_r is the relative permeability of the material
A is the cross sectional area of the magnetic path (m^2)
l is the length of the magnetic path (m)

2.2.3.1 Air Core

One potential design option is not to include a magnetic core at all, in this case the inductor will use the surrounding air as the 'core'. Obviously from a core cost perspective this option is the cheapest, however; as air has a value of 1 for μ_r, it is necessary to use a winding which has a larger number of turns than would be the case if a higher permeability core was used. Therefore in order to achieve the required inductance using an air core, increases to the cost of the winding and also the winding resistance must be accepted. Additionally, as there isn't a low reluctance path to direct the magnetic flux, it is allowed to spread out further than it would if a core was present. This can result in issues with electromagnetic interference, as the flux can couple with other components and cause issues if not taken into account. That being said, as core losses increase with frequency, an air cored inductor may become viable when operating at high frequency (>1 MHz), as at this frequency the increase in core losses may be sufficient to offset the winding losses caused by the additional turns required within the winding, if an air cored coil was used.

2.2.3.2 Silicon Steel

A further potential core material is silicon steel. Silicon steel has a high flux density saturation level of up to 2 T and an initially permeability ranging from 400 – 10,000. However, due to its relatively low electrical resistivity (0.4 – 0.7 μΩ.m), eddy current losses are large. These losses can be reduced by producing the core from insulated laminations; thinner laminations result in lower levels of eddy currents; however, the cost of the winding stack is inversely proportional to lamination thickness (as more laminations are required to make up a given core stack thickness). Hysteresis losses also contribute to the overall loss of silicon steel, the level of hysteresis loss in the material is influenced by the quantity of oxygen within the material structure; this can be controlled by the addition of silicon which removes oxygen from the structure, reducing the hysteresis losses. Limits must be imposed on the amount of silicon added to the material however, as its addition reduces the flux density saturation level of the material and makes the material more brittle [18].

2.2.3.3 Nickel-Iron Alloys

Another core material is nickel-iron alloy, (sometimes referred to as “Permalloy”, “Isoperm” or “Invar”; depending on the concentration of nickel). The addition of nickel increases the permeability of the material. However, the amount of nickel which is added is a trade-off between saturation flux and permeability. The nickel concentrations which are commonly used range between 30 % and 80 %, with the highest permeability being obtained in the case of Permalloy (80 % nickel) and the highest saturation flux density being observed in Isoperm (50 % nickel). It is worth noting that nickel is considerably more expensive than iron, so a higher concentration will increase the material cost. Nickel-iron is available in a range of thickness, some suitable for manufacturing laminations and some thin enough to be used as a tape for the manufacture of a tape wound core. Additionally it is also available as a powder suitable for the production of powder cores.

2.2.3.4 Amorphous Alloys

Amorphous alloys are another material which can be employed in the manufacture of magnetic cores; the important characteristic of these metals pertains to their structure. To manufacture this material the alloy is cooled quickly, such that the atoms within the structure do not form crystals and are completely disordered, with a structure similar to glass. (For this reason such materials are sometimes referred to as metallic glass.) As it is necessary to cool the material at a rapid rate, there are limits on the thickness of metal which can be formed; consequently amorphous metals are usually supplied in the form of tapes. Amorphous metals have a high permeability and an electrical resistivity higher than silicon steel. The saturation flux of the material varies dependant on which materials are included within the alloy, but in some instances can approach that of silicon steel [8].

2.2.3.5 Nanocrystalline Materials

Nanocrystalline materials are produced from amorphous metals by annealing the amorphous metal; the structure is altered, forming very small crystals. This alters the properties of the material and results in a material which exhibits lower losses than the original amorphous metal.

2.2.3.6 Ferrites

Soft ferrites are another possible core material; ferrites are produced from iron oxide and either Manganese-Zinc or Nickel-Zinc [19]. Due to the high oxide content the electrical resistivity of ferrites is very high resulting in very low (negligible when compared to hysteresis loss) eddy current losses. Consequently, ferrites are a popular core material choice for higher frequency applications. The primary disadvantage of ferrites is the low maximum flux density (typically below 0.45 T). To prevent saturation it is often necessary to include an air gap for high current inductors, which can result in increased losses in other areas of the component such as the windings; the reasons for which will be discussed later.

2.2.3.7 Iron Powder

The final core material to be discussed here is iron powder. To produce a core, iron powder is heated such that the surface oxidises, producing an insulated surface layer; this powder is then mixed with binders and formed into core shapes under pressure. As the iron powder particles are insulated from each other, the eddy current losses are reduced and are lower than those seen in steel [19]. By controlling the amount of iron and binder in the mixture it is possible to vary the permeability value of the material, lowering the permeability of the material, producing a ‘distributed air gap’. This potentially eliminates the need for a physical air gap in the magnetic circuit. The saturation flux density of powder cores is typically between 1.0 T and 1.3 T. As with ferrites, due to their high resistance and therefore reduced eddy current losses, powder cores are potentially useful in high frequency applications where the losses in steel would be prohibitively high. It should be noted however, that iron powder cores have a lower maximum operating temperature compared to steel or ferrites, which is typically around 75^{o}C and is set by thermal ageing; for comparison, the maximum operating temperature for soft ferrites and silicon steel are up to 140^{o}C and 150^{o}C respectively [20]. It should be noted that in these cases the maximum operating temperature is not imposed by the magnetic materials themselves, but by other materials which are required for their practical use (such as the binders in a powder core and the epoxy coating in a laminated/ferrite core). Consequently it may be possible to exceed these operating temperatures by employing different material/construction methods.

Material	**Saturation Flux (T)**	**Initial Permeability**	**Resistivity (µΩ.m)**	**Continuous Operating Temp (°C)**	**Curie Temp (°C)**
Silicon Steel	1.9 – 2.0	400 – 10,000	0.4 – 0.7	150*	720
Nickel-Iron (80 % nickel) (Permalloy)	1.0	10,000	0.15	120 – 150*	500
Nickel-Iron (50 % nickel) (Isoperm)	1.6	2,000 - 3,000	0.35 – 0.4	120 - 150*	500
Nickel-Iron (30 - 40 % nickel) (Invar)	0.6	2,000	0.75	120 - 150*	500
Amorphous Alloy	0.5 – 1.8	10,000 – 150,000	1.2 – 2	150*	350 - 450
Nanocrystalline	1.2 – 1.5	15,000 – 20,000	0.4 – 1.2	120 - 155*	600
Ferrite (MnZn)	0.3 – 0.45	100 – 20,000	10^2 - 10^4	140 - 200*	125 – 450
Ferrite (NiZn)	0.3 – 0.45	100 – 20,000	10^7 - 10^9	140 - 200*	125 – 450
Iron Powder	1.0 – 1.3	1 - 500	10^2	75**	700

Table 2.1- Summary of properties of magnetic materials (Data from [8, 20, 21])

*Limited by epoxy/casing; ** Limited by thermal aging

2.2.4 Core Shapes

In conjunction with material selection, an appropriate core shape needs to be selected for the inductor design. Although there are many variations on magnetic core shapes, they are all based on a few fundamental shapes shown in Figure 2.4 to Figure 2.7. While these figures illustrate the principle shapes used for cores, it should be noted that there are many variations on them which are commonly employed in practical inductor design Some of these variations will now be outlined.

2.2.4.1 Toroidal Core

The topology of a toroidal core can be seen in Figure 2.4. As this shape does not include any sharp corners within the magnetic circuit, the flux will be more evenly distributed than would be the case for some other core shapes. Due to the single piece construction, the introduction of an air gap into the magnetic circuit is not possible. Consequently, the properties of the core material are more significant during the design process than would be the case for other topologies, where it is possible to make adjustments to the inductor by adjusting the air gap size. An additional issue caused by the single piece nature of the core is that winding the core is more challenging, as each turn must be individually passed through the centre of the core; and the use of pre-formed windings is not possible.


(a) (b) (c)

Figure 2.4 - Toroidal Core. (a) – general profile of shape; (b) – example core; (c) – example wound inductor employing a toroidal core

2.2.4.2 C-Core

The C-core topology (sometimes referred to as the U-core) can be seen in Figure 2.5. C-cores have two parallel legs connected by a crosspiece. This crosspiece may take the form shown in Figure 2.5, using flat base and 90° corners, or the corners may be rounded. These two shapes each have their own advantages and disadvantages. For example, designing a core with square corners as shown in the figure results in a flat surface suitable for mounting/heat extraction purposes. However, in the case of a rounded base, the shape of the magnetic path is smoother and therefore the flux will be more evenly distributed at the corners of the core. Using this topology, the windings can be positioned on one or both of the core legs. This potentially offers a thermal advantage in a wound component in which the bulk of the losses come from the windings as it allows them to be spread out over multiple legs, rather than being concentrated in one place. Additionally, as the core consists of multiple parts it is possible for the windings to be pre-formed using a coil former, aiding manufacturability. Furthermore, it is possible to introduce an air gap into the magnetic circuit by separating the two halves of the core and placing a material with a lower magnetic permeability between one or both of the core legs. This allows the magnetic path reluctance to be adjusted to achieve the desired properties from the inductor.

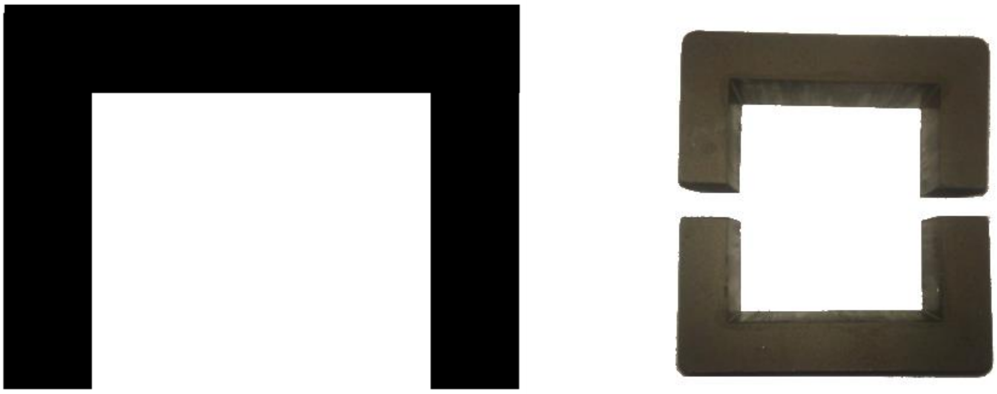

(a) (b)

Figure 2.5 – C-Core. (a) – general profile of shape; (b) – example core

2.2.4.3 E-Core

In the case of an E-core, shown in figure 2.6, the advantages are similar to those exhibited by the c-core in so much as it also possible to utilise a pre-formed coil and introduce an air gap into the magnetic circuit easily. Conventionally the windings are placed around the centre leg of the E-core. This offers the advantage that the windings are magnetically shielded from stray fields which may be generated by other components within the system by the outer legs. This is important for two reasons: firstly, it is possible that if external signals couple to the windings this will modify the performance of the component, causing unexpected behaviour to occur; secondly, high frequency magnetic fields can generate eddy currents in the windings resulting in an increased loss within the windings. Furthermore, as the outer legs form a closed path in which the flux from the inductor can flow, leakage in the opposite direction (from the inductor to other components in the system) is also reduced.

To introduce an air gap into this topology two approaches are possible. Firstly a material with a low magnetic permeability (for example plastic) can be placed between the two core halves, separating the core halves and resulting in an air gap within all three legs of the core, similar to the way in which a c-core would be gapped. It should be noted however, that if this method of gapping the core is used, fringing fields will be produced at the air gaps in the outer legs which may couple to other components. An alternative gapping strategy is to remove material from the centre leg, introducing a gap only into this leg; this approach keeps the outer core legs intact and preserves the shielding effect of the topology. It should be noted however, that this approach is also not without its drawbacks, as using this method, the air gap will have to be approximately twice as long as would be the case if all three legs were gapped in order to achieve the same path reluctance. This can contribute to increased winding losses. (This will be covered in more detail when winding losses are discussed later in this chapter). The approach chosen is dependent on the design requirements and the available manufacturing equipment, as it is necessary to grind the centre leg precisely to obtain an accurately characterised wound component. It is worth mentioning that E-cores come in several different varieties, allowing the component to be optimised to the system geometrical requirements. For example low profile planar cores such as the one shown in Figure 2.6(c) are available, facilitating the production of low profile components. Other options such as the RM core are also available; these are designed to exhibit improved magnetic shielding by extending the outer core legs around the circumference of the winding window, such that more of the winding is enclosed within the core as shown in Figure 2.6(d).

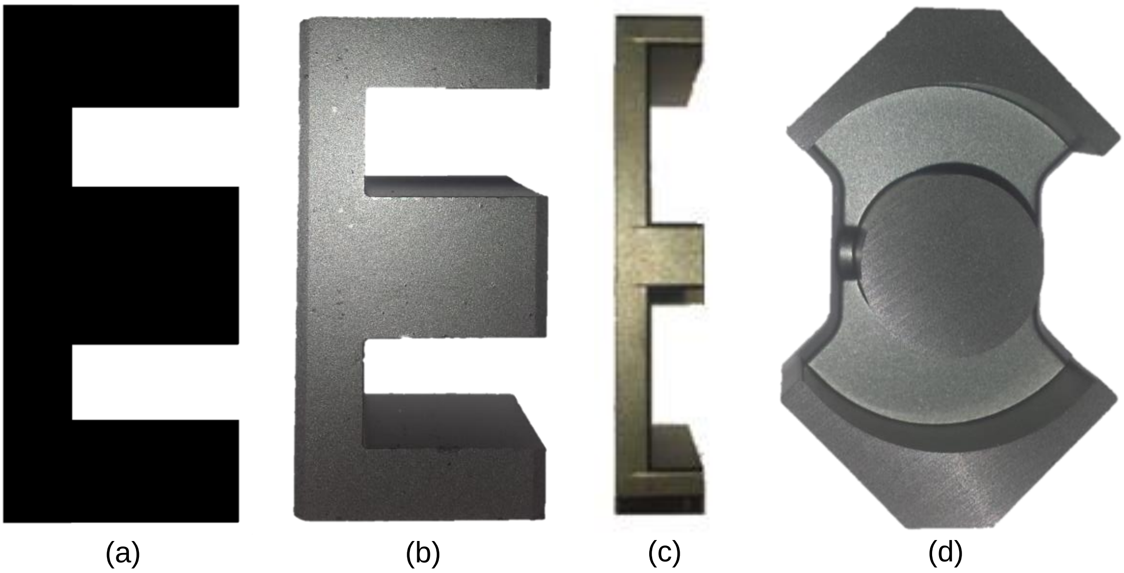

Figure 2.6 - E-core. (a) – general profile of shape; (b) – E-Core; (c) – Planar E-Core; (d) – RM core

2.2.4.4 I-Core

The I-core can be used in two different ways; the first is to use it in combination with either a C-core or an E-core to complete the magnetic path, resulting in a smaller component than would be the case if an identical pair of cores were used (but with a smaller winding window). The second way of employing I-cores is to use them as basic building blocks and produce an arbitrarily shaped custom core by assembling the cores together using an adhesive such as a cyanoacrylate based glue or an epoxy.

Figure 2.7 - I-Core. (a) – general profile of shape; (b) example core

2.2.5 Winding Configurations

2.2.5.1 Packing Factor

A decision which must be made when designing a wound component is the shape and structure of the windings being employed. When considering windings, an important property which must be included is the packing factor. The packing factor is a measure of how much of the available winding area is occupied by conductor material, expressed as a proportion of the total space. It is important to consider this parameter when designing a winding to occupy a confined space as failure to do so will result in a winding which contains fewer turns than it was designed to have. In cases in which the winding is not size constrained the desired number of turns will be achieved but failure to consider the packing factor will result in a winding which is larger than anticipated.

There are several reasons why a winding will not occupy 100 % of the available space. Firstly the shape of the conductors used to produce the winding do not fully tessellate, as illustrated in Figure 2.8. Using standard winding techniques the tessellation of the wires can be considered a hard limit to the maximum packing factor. Work has been done to allow windings to be manufactured which exhibit a packing factor in excess of this limitation by applying pressure to the completed assembly, deforming the conductors and allowing them to pack together more closely [22, 23]. Care must be taken when employing such an approach so as to avoid the risk of damaging the winding insulation during the compression process. However, tests performed in [22] showed that even when the coils were compressed under high pressure (800 MPa) the insulation remained intact.

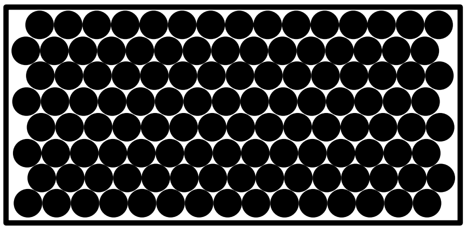

Figure 2.8 - Example winding configuration using circular profile conductors arranged using hexagonal packing, illustrating a non-perfect packing factor

In addition to the winding shape, the winding insulation material also influences the packing factor. Therefore, even if wires being employed do tessellate well, (for example, the square conductors illustrated in Figure 2.9) it is not possible to achieve a packing factor of 100 % owing to the space occupied by the winding insulation material.

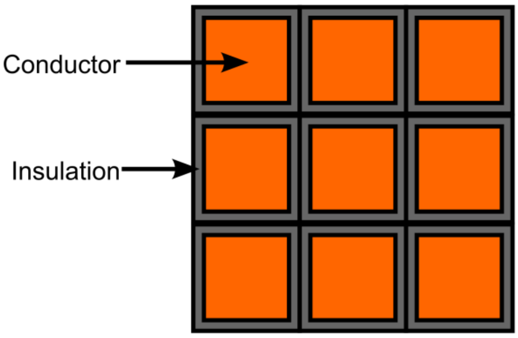

Figure 2.9 - Illustration of fill factor reduction caused by winding insulation

A further issue which must be included in the calculation of achievable packing factor is how much the winding bows due to the tension placed upon it. The level to which this is an issue is dependent on the profile of the chosen core leg. If the wire is being wound around a former which has a circular profile, the tension placed upon it is uniform and so only a small amount of bowing occurs. If however, the former has a rectangular profile, the tension on the wire will be concentrated at the corners of the former, causing the conductors to bow out and away from the former, thus reducing the packing factor of the winding [19]. This concept is illustrated in Figure 2.10.

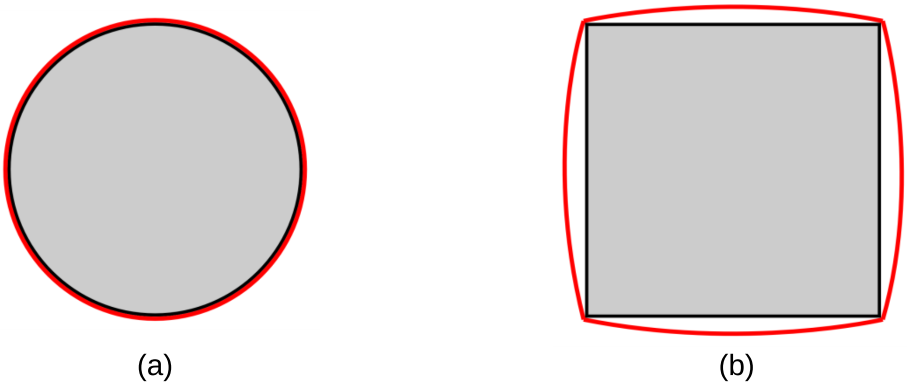

Figure 2.10 – Illustration of bowing caused by wire tension. (a) – Round former; (b) – Rectangular former

2.2.5.2 Round Wire

The most commonly employed wire shape used for producing wound components is round profile wire. This wire is readily available with a variety of insulations in a wide range of diameters on both a micron and millimetre scale.

2.2.5.3 Rectangular wire

An alternative winding shape is a rectangular cross-section; in this case the height and width of the conductors can be specified individually to meet the design requirements. One key advantage of this profile pertains to the packing factor; because the conductors possess square edges, the individual turns within a winding tessellate together well, improving the potentially achievable packing factor of the winding.

2.2.5.4 Litz Wire

For a component to operate in a thermally stable manner care must be taken during the design process to ensure that winding losses are kept to a reasonable level. To achieve this, a wire of adequate cross-sectional area must be employed. In components which operate with an ac excitation, a level of resistance associated with the ac component of the signal will manifest itself. While this will be explained in greater detail later, for now it suffices to say that to control the magnitude of this ac resistance at a higher frequency, it is necessary to decrease the diameter of the conductors used. This limits the diameter of conductor, which can potentially prevent it having a suitably large cross-sectional area to achieve the desired current carrying capabilities. This problem can be alleviated by employing litz wire. Litz wire cables consist of multiple individually insulated strands woven together, such that each strand occupies each point within the bundle at some point along the length of the cable. This allows both the maximum strand size and minimum cross-sectional area requirements to be met simultaneously [8]. Due to the many combinations of wire size, number of strands and twist pattern Litz wire is generally a bespoke component which is manufactured to order, which allows the designer to optimise the chosen Litz wire to meet the specific requirements of the component being designed. The packing factor achieved with litz wire is generally worse than that of a solid round conductor since the cables are usually manufactured from many round wires (which do not fit together well). Consequently a litz wire cable of a given cross-sectional area will be larger than the corresponding solid conductor.

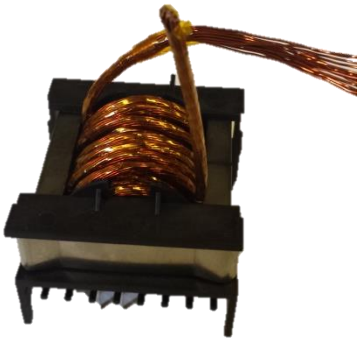

Figure 2.11 –Example litz wire inductor

2.2.5.5 Foil Windings

An alternative winding solution which can be employed to deal with frequency losses is the use of foil. When a foil is used, the dimension which is considered for frequency losses is the foil thickness. Consequently it is possible to produce a winding which satisfies the cross-sectional area requirements without exceeding the maximum thickness by using a wide, thin foil. This foil can be utilised in different ways to produce a winding. Firstly, and probably most suitably for a conventional core, the foil can be rolled up to form a winding, as shown in the example in Figure 2.12(a). Using this method, an insulation material is applied to one or both sides of the foil prior to winding to prevent short circuits between the layers [24]. An alternative approach, more suited to planar topologies is to fold the foil instead of rolling it up, producing a planar winding [25]. A diagram of such a winding is shown in Figure 2.12(b). In both instances, an advantage to using foil is the packing factor which can be achieved as foil strips fit together well. This means that the primary mechanism which reduces the packing factor in this case is the space occupied by the insulation material.

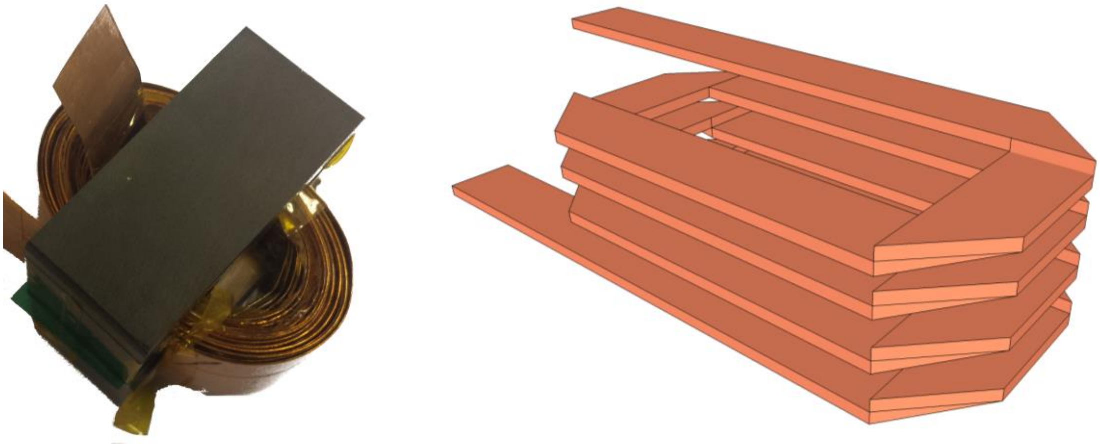

(a) (b)

Figure 2.12 – (a) - Example foil wound inductor; (b) - Example planar winding produced from foil

2.2.5.6 *PCB Windings*

A further method of producing windings particularly suited to planar applications is to etch them onto a printed circuit board (PCB). In this way the windings can either be assembled on a standalone PCB or integrated into the PCB used to construct the wider system. As the process of manufacturing PCBs is well established and reliable, producing windings in this way yields good repeatability and therefore produces windings which will have a consistent performance, in addition to the mechanical strength provided by the PCB. A sample PCB winding is visible in Figure 2.13. A disadvantage of these windings is that due to the relatively large thickness of the PCB substrate, the packing factor of windings manufactured using this method tends to be poor. This thickness can also impact upon the thermal performance of the windings, since the materials used to manufacture PCBs generally has quite poor thermal performance (0.34 W/m.K for FR4 [26]).

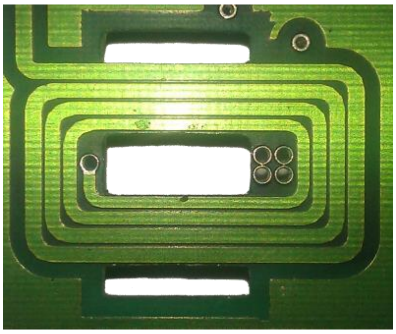

Figure 2.13 - PCB winding (magnetic core removed)

2.2.5.7 *Flexible PCB windings*

The poor thermal performance of FR4 can be addressed by utilising flexible PCBs. These PCBs differ from the conventional ones in that the thick ridged substrate is replaced by a thinner (25 μm – 75 μm), flexible layer made from kapton or some other suitable polymer. This has the twofold effect of improving the packing factor of the winding and simultaneously improving the thermal performance. Although the thermal conductivity of kapton is also poor (0.12 W/m.K [27]), the reduced thickness allows heat to transfer through it more easily.

The flexibility of the windings produced in this way also offers interesting opportunities in the design of the winding. Using this technology it is possible to produce a winding by etching it onto the PCB and then folding it up in such a way that a continuous spiral winding is formed, in a technique sometimes referred to as z-folding [28, 29]. This method is comparable to the method previously discussed which allows the production of planar foil windings. The key difference with this approach is that when the method is performed using a flexible PCB, it is possible to produce a full winding turn with one fold, whereas when foil is used, several folds are required to produce a complete turn. One point which should be noted is that the use of a PCB imposes limits upon the maximum conductor thickness which can be employed; this is limited by the PCB copper thicknesses which are available.

2.2.5.8 Plate Windings

To allow the designer access to a wider range of winding thicknesses, an alternative technique can be employed. In this method the windings are cut from sheet materials, after which appropriate insulation material is applied to the cut pieces [30, 31, 24]. This approach could be particularly amenable to mass production since it is possible to stamp out the windings using a high pressure press. These cut windings can then be assembled to form a complete winding consisting of multiple layers. In addition to offering a wider range of choice in winding thickness, this method also offers a more flexible choice of winding material compared to PCBs, which are generally only manufactured using copper.

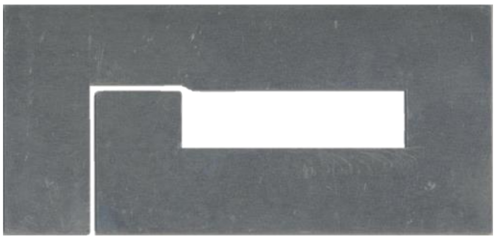

Figure 2.14 - Sample of an aluminium planar winding

2.2.6 Winding Materials

When the decision has been made which winding topology is the most desirable, the next decision is the selection of the winding material, the most commonly used of these are copper and aluminium.

When selecting the most suitable conductor material, several material properties have to be considered. These properties for pure copper, aluminium and silver (the most commonly considered materials) are listed in Table 2.2; from here a number of things become apparent. Firstly, considering silver, from the data shown here it can be seen that it has the lowest electrical resistivity of the three materials, therefore, technically if this parameter was the only concern when designing a component, silver would be the most logical choice. When other material properties are factored into the decision silver quickly becomes less attractive. Firstly, it has the highest density and therefore will produce a winding which is heavier than a similar copper or aluminium winding. When the thermal properties of silver are considered it can be observed that it does have a thermal conductivity slightly higher than copper, which would theoretically mean that a silver winding would operate a cooler temperature (silver has a thermal conductivity 7 % higher than copper). It is likely however, that such a device would reach thermal steady state more quickly than copper due to silver's lower specific heat capacity, potentially reducing the overload capacity of the component.

	Copper	**Aluminium**	**Silver**
Electrical Resistivity (nΩ.m)	16.94	26.70	16.30
Density (kg/m^3)	8960	2700	10500
Thermal Conductivity (W/m.K)	397	238	425
Specific heat capacity (J/kg.K)	386	917	234
Volumetric heat capacity (J/m^3.K)	3.459x10^6	2.4759x10^6	2.4570x10^6
Cost ($/kg)	6.0885	1.7055	536.92
Cost ($/m^3)	54,552.96	4,604.85	5,637,660.00

Table 2.2 - Conductor material properties (Data from [32, 33, 34])

Considering only the parameters discussed here so far there are advantages and disadvantages for selecting silver as a winding material over copper. The most significant parameter which destroys the use of silver as a winding material is the cost. The slight advantages which could potentially be gained by utilising silver are dwarfed by the huge difference in price. Consequently it is highly unusual to utilise silver as a winding material.

The choice of copper or aluminium is a more complex decision. From Table 2.2 it can be observed that copper exhibits superior performance in electrical resistivity. However, aluminium is less dense and cheaper. Additionally, in cases where size is not a concern, it is possible to increase the size of the aluminium conductors to compensate for the higher material resistivity, the resulting winding still being cheaper and lighter than the copper equivalent. One example where aluminium is often used is in the manufacture of distribution transformers [35, 36, 37]. In this case, the size increase required to achieve a comparable resistance in aluminium to copper can be accepted since the application does not require the component to be moved regularly and therefore size is not a primary concern.

When considering the heat capacity of the materials, the better of the two materials is dependent on which parameters of the winding are constant between the comparable windings. In some instances (e.g., if the windings are produced from the same weight of material) an aluminium winding will have a higher heat capacity than that of a copper winding. However, in other scenarios (e.g. if the windings have the same volume) the copper winding will have a higher thermal mass. It should be noted that if an inductor is being designed to be operated with a relatively consistent load for a prolonged period of time, the thermal mass is not important as the component will be operating at thermal steady state.

From this analysis it can be observed that there is not a simple ‘one size fits all’ winding material which is the optimum choice for all applications. The most suitable material will depend upon the constraints that are placed upon design and the optimisation goals. Primarily these optimisation goals will be size, weight, cost and resistance. As discussed here, there is no material which is the optimum choice for all optimisation goals simultaneously therefore the choice between copper and aluminium is an area of considerable interest. The choice between aluminium and copper will be discussed in more detail in chapter 3 of this thesis.

2.2.7 Winding Insulation

After the decision has been made as to which winding material and topology is to be employed, the next decision is the choice of winding insulation. In some instances this choice may have already been made when the winding topology was selected. (For example, if a PCB winding is being employed, the layer separation will inherently be provided by the PCB substrate.) Even in such a case, additional winding insulation may still be required. In other cases the structure of the windings does not inherently offer any insulation properties, so the choice of insulation material is left entirely to the designer.

When selecting an insulation material two factors must be considered: the maximum operating temperature of the winding and the maximum voltage which the insulation must be capable of isolating. If the chosen insulation is insufficient to meet both of these requirements it is likely that it will fail, resulting in short circuits.

In the case of circular or rectangular profile wire, it is possible to purchase the wire with insulation pre-applied to its surface, such wire is commonly referred to as ‘magnet wire’ or ‘enamelled wire’, (the latter of these names is a misnomer as it is quite unusual for wire to be insulated using enamel, more usually the insulation will consist of a plastic material, such as polyester, polyurethane or polyimide). The maximum operating temperature for winding insulation is typically specified as defined by the NEMA MG1 standard [38]; the temperature ratings, by class are presented in Table 2.3. These temperature ratings specify the maximum temperature which the insulation can operate at and still achieve a specified lifetime (typically 20,000 hours). By operating the winding at temperatures lower than the rated temperature the expected lifetime of the insulation is improved; in this respect it is potentially advantageous to over specify the temperature rating of the insulation material to improve the reliability of the winding.

Class letter	**Maximum Operating Temperature**
A	105 °C
B	130 °C
F	155 °C
H	180 °C

Table 2.3 - Insulation operating temperatures as defined by NEMA specification [38]

For magnet wire, the minimum insulation breakdown voltage is prescribed by IEC 60317 [39]; within this standard there are different breakdown voltages specified for each conductor size dependant on the grade of the conductor. Higher conductor grades have higher breakdown voltages, however, this also results in conductors which have a slightly larger diameter owing to the increased insulation thickness required to achieve the desired breakdown voltage.

To facilitate ease of use, some winding insulations are designed to be solderable. In these cases it is not necessary to remove the insulation prior to soldering, a trait which may be particularly desirable when assembling windings which employ litz wire, as a litz wire bundle consists of many individually insulated strands, (possibly well over 100) all requiring the insulation to be removed to make an electrical connection. A process which is potentially time consuming and difficult, making a method that avoids such a task desirable.

The options described here are readily available in the form of magnet wire however, as discussed previously, it is possible to manufacture bespoke windings from scratch. In these cases it is necessary for the design to include some kind of insulation material. A common material for this purpose is polyimide (sometimes referred to by the brand name kapton). Kapton is available in the form of a thin film (25 μm) and is capable of operating at temperatures up to 400 °C [27]. Practically speaking kapton is suitable for use in the production of planar windings. It is also available in the form of a tape with adhesive applied to it which can be applied to foils as insulation [24]. Additionally, as previously discussed, kapton is also used as the substrate in the manufacture of flexible PCBs, providing interlayer separation and insulation.

An interesting insulation option which applies to aluminium is the growth of a layer of aluminium oxide on the surface of the aluminium using the anodisation process. This is a potentially attractive solution due to the fact that aluminium oxide has a thermal conductivity considerably higher than that of kapton, offering a method of improving the thermal performance of the completed winding. The use of aluminium oxide as an insulation material for wires [40] and foils [41] have both been explored, the result of which suggests that aluminium oxide is potentially a viable insulation material in some topologies. However, in the case of round wires cracking is visible in the oxide layer prior to any stress being applied to the wire [40]. This can be attributed to the curvature of the surface of the round wire since comparable cracks are not visible in a similarly prepared flat profile piece of anodised aluminium. Work has been completed as part of this thesis exploring the use of aluminium oxide as an insulator in planar windings [2]. This concept will be discussed in more detail during chapter 4.

2.2.8 Winding losses

Once the conductors have been selected, it is necessary to consider the losses generated by the inductor windings.

2.2.8.1 DC resistance

The simplest and most often considered winding losses for a conductor are the dc losses. These losses are based on the dimensions of the conductor and the electrical resistivity of the material used to manufacture it. The dc resistance of a conductor can be calculated using equation (2.5). Calculation of the value of *A* is dependent on the shape of conductor. Example calculations for round and square conductors are shown in Figure 2.15 and equations (2.6) and (2.7).

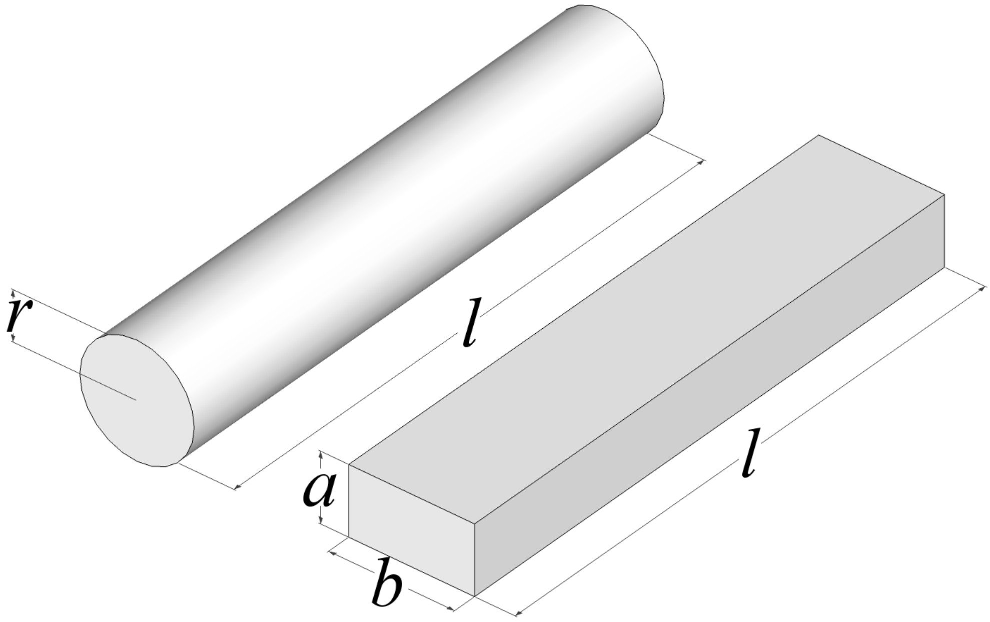

Figure 2.15 - Diagram illustrating conductor dimensions for round and square conductors

$$R_{dc} = \frac{\rho_c l}{A} \tag{2.5}$$

$$A_{round} = \pi r^2 \tag{2.6}$$

$$A_{square} = ab \tag{2.7}$$

Where:

R_{dc}	is the dc resistance of the winding (Ω)
ρ_c	is the conductor resistivity (Ω.m)
l	is the length of the winding (m)
A	is the cross sectional area of the winding (m^2)
r,a,b	are the dimensions of the conductor (see Figure 2.15) (m)

For ac applications, frequency effects can significantly alter the effective resistance of the winding, where the effective resistance is described as the sum of the dc resistance and the eddy current effects at a given frequency. Under ac current excitation, alternating magnetic fields are produced; these fields in turn induce eddy currents within the winding resulting in an increase in the winding resistance compared to its dc value. These eddy current losses can be divided into two categories: skin effect losses and proximity effect losses.

2.2.8.2 Skin Effect

Skin effect losses are caused by eddy currents induced within the conductor as a result of the conductor's own magnetic field. A consequence of this is that current within the conductor is unevenly distributed, with more current flowing near the surface of the conductor than in its centre. Skin depth is a measure of how deep within the conductor the majority of current will penetrate and can be calculated using equation (2.8) [8]. When selecting the wire size to be used within a winding, the diameter is generally limited to twice the skin depth at the operating frequency [42] due to this effect.

$$\delta = \sqrt{\frac{\rho_c}{\pi \mu f}} \tag{2.8}$$

Where:

δ	is the skin depth (m)
ρ_c	is the resistivity of the of the conductor (Ω.m)
μ	is the permeability of the conductor (H/m)
f	is the frequency of excitation (Hz)

The influence of skin effect upon the current distribution is demonstrated in Figure 2.16 using a copper conductor with a diameter of 2 mm. Furthermore the resistance of this conductor at a range of excitation frequencies modelled with FEMM, using a harmonic excitation and assuming planar symmetry is also included in Table 2.4. (In this instance the conductor length is set to 1 m.) An important issue to highlight at this point is the use of a suitable mesh size when simulating the effects of skin effect. It is important to ensure that the mesh which is used has elements smaller than the skin depth at the highest frequency of interest. If this constraint is not satisfied the results of the simulation will contain errors due to this.

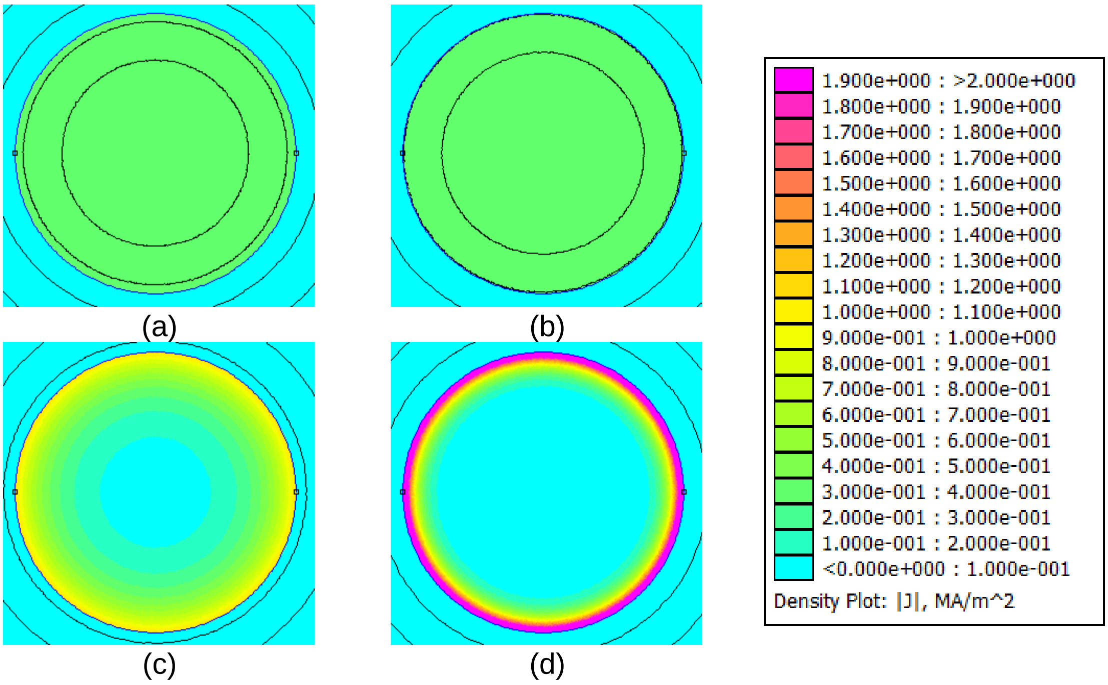

(a) (b) (c) (d)

Figure 2.16 – Simulated current distribution within 2 mm diameter copper conductor in free space at a range of frequencies. (a) – dc; (b) – 10 kHz; (c) – 100 kHz; (d) – 1 MHz

Excitation Frequency	Resistance
dc	5.489 mΩ
10 kHz	6.040 mΩ
100 kHz	14.610 mΩ
1 MHz	43.012 mΩ

Table 2.4 - Resistance of 2 mm diameter copper conductor in free space with respect to frequency (length of conductor = 1 m)

2.2.8.3 Proximity effect

In addition to skin effect, the proximity effect also contributes to the increase in effective resistance. A simulation of a group of wires demonstrating the redistribution of current as a result of this effect is provided in Figure 2.17. Here, once again the conductors are 1 m long and 2 mm in diameter; in this particular configuration the resistance increases from 32.9 mΩ at dc to 634.6 mΩ at 1 MHz. This effect is caused by magnetic fields generated by other wires/turns within the winding causing the current within the conductors to redistribute.

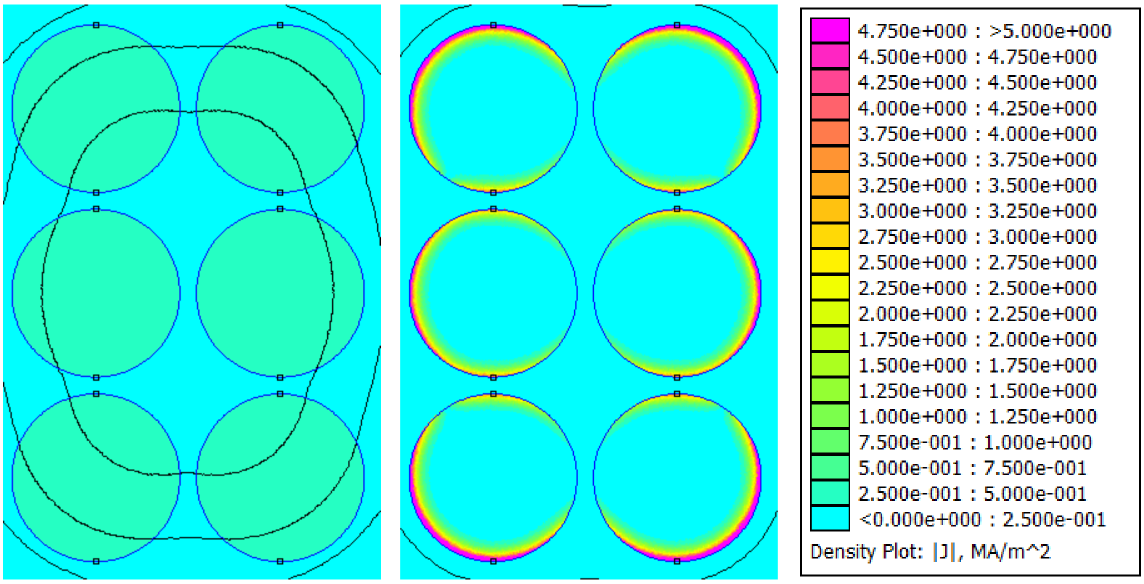

(a) (b)

Figure 2.17 – Simulated current distribution within a collection of 2 mm diameter copper conductors. (a) – dc; (b) – 1 MHz

In addition to other wires, the magnetic field fringing at the air gaps in a magnetic circuit will also contribute to the redistribution of current. This phenomenon is illustrated in Figure 2.18, where a single 2 mm diameter, 1 m long conductor is surrounded by a magnetic circuit which includes an air gap; the effect of this air gap on the current distribution can be clearly seen in Figure 2.18(b). In these simulations the winding resistance of the conductor at dc is 5.5 mΩ; this increases substantially to 350.5 mΩ at 1 MHz. This dramatic increase is caused by the fact that the fringing flux at the air gap of the core interacts with the winding and induces eddy currents within the winding. The magnitude of this effect is proportional to frequency, so at 1 MHz, the influence of this effect is considerable. As this effect is caused by interaction between the winding and airgap fringing flux, it is possible to reduce its effect by increasing the spacing between the airgap and the conductors, but at the expense of coil packing factor.

The combination of these frequency effects can have a substantial impact on the resistance of the windings at the operating frequency. Consequently, care must be taken during the design process to minimize the influence of them through appropriate selection of wire size and by keeping the conductors an adequate distance from air gaps.

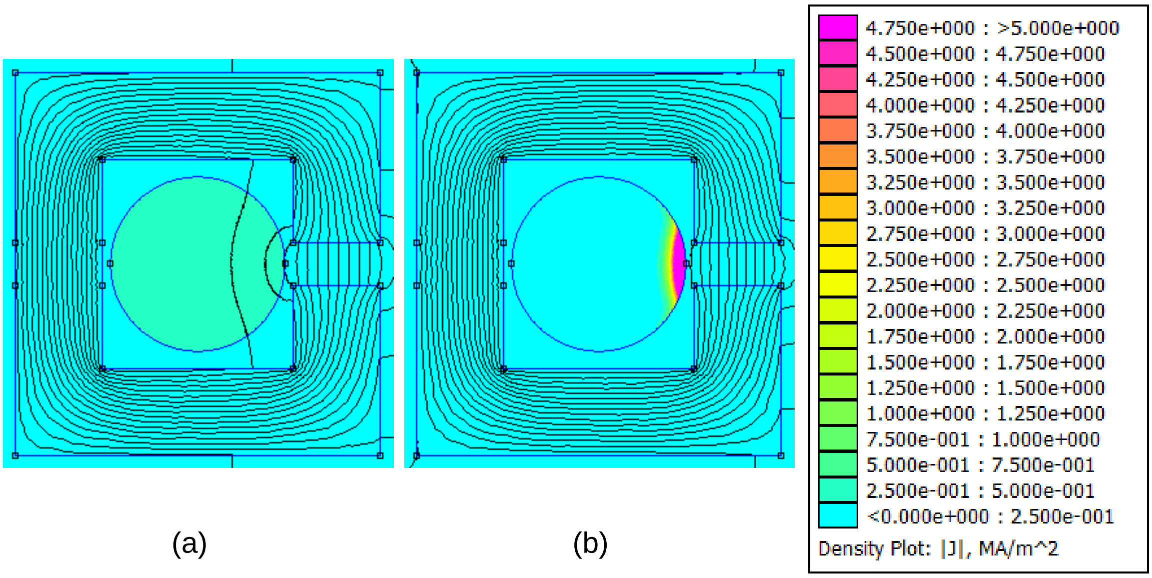

(a) (b)

Figure 2.18 – Simulated current distribution within a 2 mm diameter copper conductor contained within a magnetic path which includes an air gap. (a) – dc; (b) – 1 MHz

2.2.9 Modelling of winding losses

When examining the effects of frequency on effective ac resistance it is beneficial to define the ac/dc resistance ratio (R_{ac}/R_{dc}) (sometimes referred to as F_r in literature). This parameter is defined as the ac resistance of a conductor at a given frequency, divided by its dc resistance and is useful as a means of quantifying the effects of frequency on a given winding with respect to its dc resistance.

The modelling of ac resistance for wound components is a complex issue about which many papers have been written [43, 44, 45, 46, 47, 48, 49, 50, 51]. A brief summary of the work covered in these papers will now be provided.

The most commonly referred to method for calculating ac resistance is [43] by Dowell. This model is a 1-dimensional analysis which represents each layer of conductors within a winding as a rectangular foil. The equations required to calculate the ac resistance factor are presented here as equations (2.9) - (2.12). By assuming that the conductors are rectangular, and approximating a full layer of the winding as a single conductor, this model introduces error into the calculation of losses. Additionally, as it is a 1D model, the difference in losses along the winding window is not included. Furthermore, there is not a capacity in this model to consider the effect of an air gap within the magnetic path, limiting its usefulness in the design of inductors which include this.

$$F_R = M' + \frac{(m^2 - 1)D'}{3} \tag{2.9}$$

$$M' = real(\alpha h \coth \alpha h) \tag{2.10}$$

$$D' = real\left(2\alpha h \tanh\frac{\alpha h}{2}\right) \tag{2.11}$$

$$\alpha = \sqrt{\frac{j2\pi f \mu_0 N_l a}{\rho_c\, b}} \tag{2.12}$$

Where:

m is the number of whole layers within a winding portion
h is the height of the conductor (m)
N_l is the number of turns per layer
a is the width of the conductor (m)
b is the total winding width (m)

Addressing the assumption that the conductors are rectangular in shape is performed by Ferreira in [44]. This approach uses Dowell's work as a starting point but employs Bessel functions to account for the shape of a round conductor, yielding a solution which is more accurate for round conductors but is more complex to implement.

In some winding configurations, there is a considerable difference between the losses at the centre and at the ends of a winding. To represent this it is necessary for the model to be formulated in two dimensions [45, 46]. In both of these instances reference is given to high frequencies and foil windings since this is the scenario in which edge effects are the most pronounced.

As has been discussed previously, the inclusion of an air gap can have significant influence on the current distribution within the windings. Several methods of modelling this analytically can be found in literature [47, 48, 49]. The method in [47] uses the equivalent foil conductor assumption seen previously, whereas [48] uses circular conductors and [49] uses individual rectangular conductors. Consequently, the most suitable model will depend upon the windings being used. Due to the nature of the fringing field all three of these models are formulated as 2D models.

As the level of detail required from the model increases, so does the complexity of the model. As a result, some models can become unwieldy quite quickly; in these instances it may be advantageous to model the component using FEA. Using this method allows the designer to draw the component as accurately as required and can potentially reduce the number of assumptions being made. Care should be taken to ensure that areas being affected by eddy currents are meshed in a sufficiently fine way so as to capture the details at the frequency of interest. In some instances, this results in a model which contains a large number of elements and therefore takes a long time to solve. These longer solve times potentially limit the number of potential designs which can be considered during the design process, restricting its use for optimisation purposes.

Another approach to calculating the losses in round conductors is proposed in [50]. This approach is a hybrid, based around the use of a lookup table, populated by running simple FEA simulations. By using this approach, it is possible to use FEA as a basis for the calculation of losses without having to accept the time penalty usually associated with the use of FEA to solve the whole model. This approach is shown to give more accurate results than ordinary analytical models across a wide range of frequencies.

The work outlined previously is designed for use with single conductors; the losses in litz wire conductors are considered in [51]. In this instance, both an approximate and a rigorous solution are discussed, the rigorous solution being more complex but also having a wider range of frequencies for which it is valid.

2.2.10 Termination of aluminium windings

A point which requires discussion when considering the use of aluminium conductors is the termination of the windings. This requires consideration since poorly terminated aluminium joints are more prone to exhibiting higher contact resistance than their copper counterparts. In aluminium-to-aluminium joints this can be attributed to the thin layer of aluminium oxide which forms naturally on the surface of the material when exposed to air. This layer behaves as an insulator and reduces the amount of conducting surface area within the joint, yielding a higher contact resistance than if the oxide was not present. This higher resistance in turn leads to increased heating in the joint and potentially, joint failure. In the case of joints made from dissimilar metals, such as aluminium and copper, a further issue is galvanic corrosion, which can also lead to joint failure due to corrosion. For aluminium to be a practical conductor material it is necessary to mitigate these issues. In literature, studies have been conducted into this and a variety of methods for mitigating / reducing the impact of these issues have been proposed.

To deal with the aluminium oxide surface layer several strategies have been suggested. Depending on the scenario it may be desirable to combine several of these techniques together to achieve the maximum benefit. The first consideration is the preparation of the joint surface. It is important to ensure that the joint surface is clean, after which the surface of the conductor can be mechanically abraded to remove the oxide layer from it. To inhibit the re-oxidisation of the surface, anticorrosion grease can also be applied [52]. The choice of connector is another important factor; connectors designed specifically for aluminium should be used. An important characteristic of such a connector is the amount of sheer stress which the connector imparts to the surface of the conductors during assembly; this should be sufficient to shear the surface oxide layer [53]. An illustration of the importance of this requirement is presented in [54], where insufficient shearing of the oxide layer results in failure and overheating of pigtail splices despite the inclusion of a corrosion inhibiting compound within the connector.

An alternative to using connectors is to utilise solder as a joint medium [52]. However, to achieve reliable connections it is necessary to employ solders specifically formulated for aluminium, in combination with a flux that can break down the oxide since without this, poor joint quality is likely.

A further potential solution is to create the joint using some form of welding. In the case of welding dissimilar metals, it is important that the process is tightly controlled, because increasing the temperature of the joint beyond what is necessary will result in the formation of excessive quantities of intermetallic compounds within the joint and will therefore produce a brittle joint [55]. Types of welding which may be appropriate include laser welding [55], ultrasonic welding [56] and friction welding [57]. It is worth noting that for the case of joining copper to aluminium it may be desirable to select a different filler material from the base materials as aluminium/copper joints possess poor mechanical properties due to the presence of the intermetallic compounds mentioned previously.

The use of an alternative interface material is not limited to welding; it can also be used to combat galvanic corrosion. This can be achieved by using a lug or connecter made from an appropriate interface material, or by plating one or both of the wires with the desired interface material. Several papers have been written to evaluate the suitability of various plating materials for this purpose, considering a range of different metals and thicknesses [58] [59] [60]. From these papers it can be concluded that the best choice of plating material is nickel, as it has been shown to outperform both tin and bare copper when connecting to aluminium. Although tin is a popular choice for this purpose it has also been shown that it can be very susceptible to fretting. This occurs when the two contacting surfaces rub together, causing abrasion; the debris produced from this is trapped within the joint and oxidises, resulting in an increase in joint resistance. It has been shown in [60] that nickel is less susceptible to this, producing a longer lasting, more stable joint over its lifetime.

2.2.11 Magnetically limited designs

In a magnetically limited component, the property which prevents the component being operated at a higher current is the magnetic saturation of the core. Control of the core flux density can be achieved by adjusting the size of any air gaps which are placed within the magnetic path (as a larger gap will increase the reluctance of the magnetic circuit), thus reducing the magnetic flux. Equations which facilitate the calculation of the flux density and inductance of a component are listed as equations (2.13) - (2.16). When designing an inductor which is magnetically limited, for a given core, it is necessary to select the required air lap length and number of turns which will achieve the desired inductance, while keeping the value of B below its saturation level.

$$B = \frac{\phi}{A} \tag{2.13}$$

$$\phi = \frac{NI}{S} \tag{2.14}$$

$$L = \frac{N^2}{S} \tag{2.15}$$

$$S = \frac{l}{\mu_0 \mu_r A} \tag{2.16}$$

Where:

B	is flux density (T)
Φ	is flux (Wb)
A	is the cross sectional area of the magnetic circuit (m^2)
N	is the number of turns within the winding
I	is the current flowing within the winding (A)
S	is the reluctance of the magnetic circuit (H^{-1})
l	is the length of the magnetic circuit (m)
μ_0	is the permeability of free space ($4\pi x10^{-7}$) (H/m)
μ_r	is the relative permeability of the magnetic path material

A technique for achieving this is outlined in [61] using equations (2.17) and (2.18). This technique assumes that the reluctance of the circuit is entirely determined by the reluctance of the air gap. This is usually a reasonable assumption since the core is manufactured from a high permeability material and therefore will have a low reluctance compared to that of the air gap. This method accounts for fringing flux at the air gap by using the parameter A_g, this parameter being determined by adding the length of the air gap to each dimension of the core leg as demonstrated in equation (2.19). If it is necessary to more accurately determine the inductance, it is possible to include the effects of the core reluctance on the component by considering the total reluctance of the magnetic circuit. This can be determined from the sum of all of the reluctances in the magnetic circuit; the resultant equation for this is shown as equation

(2.21). This approach allows the design of an inductor which has the required inductance while ensuring that the flux density does not exceed the maximum saturation level.

$$N = \frac{LI}{BA_m} \tag{2.17}$$

$$l_g = \frac{\mu_0 N^2 A_g}{L} \tag{2.18}$$

$$A_{gECore} = \left(a + l_g\right)\left(b + l_g\right) \tag{2.19}$$

$$S = S_{Core} + S_{airGap} \tag{2.20}$$

$$l_g = \mu_0 \left(\frac{N^2}{L} - \frac{l_m}{\mu_0 \mu_r A_m} \right) A_g \tag{2.21}$$

Where:

l_g	is the length of the air gap (m)
A_g	is the equivalent cross sectional area of the air gap, accounting for fringing (m^2)
A_{gECore}	is the equivalent cross sectional area of the air gap in an E-core (m^2)
a,b	are the dimensions of the centre leg of an E-core (m)
S_{Core}	is the core reluctance (H^{-1})
S_{airGap}	is the air gap reluctance (H^{-1})
l_m	is the length of the magnetic circuit (m)
A_m	is the cross sectional area of the magnetic circuit (m^2)

2.3 Thermal Considerations

When designing passive components it is desirable to produce the smallest component possible for a given application in order to achieve the best possible power density. As the size of the component is reduced, the designer is left with the challenge of extracting the dissipated power from a smaller surface area. Furthermore, it is a distinct possibility that in making the component smaller, the losses will be increased (due to the potential reduction in wire size which can be accommodated within the reduced footprint). Consequently the design of a power dense inductor cannot be performed solely within the magnetic domain, it is necessary to also consider the thermal performance of the component.

2.3.1 Heat Transfer Mechanism

To accurately consider the thermal performance of a component, it is important to consider the mechanisms by which heat is transferred [62]. These mechanisms are:

- Conduction

- Convection
- Radiation

To thermally model a component it is potentially helpful to be able to visualise the movement of heat through a component using an electrical circuit analogy. To do this the thermal parameters of the system must be given meaning in the electrical domain; the thermal/electrical equivalent properties used to achieve this are shown in Table 2.5.

Thermal Property	**Electrical Analogy**
Temperature	Voltage
Power	Current
Thermal Resistance	Electrical Resistance
Thermal Capacitance	Capacitance

Table 2.5 - Thermal/electrical analogous properties

To illustrate this, the circuit diagram shown in Figure 2.19 is used. This represents a component which is dissipating power and is mounted to a heat sink. Using this example the peak temperature of the component and the heat sink temperature can both be determined by calculating the 'voltage' at the relevant nodes. The inclusion of capacitors allows the transient response of the system to be considered. The example shown here is a particularly simple case, in a more complex case there may be more than one component mounted to the heatsink. It may be desirable to consider multiple temperatures at different points within the same component, or have the capacity to include multiple sources of loss (core, windings). This can be achieved by dividing the component into multiple elements, each represented by suitable electrical components. Doing so permits the temperature to be predicted for each node within the circuit. Additionally, losses can be applied to the nodes individually, more accurately representing the location within the component at which they are generated. This technique is known as lumped parameter modelling and will be discussed in greater detail later in this chapter.

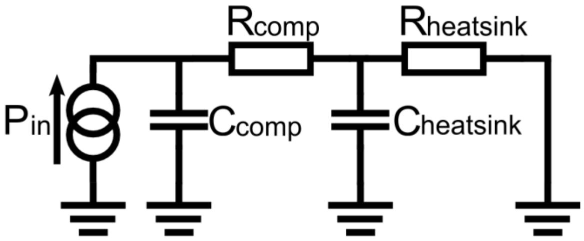

Figure 2.19 - Example circuit diagram

2.3.2 Heat Extraction Methods

As has already been stated, the drive towards increased power densities in power electronics leads to a reduction in component size. Consequently the available surface area for power dissipation into the environment is reduced. If nothing is done to address this, these smaller devices will have higher operating temperatures than their larger counterparts. This is undesirable since operating a device at elevated temperature increase its chances of failure [63]. To combat this, techniques must be employed to improve the transfer of heat from the component to the external environment. Mechanisms for extracting heat from components can be divided into four major categories: natural air cooling, forced air cooling, liquid cooling and phase change cooling.

2.3.2.1 Natural Cooling

'Natural cooling' is cooling which occurs when a component is in air; its primary dissipation mechanisms are convection and radiation [62]. The amount of power dissipated through these mechanisms is proportional to the available surface area. As a consequence of this a common way to improve cooling in naturally cooled systems is the application of a finned heat sink. The fins increase the available surface area, resulting in an increase in allowable power dissipation for a given temperature rise. Heat sinks designed to work under natural convection conditions must have a reasonable spacing between the fins because inadequate spacing will result in the effectiveness of the fins being reduced. Snelling [64] states that as a rule of thumb if there is a clearance of less than 3mm between two surfaces it can be assumed that natural convection doesn't occur within the space between the surfaces. A further issue which requires consideration when using a heat sink is how the device will be mounted to it. In some applications it is appropriate to simply apply pressure between the heat sink and device; however, if the interface between the two materials is not totally flat, pockets of air will be trapped in the gaps between them. This is undesirable as trapped air has a very low thermal conductivity (0.026 W/m.K [8]). To address this, it is not unusual for a thermal interface material (TIM) to be used to fill the gaps. Possible TIMs include thermal grease, liquid metal alloys, gels, soft metal alloys and epoxies [65]. A more detailed look at these interface materials will be provide in the next section of this chapter.

Figure 2.20 – Heat sink designed to be cooled by natural convection

2.3.2.2 Forced Air Cooling

Forced air cooling offers improvements over natural cooling by employing a mechanism (such as a fan) to make the air move around the device at a faster rate than it would normally move due to natural convection. This increases the rate at which the heat can be removed from a device through convection. In this configuration the amount of power which can be dissipated is proportional to the velocity of the air. As with natural cooling it is possible to increase the effects of the cooling by increasing the surface area by utilising a heat sink. Careful design of the heat sink can lead to a considerable increase in the amount of power which can be removed from the device through this method when compared to natural cooling [66].

2.3.2.3 Liquid Cooling

Liquid cooling can extract far more power from a device than air cooling owing to liquid's higher heat transfer coefficient compared to gases [46]. When using liquid coolants, adequate precautions against fluid leakage must be taken. Further to this, the use of liquid cooling will increase the weight of the system as the weight of the working fluid must be taken into consideration. Liquid cooling can be applied by the designer in a variety of different ways. In some applications it may be appropriate to fully immerse the device to be cooled in the working fluid. However, to do this, the fluid must be nonconductive and must not react chemically with the device. This method is sometimes referred to as direct cooling because the device is in direct contact with the coolant. Examples of the use of this technique include distribution transformers [67], motors [68, 69], and complete converter systems [70].

In some applications it is not desirable for the coolant fluid to be in direct contact with the conducting parts of the component. In these instances the fluid can be pumped through cooling channels either directly integrated into the device or built into a separate heat sink; this is referred to as indirect cooling. Construction in this manner mitigates the issues which may arise from direct contact with the cooling fluid, potentially simplifying the design process. This advantage is potentially offset by the fact that the thermal path between the location of heat generation and the extraction surface is likely to be longer than in the directly cooled case [71, 72, 73].

Also falling into the category of liquid cooling is the use of jet impingement technologies. This technique works by focusing the coolant through a nozzle and spraying it onto the surface to be cooled; owing to the velocity of the jets the coolant forms a thin boundary layer on the cooled surface, improving heat transfer when compared to that seen in the previously described technique. This technique can be used to cool the components directly or indirectly, the advantages of each are the same as explained previously [74, 75].

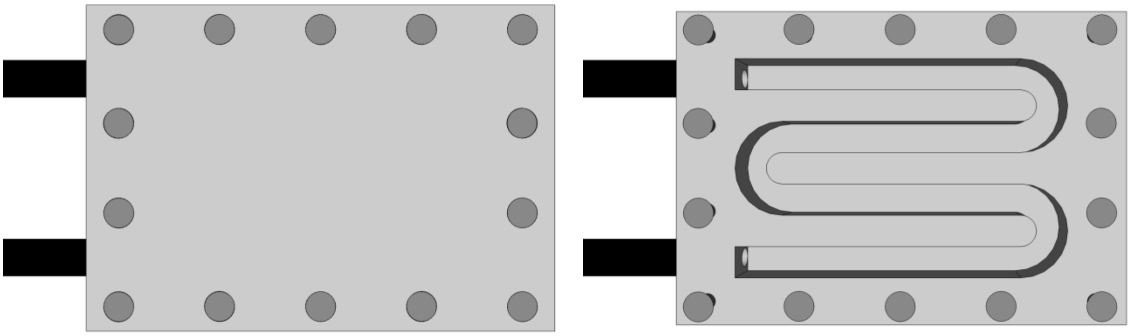

(a) (b)

Figure 2.21 - Example of a liquid cooled heatsink with serpentine channel structure. (a) – assembled structure; (b) – Top removed to expose serpentine channel.

2.3.2.4 Phase Change Cooling

Another mechanism for removing power from a device involves taking advantage of material phase changes. This cooling can be implemented by directly spraying coolant onto the device or can take place in a sealed system. In the case of direct spraying, the coolant is sprayed onto the device through a nozzle which causes the fluid to form a thin film (as is the case with jet impingement). The difference in this technique is that a fluid is used which will boil using the power dissipated in the device, resulting in even higher thermal transfer rates [63, 76]. To utilise this technique it is vital that the working fluid contains no impurities, as any impurities in the fluid will be deposited onto the surface of the device, increasing the surface thermal resistance and reducing the effectiveness of the cooling.

An alternative to spraying the working fluid onto the device is containing it within heat pipes. A heat pipe is a sealed tube which contains the working fluid. When one end of the tube is heated the fluid boils and vapour moves to the other end of the tube. Here energy is extracted from the vapour, causing it to condense back to liquid. Considering this, a heat pipe must also include a mechanism which allows this re-condensed fluid to return to the hot end of the heat pipe. To function correctly the cold end of the heat pipe must incorporate a method of extracting power from the working fluid. If this is not the case it is possible for all the fluid within the pipe to boil simultaneously, reducing the thermal conductivity of the heat pipe substantially (to that of the heat pipe case, usually manufactured from a thin piece of copper) [63, 77]. In this respect heat pipes should actually be considered as a mechanism for transporting heat around a component to a heat extraction surface, not as a means of directly dissipating heat into the environment.

2.3.2.5 Cooling of Passive Components

The above information provides a general overview of cooling; this next section will look at work which has been done specifically in the area of passive magnetic component design.

In the design of magnetic components specifically for automotive applications, the assumption is generally made that the components will be situated within an enclosed area with a relatively high ambient temperature. The cooling technologies which are assumed to be available are dependent on the drive configuration of the vehicle. For example, if the vehicle incorporates an internal combustion engine, it is reasonable to assume that access will be available to the closed loop liquid cooling system. As this system is also employed to cool the engine it must be noted that the coolant within this system is likely to be operating at a relatively high temperature (typically around 85°C) [78]. In other drive configurations, particularly those which employ a fully electric topology, it may be the case the liquid cooling loop is no longer available and so an alternative solution (for example forced air cooling) would have to be found.

To achieve optimal cooling within magnetic components it is important to minimise the temperature gradient between the areas in which the heat is generated within the component and the heat extraction surfaces. This can be achieved through a variety of different techniques, some of which will be explored now.

The first technique is to encapsulate the component using a potting compound; two examples from literature of this technique being used can be found in [79, 80]. In both of these cases the inductor is designed to be cooled using a liquid cooled cold plate, to which the inductor is bolted. To facilitate this, the aluminium box into which the component is potted incorporates mounting holes. The purpose of the encapsulant in these applications is to aid the extraction of heat from the component by providing a low thermal resistance path from the component to the case. It has also been shown in [81] that it is possible to improve the performance of potted components by tailoring the box in which they are to be potted to conform to the shape of the component more tightly. This improves the component performance by reducing the distance between the heat generation source and the heat extraction surfaces. However, this is not without drawbacks since a tailored casing is more complex and expensive to manufacture.

Figure 2.22 - Example of potted inductor

A different approach with a similar rationale is presented in [78]. Here, the inductor is embedded into an aluminium structure which is sufficiently close fitting that it is not necessary to employ an encapsulant. This is made possible in part by the winding structure which is employed within this inductor, which is planar in nature. Consequently, the windings are flat on the upper and lower surfaces, making it possible to easily produce a casing which conforms to the shape. To prevent issues arising from thermal expansion a compressible gap pad material is employed between the casing and core which creates a good thermal contact between these elements and reduces the risk of cracking the core. A further point which is raised in this work is the potential issue arising as a result of placing a conductive material (the aluminium case) in close proximity to the core air gap; in this instance the flux fringing at the air gap intersects the aluminium casing, causing eddy currents to be generated within the casing and leading to increased losses.

Further to designing parts of the casing to aid the transport of heat out of the component, it is also possible to improve the thermal path out of the component by manipulating the design of the component its self. One such example of this can be seen in [82]; in this design the core is divided into several sections perpendicular to the direction of magnetic flux flow as shown in Figure 2.23(b). When the core is assembled a thermally conductive ceramic component is placed between each of the core sections. This design allows highly thermally conductive elements to be incorporated within the structure of the core, providing a low thermal resistance path out of the component. It should be noted however, that as these thermally conductive pieces occupy space which could have otherwise being occupied by core material, the magnetic cross-sectional area of the core is reduced. An important consideration with this type of design is the quality of the interfaces between the core and heat extractors. For this implementation to be effective, a good interface is required so as not to inhibit the conduction of heat into the heat extractors.

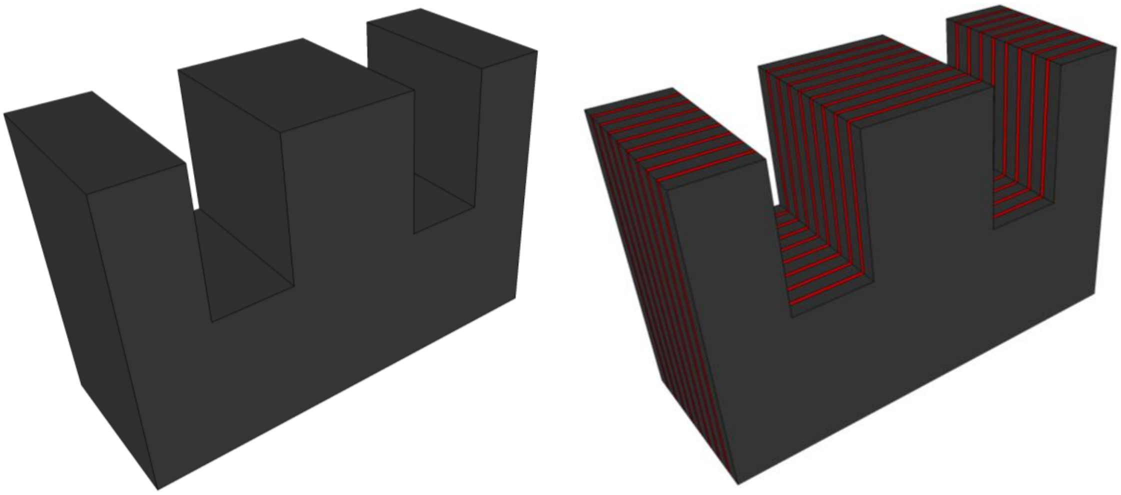
(a) (b)

Figure 2.23 – (a) – standard magnetic core; (b) – magnetic core with integrated heat extractors

2.3.3 Thermal Interfaces

An issue which requires consideration when manufacturing a component from multiple elements is the thermal contact resistance between the associated elements of the system. This is important because surfaces which appear perceivably flat and smooth are in fact, on the micron scale, not flat at all. Consequently, if two imperfect surfaces are placed together, the contact area will be considerably less than would be expected because contact only occurs in places where the peaks on the surface correspond to each other. This phenomenon is illustrated in Figure 2.24, where the contact points are highlighted by red circles. The level to which this is a problem relates to properties of the materials in contact with each other, particularly the material hardness, as this will affect the ability for the surfaces to deform and contour to each other. In places where contact does not occur, heat must conduct or be radiated across the trapped air pocket; this is a far less effective means of transfer than that exhibited by the material contact points.

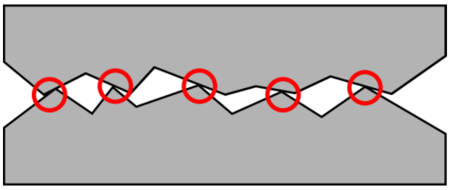

Figure 2.24 - Illustration of interaction between two uneven surfaces (exaggerated for clarity)

While it is not generally possible to eliminate the effects of thermal contact resistance there are several approaches which can be implemented to reduce it. Firstly, the surfaces can be abraded to reduce the surface roughness. Achieving a very highly polished finish on a surface can be time consuming and results in a surface which must be handled very carefully to prevent it becoming scratched. Another approach is to apply pressure to the joint. In [83] the thermal contact conductance for an assortment of different materials, at a range of different contact pressures is presented. This data demonstrates that generally speaking, the thermal joint conductance increases with respect to applied pressure.

A further option which can be employed to improve thermal contact resistance is the introduction of a filler material into the joint between the two surfaces. This approach improves the contact resistance by displacing the air which would be trapped within the gaps between the two materials and replacing it with a more thermally conductive material. For this purpose a wide variety of materials can be used, the choice of which will be determined by factors such as practicality of assembly, level of desired improvement and cost. An additional practical consideration is whether the filler should also perform as an adhesive to hold the two surfaces together; if this is not desirable it is necessary to supply an alternative mechanism for holding the surfaces together.

Technique	Thermal Conductivity (W/m.K)	Adhesive
Thermal Grease	0.5 – 2.9	No
Thermal Epoxy	0.8 – 1.4	Yes
Metallic Foil	35.0 – 384	No
Gap pads	0.8 – 5.0	No
Solder	17 – 78	Yes
Silver sintering	150 – 200	Yes

Table 2.6 - Comparison of mounting techniques (Data from [84, 85, 83, 86, 87, 88])

2.3.3.1 Thermal Grease/Epoxy

One such material available for this purpose is thermal grease. Thermal greases fall into two categories; filled and unfilled. Unfilled grease is produced entirely from the grease material and exhibits a thermal conductivity higher than that of the air it is designed to displace. Filled grease is produced by combining grease with a filler material which exhibits thermal conductivity in excess of that of the grease. The addition of this filler material enhances the thermal conductivity of the grease, improving its performance as an interface material. If it is desirable for the interface material to also provide an adhesive property, it is possible to employ a thermally conductive epoxy in place of the grease. This option provides a more permanent mounting solution and potentially dispenses with the requirement of thermal grease to employ some external holding force to keep the component in place.

2.3.3.2 Metallic Foil/Gap Pads

An alternative to utilising greases is the use of a thin soft foil material. It has been shown in [83] that selection of a foil of suitable thickness is important as it impacts on the resultant joint resistance. The data presented in this paper does not specify how to select the optimal foil thickness; it is logical to conclude however that this thickness will be directly related to the level of surface roughness present at the interface. Optimally speaking, the foil used needs to be sufficiently thick to fill the gaps within the joint, but no thicker, as excess thickness will cause the surfaces of the joint to be pushed further apart, increasing the conduction distance. This study also includes the effect of joint pressure, showing that increasing the joint pressure consistently improves the thermal quality of the joint regardless of which foil material is employed. This approach also potentially offers the advantage that it is cleaner to use than thermal greases (as the gap material is supplied as a single piece and does not need to be applied in the same manner as greases). An alternative to foils are gap pads; these are designed to be inserted into the gap between two components in much the same way as a foil. However, one key difference between them and a foil is electrical conductivity, since gap pads are commonly manufactured from electrically insulating materials and so are suitable for applications in which the component should be electrically isolated from the heat sink. Moreover, it should be noted that gap pads exhibit a lower thermal conductivity than their foil counterparts and are generally thicker. While this increased thickness will contribute to a higher thermal joint resistance it can also be used when producing assemblies from different materials in order to accommodate for expansion between the parts [30].

2.3.3.3 Solder

If electrical isolation is not a concern, (or is undesirable) it may be possible to mount the component using solder. Solder is a potentially attractive choice owing to its relatively high thermal conductivity (compared to thermal grease); additionally it also performs in an adhesive capacity. In the case of a mass produced product which employs reflow techniques to mount components, it may also be possible to perform the soldering as part of the same process, removing the need to implement an additional assembly step during construction. It is important to note however, that for this technique to be viable the solder must be able to wet to both surfaces. If this is not the case, the component will not be attached properly and poor joint performance will result. It may be possible to apply a solderable contact to the base of a component to facilitate soldering, as demonstrated in [89]. Here, a titanium gold contact is applied to the base of a ferrite core. In this instance the joint exhibits a comparable performance to a joint manufactured using thermal epoxy. This is a surprising result as the solder possesses a much higher thermal conductivity than that of the epoxy. It does however highlight an important issue which arises when soldering large area components, that being the entrapment of air beneath the component within the solder layer. It is necessary to take precautions against this when producing such a joint, for example, by performing the soldering operation in a reduced pressure environment, as this would aid the trapped air in escaping [90].

2.3.3.4 Silver Sintering

A further technique for producing thermal connections is the use of silver sintering. This process employs a silver based sintering compound which is applied between the component and mounting surface. A joint is formed by the application of pressure and heat to this assembly; sintering the material and producing a joint. As with soldering it is necessary to have a metal contact on both of the joint surfaces to produce the joint [91]. To achieve the optimal joint it is necessary to fine tune the sintering process by adjusting the pressure, temperature, sintering time and atmosphere. It is possible that one or more of these parameters will be limited by the components being joined and any profile which is devised must be sympathetic to this. Considering maximum operating temperatures, sintering potentially possesses an advantage when compared to soldering in that to produce a soldered joint it is necessary to heat the solder to a temperature high enough to melt it which is not the case with sintering. Therefore, if the device is capable of it, it is possible to use a sintered joint at temperatures higher than the sintering temperature. The same is not true with a soldered joint, as raising the temperature above soldering temperature will melt the joint [92].

Within this thesis, the major point at which thermal interface resistance is an issue is during the construction of the aluminium oxide insulated planar inductor considered in chapter 4; here a filled thermal grease is employed between the planar layers to improve the heat transfer between the layers of the inductor. This was selected as it was necessary for the interface to be as thin as possible, be an insulator and be non-adhesive, making this the best choice of material.

2.3.4 Thermal Modelling

In this section methods of thermally analysing components will be presented and discussed. These methods can be divided into two broad categories:

- Lumped parameter modelling
- Numerical Modelling (Finite Element Analysis (FEA) / Computational Fluid Dynamics (CFD))

2.3.4.1 Lumped Parameter Modelling

Lumped parameter models are produced by representing the thermal paths within a component as an electrical circuit. The components within the lumped parameter model can be sized using:

- the geometry of the component and material properties;
- finite element models;
- experimental results (empirically).

The advantage of lumped parameter models is that, compared to numerical models, they are relatively simple to solve and consequently can be solved in real-time, facilitating their use in a monitoring or control environment. Examples of this have been shown in literature previously [93, 94].

When devising a lumped parameter model, the system can be divided up into multiple parts allowing the temperature to be calculated at multiple points within the component. This is done by ensuring that there is a node within the model which represents the position of interest. This allows the required detail to be obtained from the model whist still being simple enough to be evaluated in real time. A simple lumped parameter model has been shown by way of demonstration previously in Figure 2.19 (section 2.3.1).

Several different resistor based, lumped parameter, thermal network models have been proposed in literature [10, 79, 95, 96, 97]. The amount of detail in each model differs, as does the method in which the resistances were determined.

In [10] a simple network involving only three resistors is used; this is the simplest model which can be used while still being capable of considering the core and windings separately, calculating a temperature for each. Here, losses are divided into core and winding losses, allowing them to be modelled individually and applied to the appropriate components within the model. The method used to determine the resistance values in this case is not specified. Since this model does not contain any capacitors, it can only be used to model the component at steady state and not for analysis of the transient response of the component because the lack of capacitors in the model prevents the incorporation of time constants into the system.

In [95] the model divides the component into several blocks and models the thermal resistances of each section. In this case the thermal resistances are calculated based on the geometry of the device; once again this approach does not include any consideration for transients. However, as the component is subdivided into several sections, more detailed predictions about the component at steady state can be obtained.

In [79, 96, 97] thermal conduction is modelled between every constituent part in the component. This allows significantly more information about temperature distribution within the component to be obtained from this model than those discussed previously. Additionally, capacitances are included for each node allowing the transient response of the component to be considered. In this case, the resistance values are determined based on a 2D FEA model of the device, while the capacitances are determined based on the geometry of the component using their respective volumes and heat capacities.

Another approach to generating a lumped parameter model is to divide the component into a range of primitive elements such as cuboids and arc segments [98, 99]. This approach potentially allows a lumped parameter model to be constructed which includes detail in a similar manner to FEA, but does not have the large overheads associated with it. Part of the speed obtained through using these models comes from the fact that areas of complex geometry, such as the windings, are not represented on a strand level as would be the case in FEA, but are instead represented by a bulk thermal conductivity for the region which allows the model to be constructed using far fewer nodes than is the case when FEA is used. The acquisition of these bulk parameters is outlined in [98, 15, 100].

2.3.4.2 Numerical Modelling

The use of numerical methods such as CFD and FEA could be considered as an alternative to lumped parameter modelling of a system is. Both of these methods require the production of a computerised representation of the object within the software which is then divided into a mesh of elements. The software then performs calculations on each of these elements to determine the state of the model at each point within the object. The nature of the problem and the desired information to be obtained from the model will determine if it is more appropriate to use CFD, FEA or a combination of the two. CFD is used to model fluid flows and so is useful for the modelling the cooling effect of fluids such as air convection, water cooling or other similar problems. FEA on the other hand, is designed to be used with solid objects, and is therefore better suited to problems such as the modelling of heat conduction within a component. If it is to be used on its own, it is necessary to define boundary conditions to capture the influence of heat flow at surfaces affected by fluid flows. To produce a complete model of a component under operating conditions it is possible to produce a model which incorporates both CFD and FEA, allowing both the component heat distribution and (for example) the airflow around it to be modelled.

Models for this purpose can be produced in either 2D or 3D. A 2D solution will require approximations to be made about the symmetry of the component geometry but will also be less computationally intense to solve. The two most commonly employed topologies for 2D modelling are the planar and axisymmetric configurations. It will generally be the case that a component will be better suited to being modelled by one of these methods than the other; in this case, the selection of the wrong model type can result in considerable errors in the predictions.

3D implementations allow an object to be modelled in more detail using fewer approximations; this is achieved at the expense of a significantly longer processing time. It should be noted that both 2D and 3D implementations are too complex and slow solving to be run in real time for use in applications such as observer based systems.

2.3.5 Thermally limited design

If a design is thermally limited it would be possible to operate it at a higher current level, except for the fact that this would cause the component to run at an excessive temperature. Here the definition of excessive may be set by limitations of the material, but may also be due to a specified maximum temperature for the component. In such a case it may be possible to increase the operating current if one or more of the following are done:

- Improve heat extraction from the component
- Improve heat transfer within the component
- Reduce level of loss within the component

Potential methods of achieving these objectives have already being discussed in this chapter through the design decisions presented to a component designer.

As a basic method of predicting temperature rise within a component it is possible to use the thermal resistance values for the magnetic core which will be specified by the manufacturer. However, this value is only valid if the inductor has been constructed in a conventional manner. If this is not the case, for instance, if the component is encapsulated, the core thermal resistance alone will not yield a good prediction and the component will have to be modelled in more detail using one of the techniques described in section 2.3.4. If the temperature increase predicted by these methods is more than the maximum allowable, it may be necessary to redesign the component to incorporate additional cooling technologies or to utilise a larger core size such that the component will operate at below the desired maximum temperature.

2.4 Conclusions

This chapter has highlighted the wide range of factors which an inductor designer must consider to produce a well-designed inductor. These factors are divided into two broad categories: magnetic and thermal. From the magnetic perspective considerations regarding the core (*e.g.* material; shape) and the windings (*e.g.* material; insulation; topology) were discussed. Regarding thermal aspects, design considerations such as methods of transferring heat from within the component to the environment are discussed. Additionally, other considerations such as device structure and packaging are also considered. Based on these considerations the complexity required to produce the optimal inductor can be clearly seen.

The potential optimisation criteria for an inductor are: power density; efficiency; cost and reliability. Unfortunately it is not possible to produce an inductor which is optimal in all of these categories simultaneously so consequently it is necessary to know which criteria is a priority for the application for which the inductor is being produced.

In the coming chapters, consideration will be given to a variety of potential methods of improving the power density of inductors. This includes considering the use of a lighter winding material to produce the winding (aluminium); utilising winding insulations with improved thermal properties (aluminium oxide) and employing encapsulant composites to improve thermal transfer within the inductor.

Chapter 3

Comparison of ac resistive losses for copper and aluminium conductors

In the previous chapter a range of potential decisions available to inductor designers were discussed. One such consideration was the choice of winding material. On this subject it was concluded that the decision between aluminium and copper windings is a choice which is steered by the overall optimisation objectives for the component. In this chapter, by considering the influence of frequency effects, it is shown that in some configurations aluminium exhibits a lower ac resistance than copper at a range of frequencies. This presents the opportunity to produce windings which retain all of the advantages of aluminium, but have a lower ac resistance than copper.

When manufacturing wound components, the material chosen for the windings is almost always copper. This can be primarily attributed to its high electrical conductivity. The low cost and mass of aluminium, however, could prove advantageous in the development of magnetic components for applications in which these properties are a key concern, such as in the automotive and aerospace industries. Within a power electronic converter system, a large proportion of the weight and size is attributed to the passive components (inductors, capacitors, transformers). Consequently, methods of reducing the size and weight of these components are highly desirable, as they greatly influence the total size and weight of the final system.

The remainder of this chapter is structure in the following way:

- The material properties of copper and aluminium are compared
- The effect of frequency on ac resistance is explored
- The influence of winding topology on ac resistance is considered
- Prototype air-cored and ferrite-cored inductors are produced to allow the winding losses to be compared in a practical manner

3.1 Material Properties

The factors which can be considered when choosing between copper and aluminium as a conductor material have already been highlighted in chapter 2 of this thesis; the literature considered previously generally operates on the assumption that an aluminium conductor will have to be larger than a copper conductor or it will have higher losses. The acceptability of this condition is dependent on the specific application of the component and therefore, the desired optimisation goals. In the case of vehicle / transport applications where an increase in size would generally be considered undesirable, this would appear to make aluminium a poor choice, unless an increase in losses can also be tolerated. Table 3.1 shows the properties of conductor grade copper and aluminium. From this it can be seen that the electrical resistivity of conductor grade copper is 17.2 nΩ.m [101] which is considerably lower than that of aluminium (28.3 nΩ.m [101]). However, if it is necessary to achieve the same dc resistance for 2 comparable windings, the resulting increase in aluminium cross-sectional area still results in a winding which is still over 50% lighter than the copper equivalent, with a considerably cheaper material cost; however, a volume penalty of 64.5% must be accepted. A complete comparison of aluminium windings which match one of the properties of a normalised copper winding are listed in Table 3.2.

	Copper	**Aluminium**
Electrical Resistivity (nΩ.m)	17.2	28.3
Density (kg/m^3)	8920	2700
Cost (\$/kg)	6.0885	1.7055
Cost (\$/m^3)	54,552.96	4,604.85

Table 3.1 - Comparison of conductor grade copper and aluminium properties (Data from [101, 32])

	Copper	**Aluminium (Equal Volume)**	**Aluminium (Equal DC Resistance)**	**Aluminium (Equal Weight)**	**Aluminium (Equal price)**
Cross sectional area	1	1	1.64	3.30	11.85
Resistance	1	1.64	1	0.49	0.138
Weight	1	0.274	0.449	1	3.587
Price	1	0.084	0.138	0.280	1

Table 3.2 - Comparison of aluminium windings to a normalised copper winding

3.2 Effects of operating frequency on wound components

As outlined previously, when a conductor is excited by an ac current, the changing current produces a changing magnetic field, which in turn induces eddy currents within the conductor. In a single conductor in free space, skin effect causes the current within a conductor to be unevenly distributed, with more current flowing closer to the edges of the conductor than in its centre. The equation for calculating the skin depth is restated here as equation (3.1) [8]. Of particular significance in this equation is the fact that conductor resistivity influences skin depth, such that a higher resistivity results in a larger skin depth. This point is important when considering the comparison between aluminium and copper, as due to aluminium's higher resistivity, it also has a higher skin depth at any given frequency. This means that at frequencies where skin effect needs to be normally considered, more of the conductor cross-sectional area will be used to carry current in an aluminium conductor than in a copper conductor of equal diameter, and therefore the ac resistance of aluminium will increase less than copper at a given frequency. The equations used to calculate proximity effect are more complex than that of skin effect and were discussed previously. For the purposes of this explanation it is sufficient to state that proximity effect is also influenced by resistivity in the same manner as skin effect is, that is to say, that the increase in ac resistance due to proximity effect in an aluminium conductor will also be reduced when compared to that of a copper conductor [101].

Due to the fact that skin depth is inversely proportional to the operating frequency, as frequency increases, the maximum conductor size which can be effectively used is reduced, increasing the dc resistance of the conductor. This can be problematic if the inductor current contains a large dc component (as will be discussed later in section 3.4). To address this, it is possible to employ multiple strands in parallel, allowing the dc resistance to be maintained, while still meeting requirements imposed by the frequency effects. In depth consideration of this is beyond the scope of this analysis, but this option is mentioned here for completeness.

This analysis primarily considers the substitution of a copper winding with an aluminium winding of identical geometry. Such a substitution will result in a winding which is lighter than the original copper winding. In some applications, where size is not of primary concern, it may also be possible to employ a larger cross-section aluminium winding, which is still lighter than its copper equivalent. In designs which employ a core this may necessitate the use of a larger core, which will also contribute to the weight of the component. This conclusion results in an optimisation problem which is beyond the scope of the analysis performed here, however in some designs it may be worth considering.

$$\delta = \sqrt{\frac{\rho_c}{\pi \mu f}} \tag{3.1}$$

Where:

δ is the skin depth (m)

ρ_c is the electrical resistivity of the conductor (Ω.m)

μ is the permeability of the conductor (H/m)

f frequency of excitation (Hz)

3.2.1 Characterising the shape of the R_{ac} curve

To illustrate the overall shape of the ac resistance curve for an air cored inductor, the inductor shown in Figure 3.1 was constructed, the specifications of this inductor are listed in Table 3.3. The experimentally obtained ac resistance (R_{ac}) of this inductor measured using a Hioki 3522 LCR meter is shown with respect to frequency in Figure 3.2.

Core Material	Air
Winding Former	40 mm diameter; Circular winding path
Winding Material	Copper
Winding Profile	2.2 mm diameter; Circular wire
Total Number of Turns	30
Number of Winding Layers	6
Winding Turns / Layer	5

Table 3.3 - Specification of inductor shown in Figure 3.1

Figure 3.1 - Sample copper air-cored inductor wound with 2.2 mm diameter wire, 6 layers, 5 turns/layer

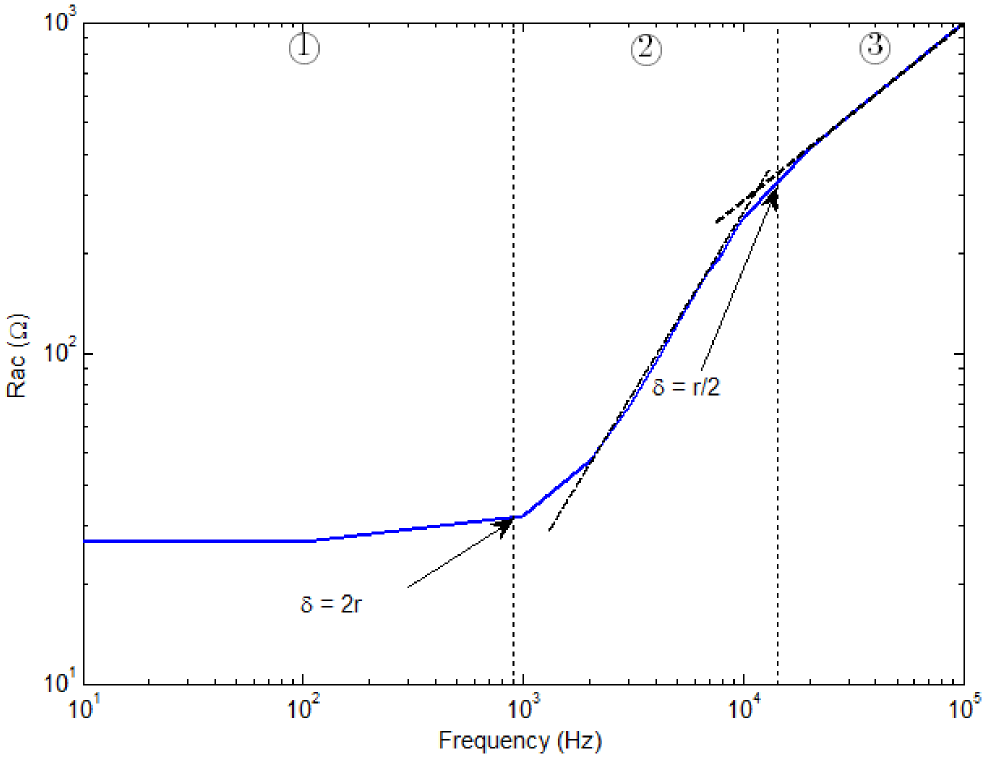

Figure 3.2 – Measured R_{ac} values for sample copper air-cored inductor wound with 2.2 mm diameter wire, 6 layers, 5 turns/layer

The shape of the curve shown in Figure 3.2 can be divided into three distinct regions. Region 1 contains frequencies for which the skin depth is greater than twice the radius (*r*) of the wire used. At these frequencies the effects of eddy currents are small and therefore have little influence on the current distribution within the conductor; in this region frequency effects are minimal and so only a small change in series resistance is observed. In region 2 the conductor is being driven at frequencies such that the skin depth is less than the diameter of the conductor. In this region the current is distributed within the winding in a non-uniform manner, increasing the series resistance of the winding considerably. In region 3 the skin depth is less than half of the conductor radius. Here the series resistance still increases with respect to frequency, however, this increase now occurs at a slower rate than that observed in region 2 as a result of self-shielding effects on the windings [102]. Self-shielding effects occur as a result of the magnetic field generated by the eddy currents; as this field grows in magnitude, it works in opposition to the proximity effect field, resulting in a slower increase in resistance compared to that seen in region 2 [51]. When designing an inductor, it is generally the case that the radius of the wire which is selected for the windings will be smaller than the skin depth at the desired switching frequency. This allows the winding to be operated within either region 1 or the lower half of region 2 where the losses are lower.

An interesting parameter as it pertains to the shape of this curve is the equation which describes the line fitted to the R_{ac} curve within region 2. The equation of this line can be described in the form shown in equation (3.2). With the two curve fitting constants *k* and *a* being calculated using equations (3.3) and (3.4) respectively.

$$R = af^{k} \tag{3.2}$$

$$k = \log_{\frac{f_a}{f_b}}\left(\frac{R_a}{R_b}\right) \tag{3.3}$$

$$a = \frac{R_a}{{f_a}^{k}} \tag{3.4}$$

Where:

R	is the resistance of the inductor at frequency f (Ω)
f	is the frequency being evaluated (Hz)
a	Is the intercept point of the curve of interest
k	Is the slope of the curve of interest
(R_a, f_a)	is a point on the line being described
(R_b, f_b)	is another point on the line being described

3.2.2 Effects of core loss on measured resistance

The method used to determine the resistance and inductance of an inductor is based around the determination of the real and imaginary parts of the measured impedance of the component. Thus far it has been assumed that the real part of this measurement is entirely contributed by the resistance of the windings. In the case of an air cored inductor this is a valid assumption, however if a core is present the losses contributed by the core will also influence this measurement. An equivalent circuit diagram demonstrating this can be observed in Figure 3.3. Unfortunately it is not a simple matter to separate the core losses from the winding losses. Consequently, in cases in which a core is present, the results will have the axis will be labelled ‘real impedance’ rather than winding resistance to reflect this fact. For the measurements being performed here using the Hioki LCR meter, the core losses will be low due to the low excitation current being used. Additionally, as the core losses are proportional to current, and both the aluminium and copper prototypes are tested under the same excitation level, this resistance contributed by the core will not change and therefore, the frequencies for which aluminium exhibits superior performance to copper will not be affected; rather the core resistance will appear as an offset in both measurements, which is constant for a given frequency.

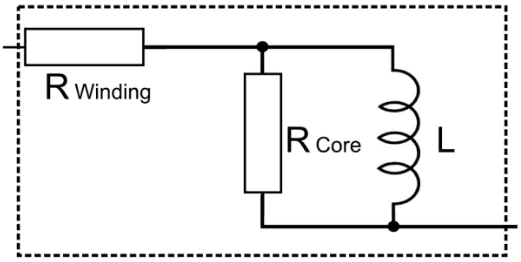

Figure 3.3 – Inductor equivalent circuit

3.3 Comparison of aluminium and copper winding resistance with respect to frequency

As a consequence of the eddy currents, the ratio of the effective resistances between copper and aluminium conductors will not simply be the ratio between the material resistivities. To explore this further the parameter $R_{Al/Cu}$, which is defined as the ac resistance of an aluminium winding divided by the ac resistance of a copper winding arranged in the same topology/winding configuration at a given frequency is considered. Examples which show that $R_{Al/Cu}$ is not a constant value with respect to frequency are presented in literature. One such case is provided in [101]; where an example is given of the value of $R_{Al/Cu}$ approaching unity for some frequencies. Further to this, in [103] cases where aluminium exhibits a lower ac resistance than copper ($R_{Al/Cu} < 1$) are presented; in this case, the behaviour of the samples at higher frequencies are not explored.

This behaviour can be explained by the fact that copper, owing to its higher electrical conductivity, and therefore lower skin depth, enters the area denoted as region 2 in Figure 3.2 at a lower frequency than an equivalent aluminium winding. Consequently, the copper windings exhibit the sharp increase in resistance associated with this region, while the aluminium winding remains in region 1. This causes the resistance values to become closer than would be predicted based on the dc resistance values, reducing the value of $R_{Al/Cu}$.

3.3.1 Scaling of R_{ac} curves

At this point it is also useful to consider how the resistance of a copper conductor compares with that of an aluminium conductor of the same topology. If the values of the R_{ac} curve are known for a copper conductor, it is possible to generate the R_{ac} curve for the equivalent aluminium inductor by scaling the copper values in both the resistance and frequency axes.

If two inductors of the same topology are compared, they will have equal values for R_{ac}/R_{dc} at the point on the curve for which the skin depth is equal; therefore equation

(3.5) must be valid. Rearrangement of this yields equation (3.6) which shows that the scaling factor for the frequency axis is equal to the ratio of the material conductivities. Scaling in the resistance axis can be done by considering the dc case of both of the configurations which means that the scaling factor in the resistance axis is also equal the ratio of the material resistivities.

$$\delta = \sqrt{\frac{\rho_{Cu}}{\pi\mu f_{Cu}}} = \sqrt{\frac{\rho_{Al}}{\pi\mu f_{Al}}} \tag{3.5}$$

$$f_{Al} = \frac{\rho_{Al}}{\rho_{Cu}} f_{Cu} \tag{3.6}$$

An example of this scaling is presented in Figure 3.4; the specification of the inductor used for this purpose is listed in Table 3.4. Here, the inductor is simulated using both copper and aluminium wire using FEA. Further to this, the scaling method proposed here was implemented on the FEA data for the copper wire. It can be observed from this figure that the scaled results show a good correlation with the FEA results for aluminium, validating this scaling technique.

Core Material	Air
Winding Former	40 mm diameter; Circular winding path
Winding Material	Copper/Aluminium
Winding Profile	1 mm diameter; Circular wire
Number of Winding Layers	4
Winding Turns / Layer	4

Table 3.4 - Specification of simulated inductors used to illustrate scaling shown in Figure 3.4

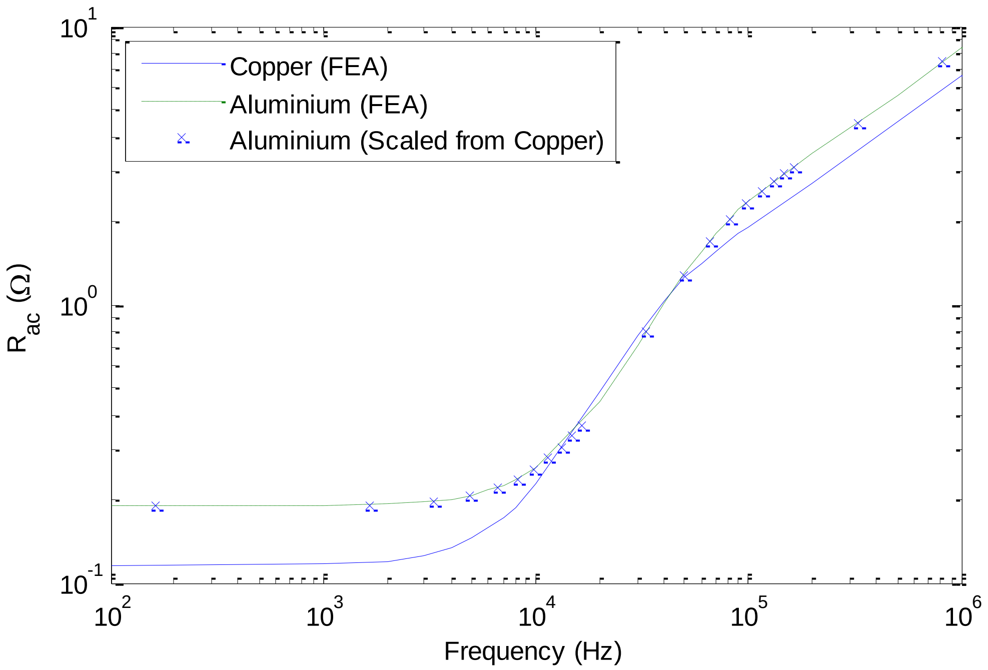

Figure 3.4 - Simulation results validating proposed scaling method

By establishing this relationship between the ac resistance curves for copper and aluminium windings, it is possible to establish the criteria for which aluminium will exhibit lower ac resistance than copper for a range of frequencies. It was determined that in cases in which the value of *k* (the gradient of the curve in region 2) is greater than 1, aluminium will exhibit a lower resistance than copper for a range of frequencies. This finding was verified by performing a wide range of FEA which confirmed that in configurations in which the gradient parameter of the curve in region 2 is greater than 1, aluminium will exhibit lower losses than copper for a range of frequencies.

3.3.2 Effect of number of winding layers on $R_{Al/Cu}$

It is interesting to note that the number of layers in a winding influences the rate at which the ac resistance increases; this is a consequence of the proximity effect. In Figure 3.5 the results of 2D finite element simulations can be seen in which the effect of additional winding layers on frequency related losses are explored. The specification of the inductors used for this simulation are presented in Table 3.5; here the results which are presented are normalised to the dc resistance in each case. From this figure it can be deduced that windings incorporating a higher number of layers will exhibit a lower value for $R_{Al/Cu}$ at some frequencies, even possibly exhibit behaviour where $R_{Al/Cu}$ has a value less than unity, due to the increased gradient of the curve in region 2. This phenomenon is demonstrated in Figure 3.6. In this figure the ac resistance values for copper and aluminium inductors are both considered. Here the data is normalised to that of the dc resistance of the copper winding with the same number of layers. It can be observed that in configurations with a low number of layers the aluminium resistance remains consistently higher than the copper. However, as the number of layers increases, this no longer remains true, and copper exhibits a higher resistance than aluminium over a range of frequencies. This can be attributed to the increased gradient of the resistance curve in region 2, due to the increased impact of proximity effect, as previously explained. Also presented in Figure 3.7 are the $R_{Al/Cu}$ values for the data across the frequency range. The point at which $R_{Al/Cu}$ is equal to unity is highlighted with a bold contour; points which fall within this region are the designs for which the use of aluminium in place of copper would yield a lower ac resistance.

Core Material	Air
Winding Former	40 mm diameter; Circular winding path
Winding Material	Copper/Aluminium
Winding Profile	1 mm diameter; Circular wire
Number of Winding Layers	Various (1 – 10)
Winding Turns / Layer	4

Table 3.5 - Specification of simulated inductors used to generate data shown in Figure 3.5, Figure 3.6 and Figure 3.7

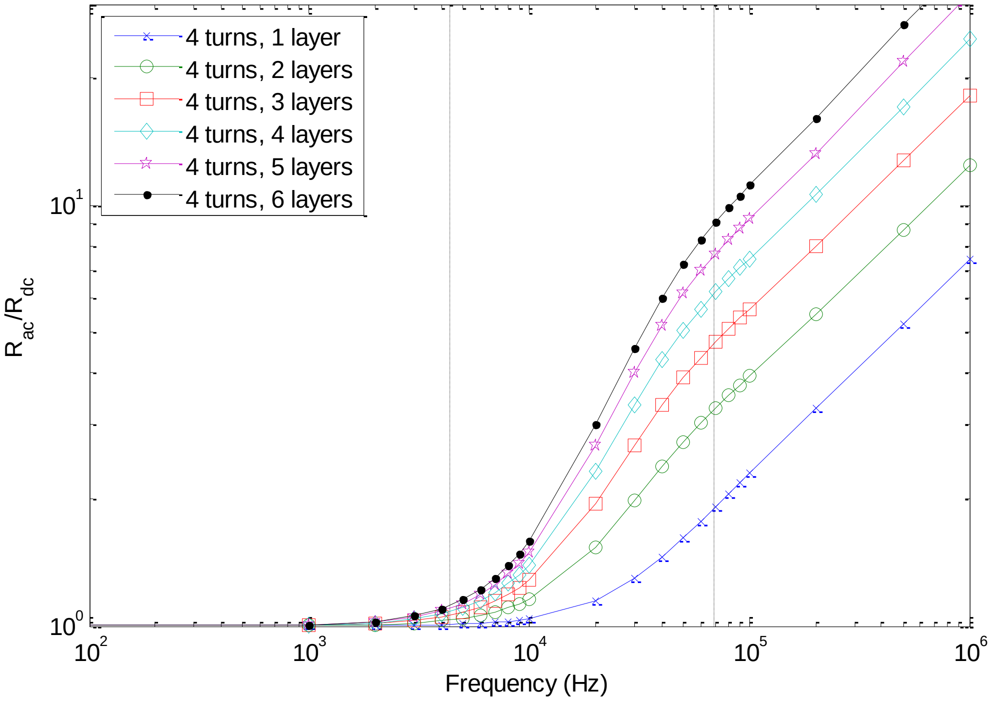

Figure 3.5 – FEA simulations showing the effect of number of layers on R_{ac}/R_{dc} (each layer contains 4 turns) (Results are for copper inductors)

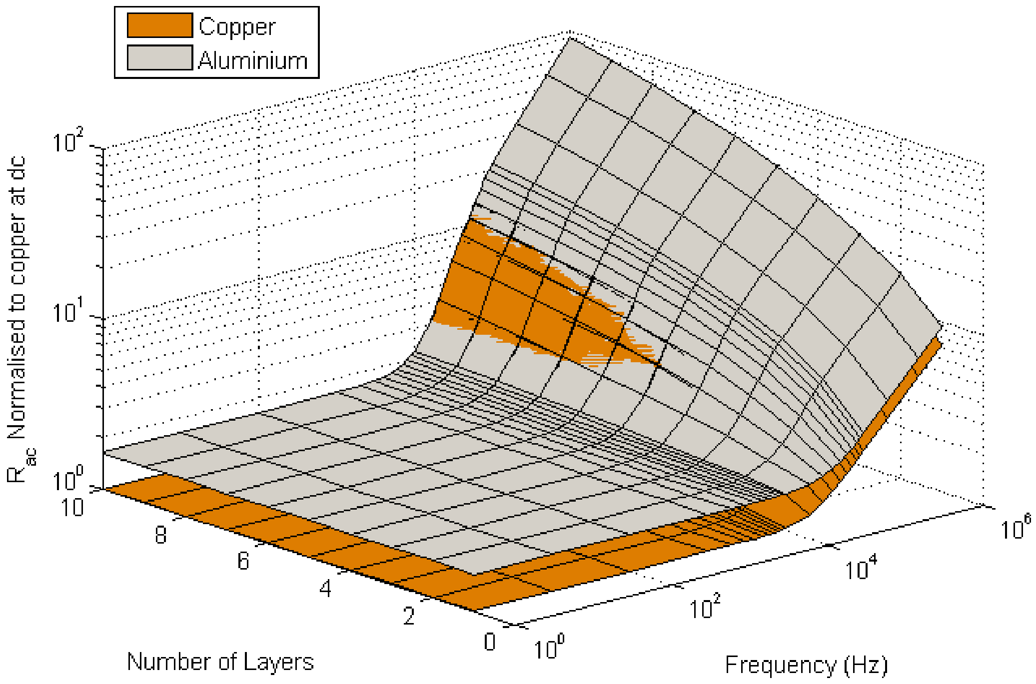

Figure 3.6 – FEA simulations showing the effect of number of layers on R_{ac} in copper and aluminium (each layer contains 4 turns)

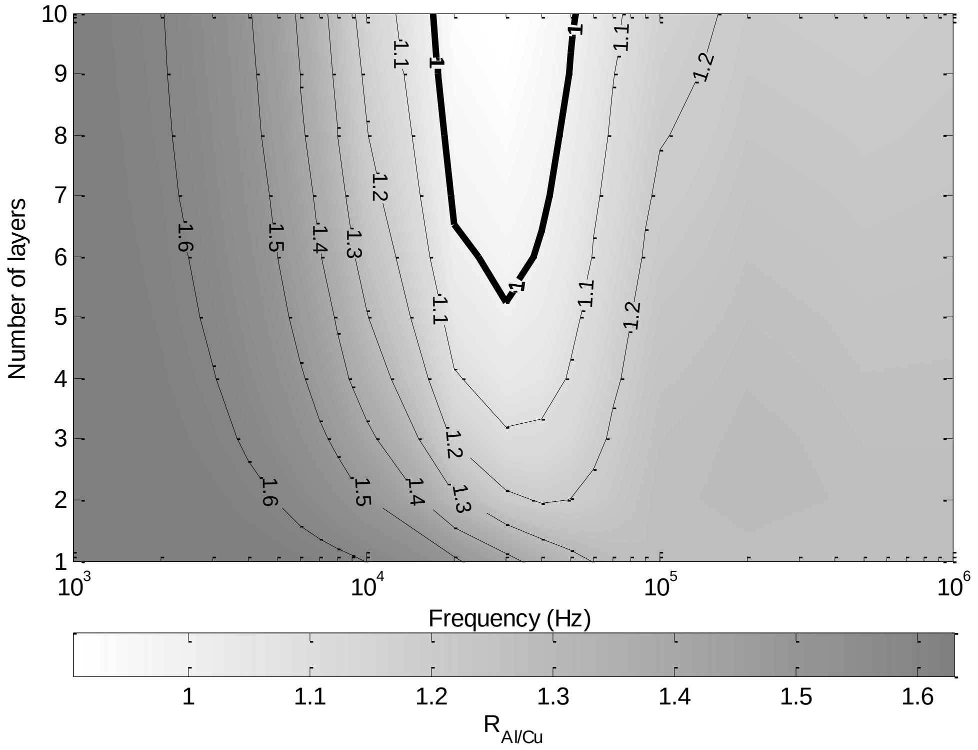

Figure 3.7 - Contour plot showing simulated $R_{Al/Cu}$ Ratios obtained from FEA simulation used in Figure 3.6

3.3.3 Effect of wire diameter on $R_{Al/Cu}$

In addition to the winding configuration, the diameter of the wire used to construct the inductor will also influence the ac resistance and $R_{Al/Cu}$. In Figure 3.8 simulated winding resistance is plotted against frequency and wire diameter for both aluminium and copper conductors. The specification of this inductor is listed in Table 3.6. From this analysis it is found that in this configuration, aluminium exhibits a lower ac resistance than the copper equivalent at some frequencies for each wire diameter considered. To assist this observation, $R_{Al/Cu}$ is shown on a contour plot in Figure 3.9. The points for which $R_{Al/Cu}$ is equal to unity are again highlighted by a thicker black line; points which are enclosed within this area are the operating points for which aluminium exhibits an advantage over copper.

Core Material	Air
Winding Former	20 mm diameter; Circular winding path
Winding Material	Copper/Aluminium
Winding Profile	Various diameters (0.05 mm – 1.5 mm); Circular wire
Number of Turns	36
Number of Winding Layers	6
Winding Turns / Layer	6

Table 3.6 - Specification of simulated inductors used to generate data shown in Figure 3.8 and Figure 3.9

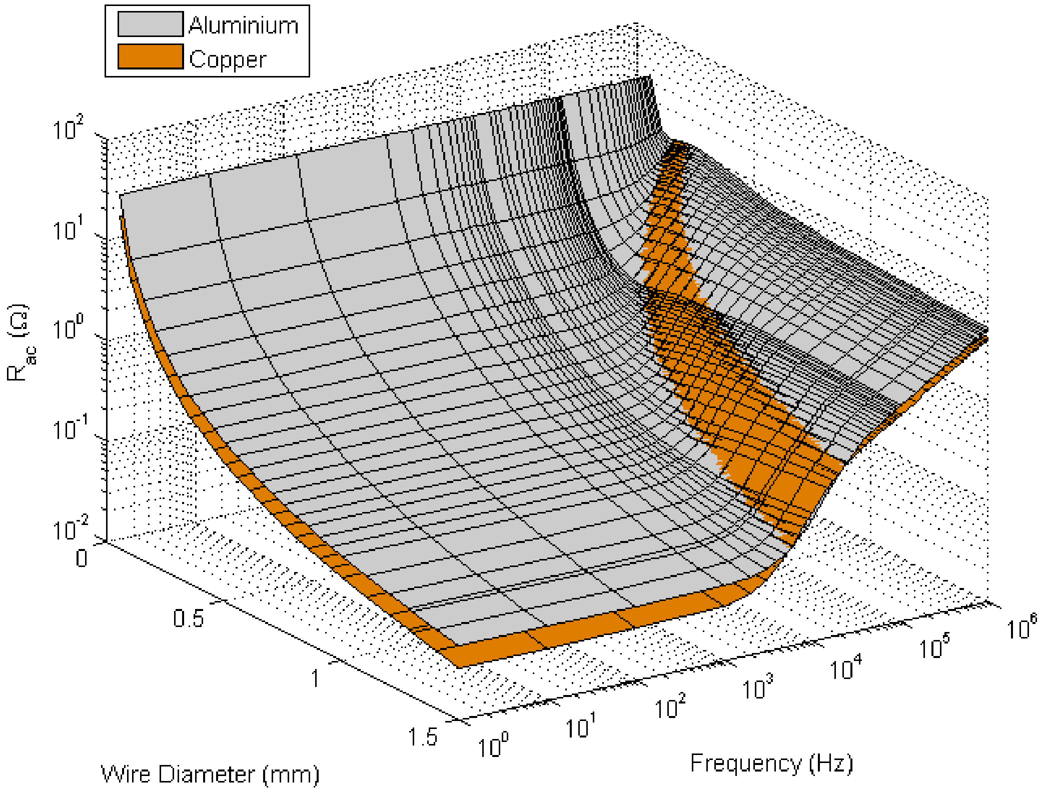

Figure 3.8 - FEA simulated R_{ac} Values for aluminium and copper windings

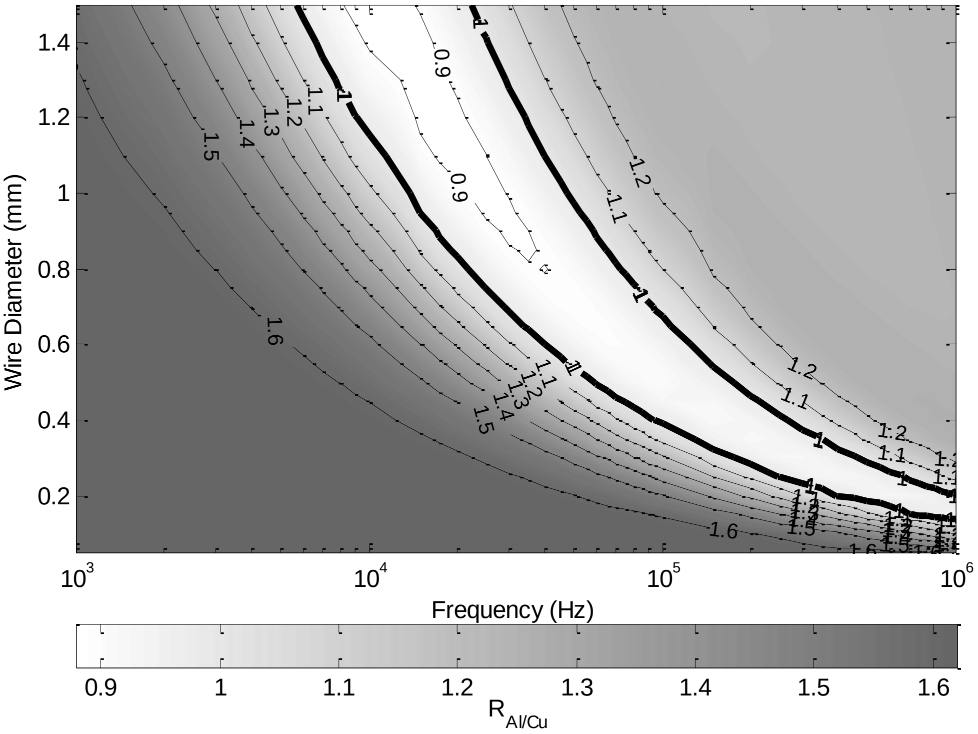

Figure 3.9 – Contour plot showing simulated $R_{Al/Cu}$ Ratios obtained from FEA simulations used in Figure 3.8

Considering the data presented within Figure 3.8, in instances for which a winding is to be excited solely by a single sinusoidal frequency, the lowest loss can be obtained by selecting the configuration which exhibits the lowest resistance at the excitation frequency.

3.4 Effects of signal containing multiple frequencies

Selecting the wire size used to construct an inductor based on the lowest loss at a given frequency will result in the optimum loss solution for components which are excited by a single sinusoidal frequency. However, it is not always the case that the component will be excited in this manner. In other applications the excitation current will contain components other than the fundamental frequency. Consequently, the performance of the winding at these other frequencies must also be considered. To illustrate this point the inductor within the boost converter shown in Figure 3.10(a) is considered. Under normal operation the MOSFET is driven by a pulse width modulation (PWM) signal. By varying the duty cycle of this signal, the output voltage across the resistor is boosted, producing a voltage greater than the input voltage across it. When this circuit is operating in continuous current operating mode, the inductor current is always greater than zero, and is triangular in shape as shown in Figure 3.10(b).

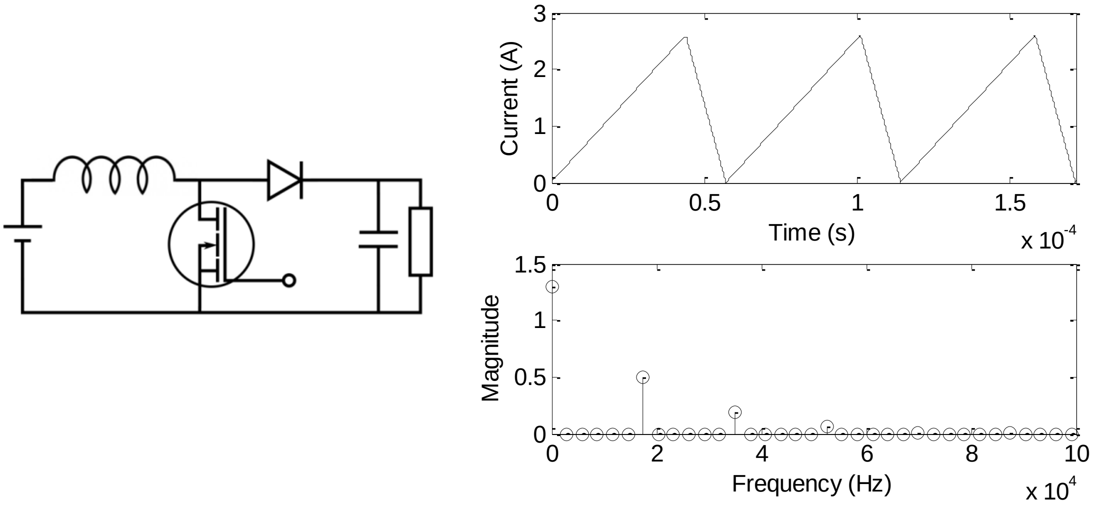

(a) (b)

Figure 3.10 – (a) - Boost converter topology; (b) - Example boost converter inductor current and Fourier transform of signal

In this example, the selected operating frequency is 17.5 kHz. (At this frequency the skin depth in copper is equal to 0.5 mm, which is the radius of the wire used to manufacture our verification prototypes later in this work.) In addition to the simulated waveform of the inductor current, a Fourier transform of the waveform can also be observed in Figure 3.10(b); from this it can be seen that inductor current has considerable dc content. Further to this, multiple harmonics are also present within the signal, due to the current’s triangular shape. The importance of these harmonics cannot be overlooked as they too will contribute to the losses. For simplicity in this analysis only the dc component and the first two harmonics are considered. (As beyond this the influence is diminished sufficiently that it can be omitted without much detriment to the solution obtained.) Combining the harmonic content of the inductor current with the R_{ac} values obtained from FEA it is possible to estimate the winding losses for the inductor at each of the frequencies of interest, and therefore, by addition of these values, determine the total inductor winding losses, a technique demonstrated in [104]. The results of this can be seen in Figure 3.11; the data in this figure was obtained by combining the effective resistances calculated for the inductor discussed in Figure 3.8 with the harmonic currents in Figure 3.10(b), with the results for aluminium wire being presented in Figure 3.11(a) and copper wire being presented in Figure 3.11(b). For ease of comparison the total predicted loss of copper is also included in (a) and the total aluminium loss is included in (b). From this result it can be seen that considerable contributions to the power loss occur at frequencies other than the operating frequency.

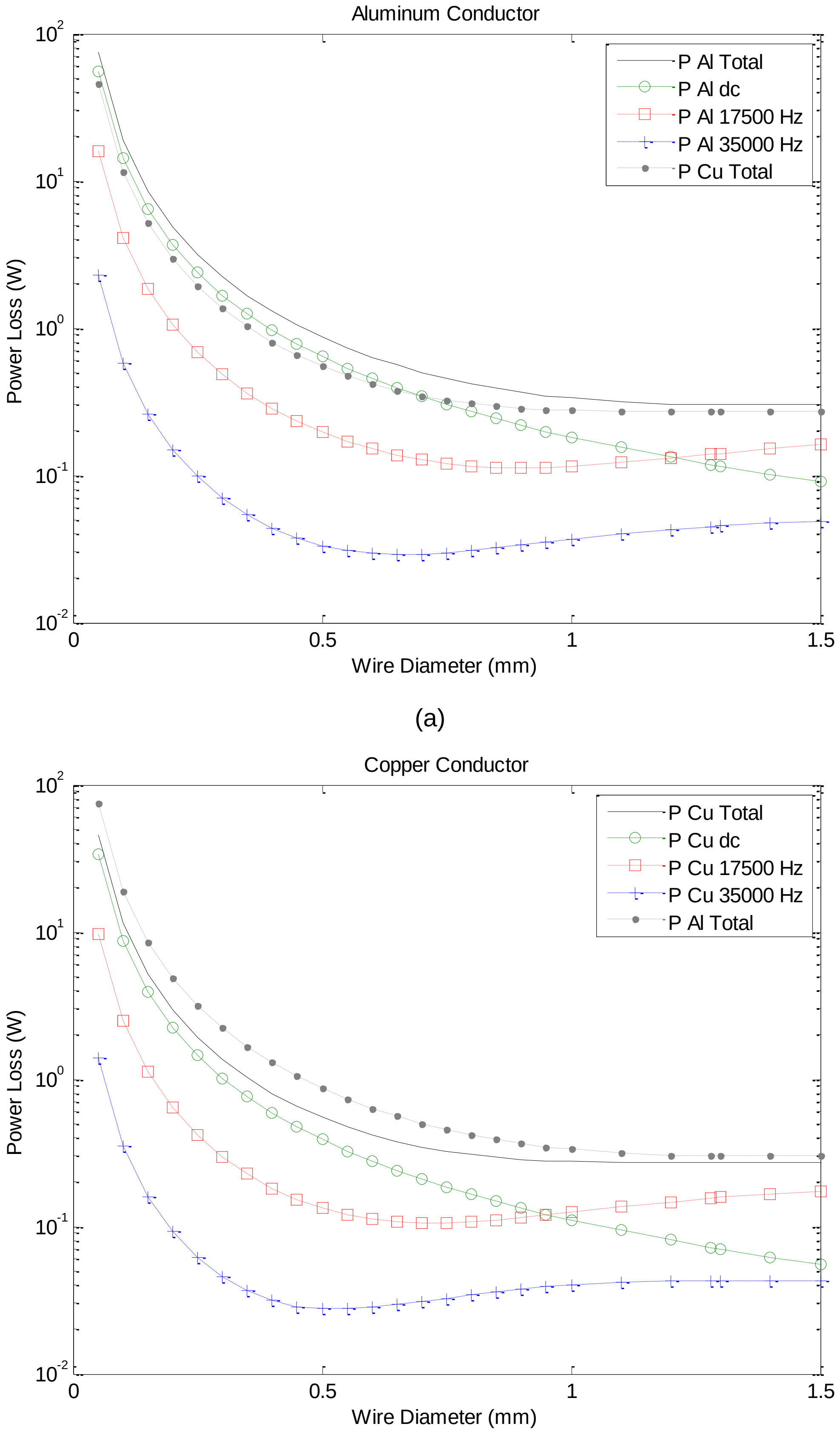

(a)

(b)

Figure 3.11 - Comparison of power loss for different wire diameters. (a) Power losses in aluminium conductors; (b) Power losses in copper conductors

Under this operating condition, owing to the considerable dc content of the signal, there is an advantage to be gained by increasing the wire diameter. However, the wire diameter cannot be increased without limit, as doing so results in increased ac losses, negating the advantage of the larger conductor. As shown in Figure 3.11, for signals which contain significant dc content, aluminium conductors cannot match the loss performance of their copper counterparts; however the aluminium conductors are still considerably lighter and so can be considered as a compromise.

3.5 Effects of conductor cross sectional area on conductor length

It was previously stated that to match the dc resistance of a copper winding an aluminium winding would require a conductor cross sectional area that is 1.645 larger. This is based on the assumption that the conductor length is constant and independent of the cross sectional area of the conductor. This assumption is flawed, as increasing the diameter of a conductor results in an increase to its length; the reason for this will be demonstrated through mathematical analysis. For the purpose of this analysis the case of a winding produced using circular conductors, formed around a circular coil former, such as would be the case in an ETD or ‘pot’ core will be considered. It is possible to derive similar equations for other winding geometries but the conclusions drawn from them would be broadly the same, and consequently this is not included here.

In an inductor containing multiple layers, the turn length of the outer layers is greater than the inner ones because the outer turns have to be wound over the previous layers. Figure 3.12(a) illustrates this by showing a cross-section of an air-cored inductor wound around a circular former shown with rotational symmetry. In Figure 3.12(b) the same inductor can be seen drawn from a top-down perspective, with quarter symmetry; in this view the average conductor length for each layer is denoted by the dotted line situated in the middle of the conductors. From this, the length of a single turn in layer *n* can be calculated using equation (3.7) . By extension, considering the example case of an inductor with six layers, each consisting of six turns, the total winding length can be determined by equation (3.8). From this equation it is clear to see that the radius of the conductor has a direct effect on the total length of the winding. Consequently, increasing the winding cross sectional area by the previously stated factor of 1.645 will not achieve the desired matching of resistance at the dc level. The precise value it must be increased by is determined not only by the conductor size, but also the size of the former and the thickness of the insulation.

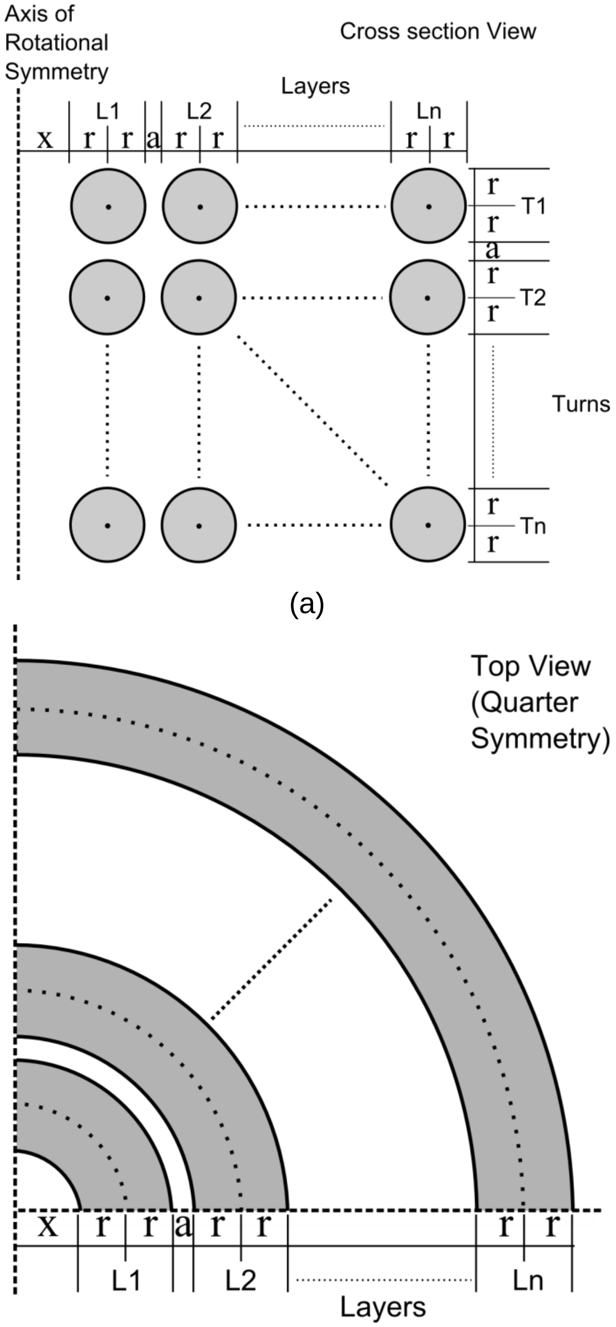

(a)

(b)

Figure 3.12 - Diagram of relevant dimensions for an air-cored inductor; (a) cross sectional view; (b) top down view (drawn with quarter symmetry)

$$LL_n = 2\pi(x + (2n-1)r + (n-1)a) \qquad (3.7)$$

$$WindingLength = 6\sum_{n=1}^{6} LL_n = 12\pi(6x + 36r + 15a) \qquad (3.8)$$

Where:

n is the layer number

LL_n is the average length of a turn in layer n (m)

r is the conductor radius (m)

x is the winding former radius (m)

a is the inter-turn spacing accounting for layer insulation, etc (m)

3.6 Experimental evaluation

3.6.1 Sample Inductors

To demonstrate cases in which aluminium conductors exhibit a lower ac resistance than copper, two different inductor topologies were manufactured; in each case, one inductor was wound with aluminium and another was wound with copper. The first topology was an air-cored inductor, the details of which are presented in Table 3.7.

Core Material	Air
Winding Former	20 mm diameter; Circular winding path
Winding Material	Copper / Aluminium
Winding Profile	1 mm diameter; Circular wire with plastic insulation 0.34 mm thick
Total Number of Turns	36
Number of Winding Layers	6
Winding Turns / Layer	6

Table 3.7 - Specification of air-cored inductor used to demonstrate lower resistance in aluminium than copper

Figure 3.13 – Air-cored inductor wound with 1mm plastic insulated copper wire, 6 turns per layer and 6 layers

The second inductor incorporated an E80/38/20 core in an E-I configuration made from N87 ferrite material. The design of this inductor is outlined in Table 3.8.

Core Material	N87 Ferrite
Core Shape	E 80/38/20 in an E-I configuration
Core Air Gap	0.5 mm in all 3 core legs
Winding Material	Copper / Aluminium
Winding Profile	1 mm diameter; Circular wire with plastic insulation 0.55 mm thick
Total Number of Turns	42
Number of Winding Layers	7
Winding Turns / Layer	6

Table 3.8 - Specification of ferrite-cored inductor used to demonstrate lower resistance in aluminium than copper

Figure 3.14- Ferrite-cored inductor wound with 1mm, plastic insulated aluminium wire, 6 turns per layer and 7 layers

3.6.2 Experimental measurement of ac resistance

The sample inductors were evaluated at a range of excitation frequencies from 100 Hz to 100 kHz using a Hioki 3522 LCR meter. Prior to undertaking these experiments, the equipment was calibrated to eliminate any effects of the test fixtures. A limitation associated with this type of equipment is that testing occurs at a relatively low current level (~100 mA), which is not representative of the actual operating conditions that the component is likely to encounter under normal service. Consequently, any nonlinearity which influences the component's behaviour at the operating point will not be represented. Although this may appear problematic, previous work considering ac winding resistance suggests that the winding resistance for a given winding configuration is relatively unaffected by the excitation current level [103, 105] with nonlinearities having a much larger influence on the core losses than the winding losses. When measuring the prototypes it was important to ensure that the current level remained constant at all frequencies, consequently, the current level used to measure the ac resistance of the windings was selected (for each topology), such that the LCR meter did not reach its maximum output voltage (as if this occurred the equipment would switch to a voltage controlled mode and not a current controlled mode). In the case of the air cored inductor, the impedance was sufficiently low across the measurement range, such that 100 mA could be used (the limit of the LCR meter) without reaching the voltage limit of the meter. In the case of the ferrite cored inductor, the impedance at high frequency was higher and therefore this current level had to be reduced to 4 mA to prevent voltage saturation.

3.6.3 Experimental results

The real component of the inductors impedance, obtained from the LCR meter at a range of frequencies can be seen in Figure 3.15 and Figure 3.16; additionally plotted in these figures are the $R_{Al/Cu}$ values for the experimental data. From this it can be seen that the resistance of the aluminium windings does fall below that of the copper windings ($R_{Al/Cu} < 1$) for both inductor topologies. For the air-cored inductor (sample 1) this occurs between 29 kHz and 41 kHz. In the case of the ferrite-cored inductor (sample 2), it occurs from 26 kHz to 42 kHz. Also included in Figure 3.17 and Figure 3.18 are the R_{ac}/R_{dc} values for the inductors. From this it can be seen that the R_{ac}/R_{dc} value in aluminium is constantly lower than that of copper. This conforms to the predictions made previously, owing to the higher electrical resistivity of aluminium, and therefore higher skin depth for a given frequency.

The gradient coefficient of sample 1 was calculated to have a value of 1.02, whereas the value calculated for sample 2 was 1.11. It was stated previously that $R_{Al/Cu}$ would be less than 1 in configurations in which this gradient value was greater than 1. This is supported by these experimental results.

A point which should be mentioned at this point is the effect of the core loss resistance on these results, this is only applicable to the ferrite cored inductor, as the air cored inductor will not have core losses. During testing it was ensured that the excitation level was a fixed current, this was done to ensure that the core losses generated within both the aluminium and copper wound inductors were consistent for a given frequency. In doing this, the core losses are present within the results as an offset value, which influences both inductors equally. Consequently, at the frequencies at which copper has a higher resistance than aluminium, this can be entirely attributed to the winding frequency effects. One parameter which will be influence by the core loss offset is the $R_{Al/Cu}$ value, as both components used in calculating this value contain the offset. This means that this value will vary with current, unlike the case in which only winding losses are considered. A point which should be noted here is that as the magnitude of the current used to test the inductors is small, the core losses will also be small, and so in the case of the results presented here the magnitude of the offset values will be small.

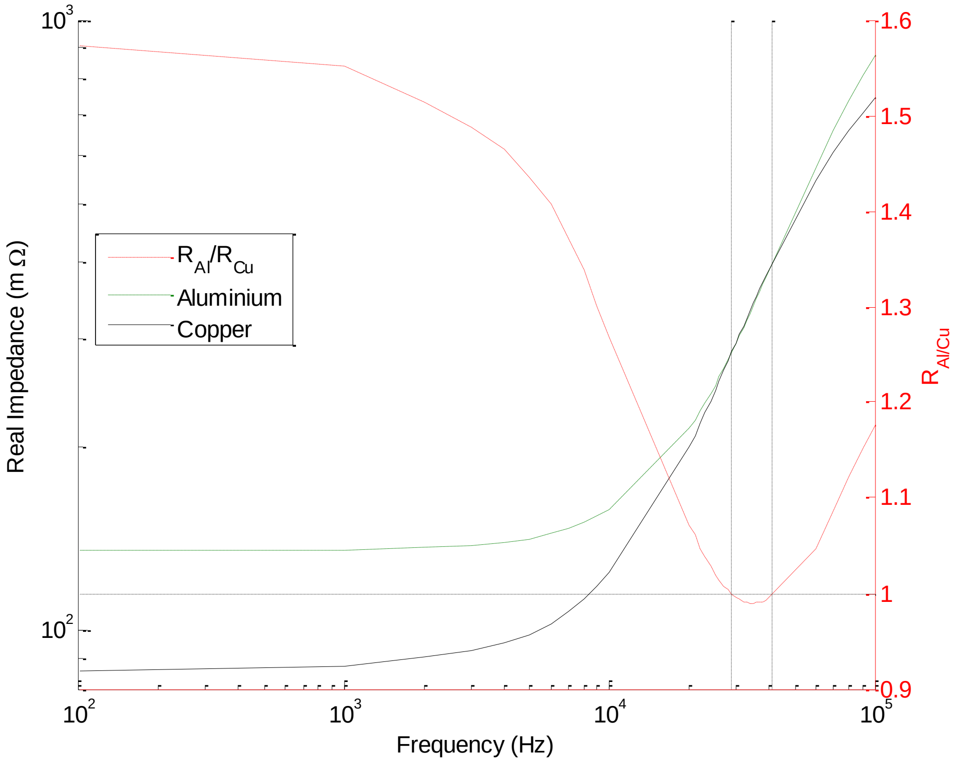

Figure 3.15 – Measured Real Impedance and $R_{Al/Cu}$ for air-cored inductors

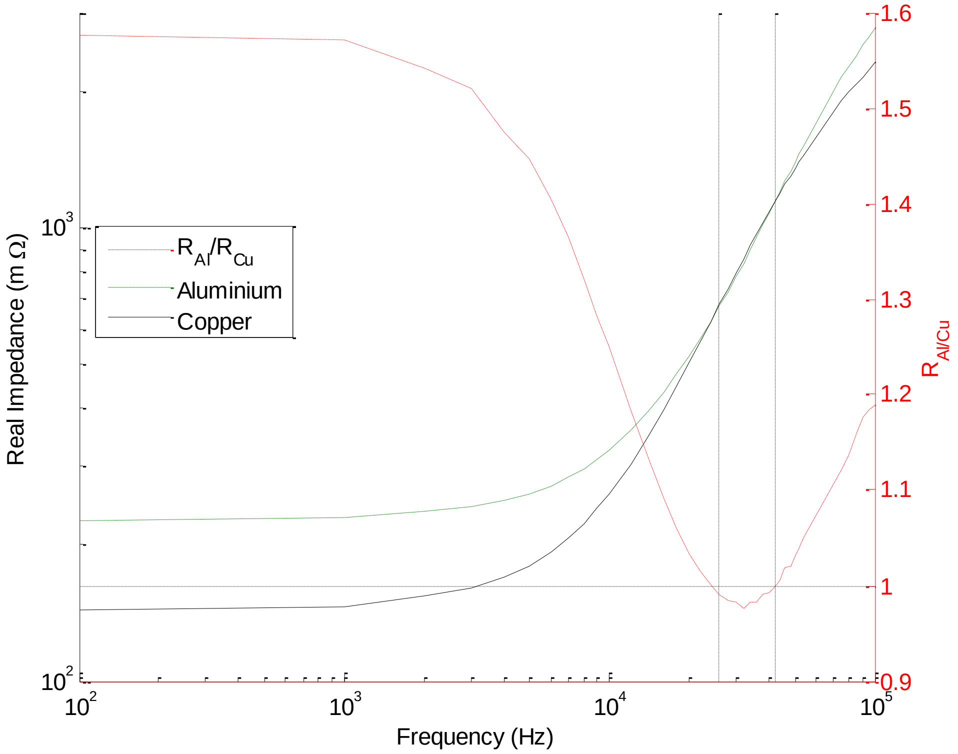

Figure 3.16 – Measured Real Impedance and $R_{Al/Cu}$ for E-cored inductors, airgap = 0.5 mm

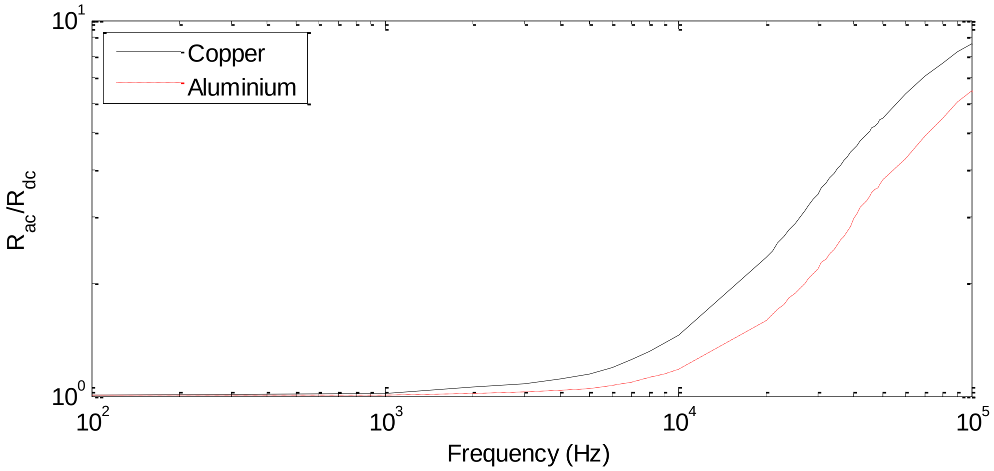

Figure 3.17 - Measured R_{ac}/R_{dc} for air cored inductors

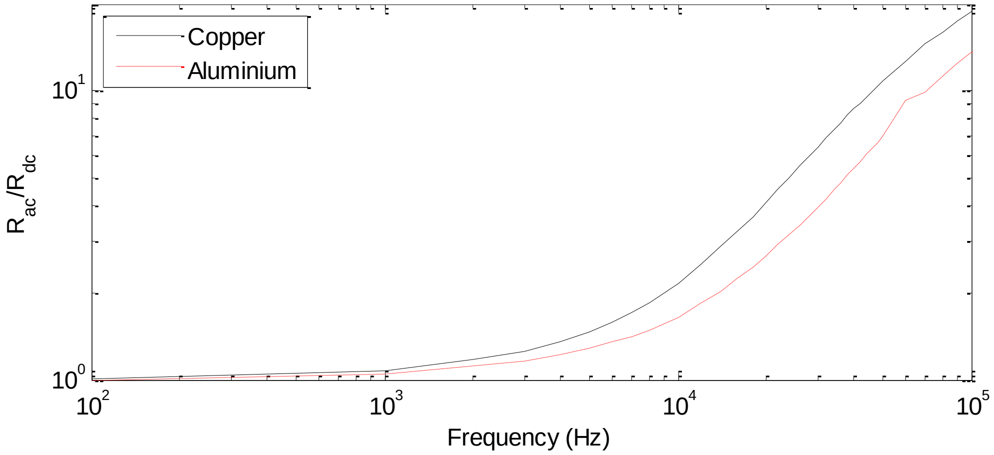

Figure 3.18- Measured Rac/Rdc for E-cored inductors, air gap = 0.5 mm

3.7 Experimental results discussion

When considering the experimental results it is also worth looking at the frequencies at which significant skin depths occur with respect to the wire size used. Equation (3.1) can be rearranged to give equation (3.9). Using this equation it is possible to calculate the frequency at which the skin depth in a material will be equal to a given depth. In our samples the wire used was 1 mm in diameter; other depths also evaluated here are those for the radius of the wire (*r*) and half of the radius (*r/2*), the results of these calculations are shown graphically in Figure 3.19. Also included in this figure are the frequencies for which $R_{Al/Cu}$ is less than unity for each sample. It can be observed from this figure that in both cases the frequency at which aluminium starts to exhibit a lower ac resistance is above the frequency where copper has a skin depth equal to the radius of the wire. Further to this, in both cases, copper returns to exhibiting a lower resistance before the frequency at which the skin depth in copper is equal to half of the conductor radius. This can be explained by the shape of the ac resistance curve with respect to frequency as outlined previously in section 3.2.

$$f = \frac{\rho_c}{\pi \mu \delta^2} \tag{3.9}$$

The frequency band at which this effect occurs is potentially very useful for a designer, as conventionally when frequency losses are a concern, the wire diameter selected is smaller than two skin depths at the operating frequency [42]. Under this criterion the example inductors would not be operated at above 17.5 kHz in copper, or 28 kHz in aluminium. From the results presented it can be observed that at 17.5 kHz both sample topologies exhibit less than 10 % difference between the copper and aluminium windings; far less than the 64.5 % suggested by the dc resistivity values. At 28 kHz the air-cored inductor exhibits only a 1 % variation in resistance between aluminium and copper conductors and in the ferrite-cored inductor, aluminium exhibits a resistance 1.5 % lower than copper at this frequency. Consequently it is possible to exchange the winding material whilst only having a small effect on the losses at these frequencies.

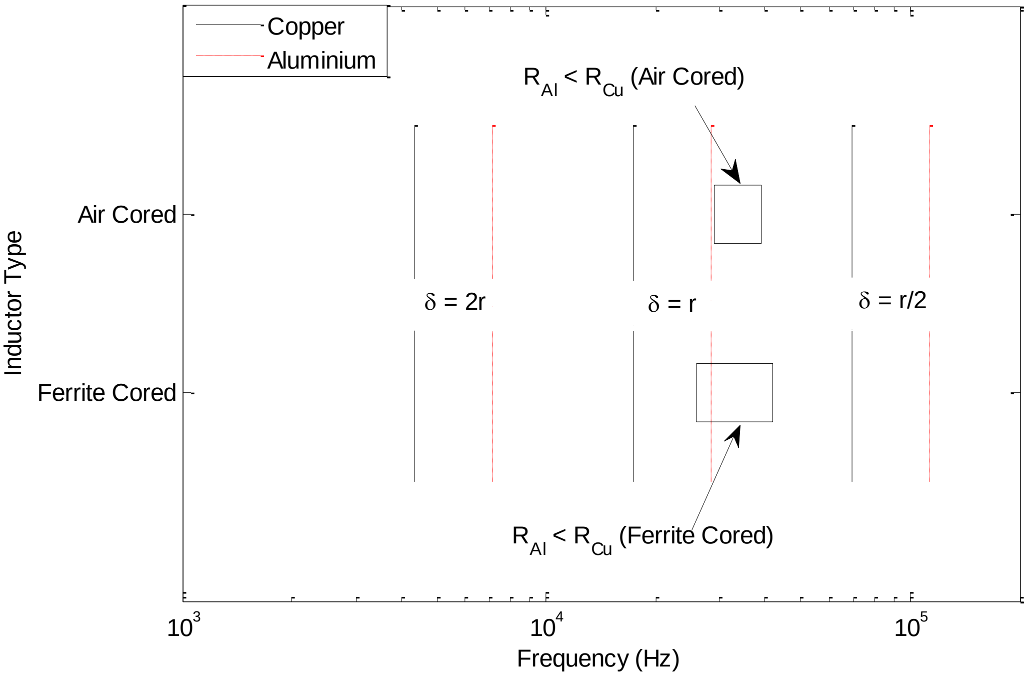

Figure 3.19 - Visualisation of resistance crossover points shown with different skin depths

3.8 Conclusions

The case has been made for the use of aluminium as a replacement for copper in inductor windings. Although at dc it is necessary to increase the cross sectional area of aluminium conductors by a factor of approximately 1.645 to match the losses of copper conductors, it has been shown that at higher frequencies this is not the case. This can be attributed to the effects of eddy currents being lower in aluminium than copper as a result of its higher resistivity. Furthermore, for the inductor configurations considered here, it can be seen that for a range of frequencies aluminium exhibits lower losses, outperforming copper windings. This fact combined with the reduced raw materials, cost and weight of aluminium, when compared to copper; makes a strong case for its use as a winding material, especially in applications where the component is excited primarily by a sinusoidal waveform at certain frequencies. For signals with a large dc content the loss advantages are diminished due to the higher dc resistance of aluminium, however, in this case, the cost and weight advantages still persist, making aluminium a favourable selection for certain optimisation objectives.

It was discussed in chapter 2 that there are potential problems relating to the termination of aluminium wire; these problems are avoidable by taking the correct precautions and using the correct hardware designed for aluminium. Furthermore, using aluminium as a conductor material opens up the opportunity to utilise aluminium oxide as an insulation material. This presents the interesting possibility of improving the thermal performance of the winding compared to conventionally used varnishes or plastic films. This technique was not employed within the samples produced here as it would not have been possible to manufacture an equivalent for the copper winding, and consequently, it would not be possible to determine if the effects being observed were due to the winding materials or the difference in insulation.

In this chapter the case for using aluminium as a winding material has been made. As has already been stated, selecting aluminium opens up the potential to employ aluminium oxide as a winding insulation material. This is an attractive proposition due to the improved thermal properties of aluminium oxide, when compared to conventional winding insulation materials. The next chapter of this thesis will explore the use of aluminium oxide to produce planar windings with enhanced thermal performance.

Chapter 4

Aluminium Oxide Insulated Planar Windings

In the previous chapter a case has been made for the use of aluminium as a potential winding material. During this discussion, it was noted that a factor which contributes to termination issues when using aluminium wire is the naturally forming oxide layer on the surface of the material. At the thicknesses which form naturally, the aluminium oxide can be considered as an inconvenience, as it inhibits the creation of a good joint. It is not, however, thick enough to be used as an insulating material.

It is possible using the anodisation process to increase the thickness of the oxide layer, making it suitable for use as an insulator. This offers an exciting opportunity to allow aluminium oxide to be used as a replacement for materials such as plastics which are commonly used as insulation. Such a replacement is of interest due to aluminium oxide's superior thermal performance when compared to plastics. This leads to the potential to reduce the operating temperatures in the windings by enhancing the heat transfer out of the component from the centre of the winding to the surface.

This chapter will therefore use aluminium oxide as an alternative insulation material and will discuss:

- The production of an aluminium oxide layer suitable for insulation purposes;
- The topology of the windings used within this work;
- Potential methods of connecting winding plates together;
- Thermal comparisons between aluminium oxide and kapton (a conventionally used insulation material);
- Consideration of the electrical properties of the insulation layer;
- Evaluation of a manufactured prototype.

Bulk material properties for both aluminium oxide kapton are shown within Table 4.1. Also included in this table are the properties for heat sink compound and whilst this is not used as an insulation material in its own right, its use in combination with aluminium oxide insulation will also be explored later in this chapter.

	Kapton	**Aluminium Oxide**	**Heat Sink Compound**
Thermal Conductivity (W/m.K)	0.12	16.6 – 36	0.9
Density (g/cm^3)	1.42	3.97	2.10
Specific Heat Capacity (J/cm^3.K)	1.55	3.74	-
Breakdown Voltage (kV/mm)	154 – 303	9.1 – 17.7	18
Relative Permittivity	3.4	8.7 – 20.5	4.9

Table 4.1 – Bulk material properties of some materials used in this work (Data from [27, 106, 107])

The novelty of this section lies in the combination of a planar transformer winding topology with aluminium oxide insulation in a way not previously seen. This method is advantageous over other methods of using aluminium oxide in that it allows the winding shape to be produced prior to the anodisation process, removing the need to bend the anodised material which can cause cracking to occur in the oxide layer.

4.1 Aluminium oxide as an insulation material

Aluminium oxide is classified as a ceramic material which naturally forms in a very thin (nm) layer on the surface of aluminium. In this form it is too thin to be utilised as an insulation material, but acts as a barrier, preventing further natural oxidisation of the aluminium surface. That being said, it is possible to produce a thicker oxide layer using the anodisation process.

4.1.1 Aluminium oxide layer grown by anodisation

Anodisation is a process used to manufacture an aluminium oxide surface layer on pieces of aluminium; the key point about this surface oxide layer is that it is much thicker than the naturally forming oxide layer and therefore is potentially suitable for use as an insulator. A diagram illustrating the equipment required to perform this process can be seen in Figure 4.1. In this process a dc power supply is connected to two electrodes, both of which are submerged within a suitable electrolyte. The work piece forms the anode of the circuit, while the cathode is produced from a suitable metal such as aluminium, lead or stainless steel. When dc current is applied to this setup an oxide layer builds up on the surface of this work piece. The chemical half equations describing this process are listed here as equations (4.1) and (4.2)

At the anode (4.1)

$$2Al + 6OH^- - 6e^- \rightarrow Al_2O_3 + 3H_2O$$

At the cathode (4.2)

$$6H^+ + 6e^- \rightarrow 3H_2$$

There are several different variations of anodic coating as defined by MIL-A-8625 [108], the most suitable of which will depend upon the desired oxide thickness. The distinction between these classes (in addition to the oxide thickness) is the choice of electrolyte; a list of the anodising classes are shown in Table 4.2. Further to the class (and therefore electrolyte chosen), other parameters such as the supply voltage, anodising current, temperature and time can also be varied; such variations will influence the properties of the resultant oxide film.

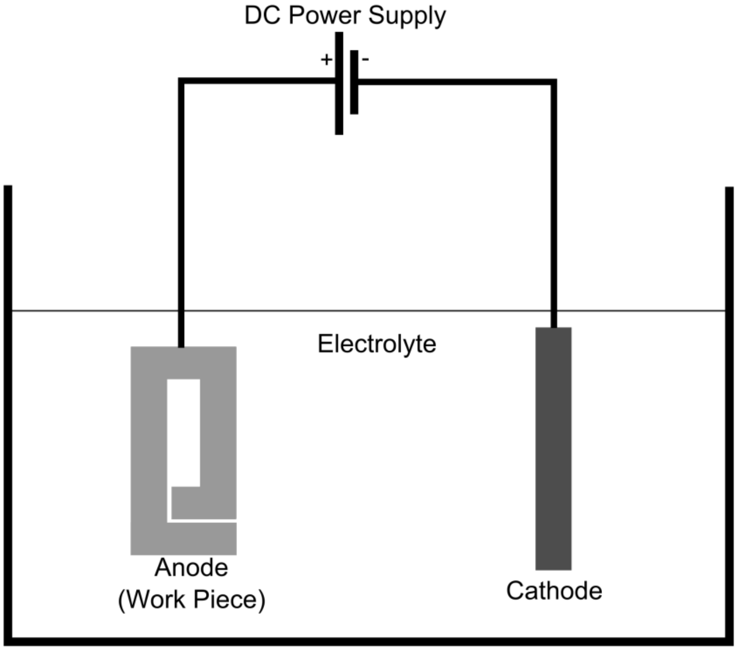

Figure 4.1 - Diagram of anodising process

Type	Electrolyte	Min Thickness	Max Thickness
I	Chromic Acid	0.5 μm	18 μm
II	Sulfuric Acid	1.8 μm	25 μm
III	Sulfuric Acid	13 μm	114 μm

Table 4.2 – Anodisation classification (Data from [108])

4.1.2 Topologies most suited to anodised insulation

Using the anodisation process, oxide layers which are of the order of microns in thickness can be produced. Layers of this thickness are potentially viable for use as insulation material. In chapter 2, a review of the use of aluminium oxide as an insulator by previous authors was considered. In this it was noted that the oxide layer was particularly prone to cracking when produced on curved surfaces (for example, the surface of a round wire); in this instance the cracking was visible on the curved surface prior to the application of any external stress [40]. The same was not true in samples which were flat in profile.

It should also be considered that due to the brittle nature of the oxide, any attempt to shape a winding from the material after the anodising process has been performed may result in the oxide cracking due to the applied stress when bending the material. Consequently such an insulation material is best employed in topologies which permit the windings to be shaped prior to the anodisation process. Considering this fact, in this work we consider a planar wound inductor, constructed from preformed winding plates.

4.2 Winding topology

The prototype winding shape which was manufactured for this work can be seen in Figure 4.2. This winding was manufactured from sheets of 0.5 mm thick aluminium which were anodised using the type II process, achieving a 25 μm thick aluminium oxide layer. The growth of the oxide layer upon the surface of the plates was performed by an external company; this was done due to the fact that the external company had prior experience of the process and knowledge of how to best produce a satisfactory anodisation layer. The shape of the plates was designed to make it possible to produce a continuous winding using only a single design; this is achieved by alternating the side of the plate which is placed on the top during the stacking of the plates, as illustrated in Figure 4.3. The dimensions of the windings were designed to allow the winding to be used with an E 58/11/38 planar ferrite core.

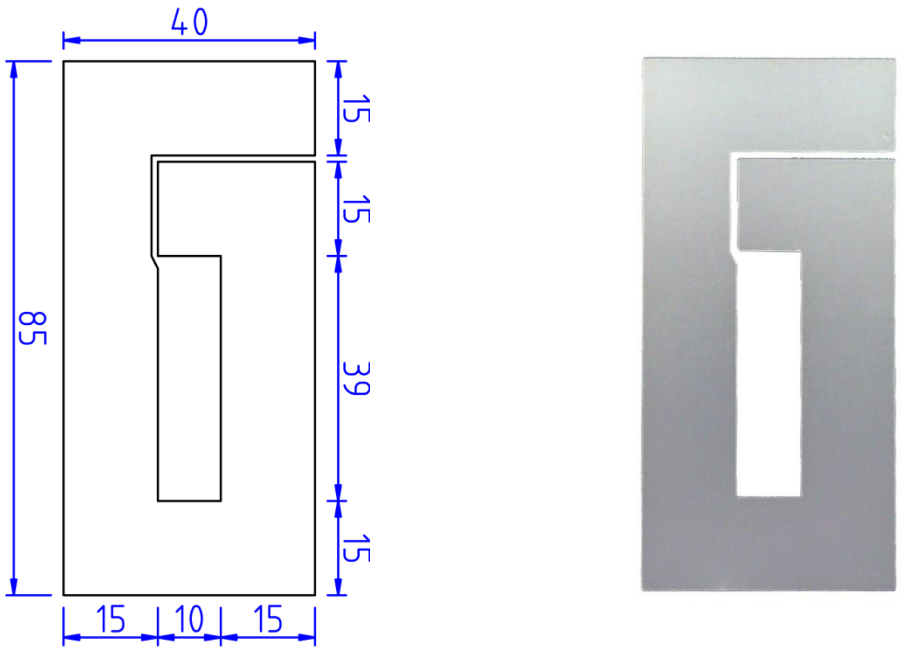

(a) (b)

Figure 4.2 - Prototype winding design employed in this work. (a) - dimensions of windings; (b) - anodised aluminium winding.

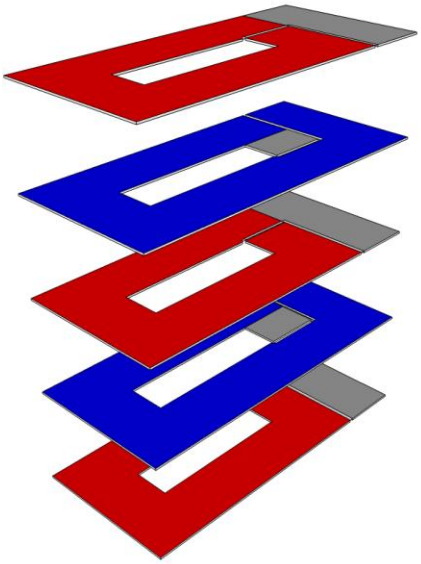

Figure 4.3 - Exploded view of a winding stack produced from five winding layers. (exposed contact areas in grey)

4.3 Winding connection considerations

As previously stated, the winding design which is employed within this prototype is constructed from multiple layers which are connected together both electrically and mechanically.

To this end, a variety of potential methods for connecting pieces of metal together were considered. Unfortunately, several of the methods considered are of limited use for this application due to the application requirements. For a technique to be suitable for this application two major criteria must be satisfied:

1. It must be possible to produce the connection without damaging/removing the insulation material, except in places where the joint is being made. This requirement is necessary because compromising the integrity of the winding insulation is undesirable and could lead to failure of the component.
2. It must be possible to produce the connection with access to only one side of the joint. This is applicable because in the context of a winding stack one side of the joint will be obstructed by the previous layer of the stack and so will be inaccessible for the purpose of producing a connection

Techniques which were considered for this application are listed in Table 4.3 along with a general overview of the techniques suitability.

Technique	**Does not damage insulation**	**Made with access to one side**
Soldering	✗	✓
Fasteners (bolts/rivets)	✗	✗
Fasteners (screws/blind rivets)	✗	✓
Spot Welding	✗	✗
Blind Spot Welding	✗	✓
Clinching	✗	✓
Electrically Conductive Epoxy	✓	✓
Electrically Conductive Tape	✓	✓
Pressure Contacts	✓	✓

Table 4.3 - Comparison of potential techniques for joining winding layers, evaluated against major criteria

4.3.1 Soldering

One method considered as potentially suitable for this application was soldering. To evaluate this method a winding was placed into a reflow oven at 260 °C and was soldered using multicore alu-sol 45D aluminium solder. When the plate was removed from the oven, visible cracks in the aluminium oxide layer could be observed; an image of the winding plate after removal from the reflow oven can be seen in Figure 4.4. These cracks are caused by a mismatch in the co-efficient of thermal expansion between the aluminium and aluminium oxide in addition to the brittleness of the oxide layer. This damage to the oxide layer leads to the conclusion that this technique is not a suitable way to join the winding plates together.

Figure 4.4 - Visible insulation cracking which occurred during soldering process

4.3.2 Fasteners

In some applications it may be viable to connect the windings together using fasteners such as bolts or rivets; in this application it would be necessary to bolt the whole stack together using a single fastener since the individual winding plates are too thin to accommodate a fastener for each connection while still allowing the windings to be stacked together correctly. Consequently a hole would have to be drilled through the entire winding stack, compromising the insulation. Additionally, if this approach were to be taken it would be necessary to ensure that a suitable insulation was applied to the fastener to prevent the entire stack from being short circuited, unless a fastener made from an insulating material such as nylon could be used.

4.3.3 Spot Welding

Spot welding joins sheets of metal together by passing a large current through the weld point, causing the metals to melt locally and fuse together producing a joint. To achieve this, the welding electrodes must be in electrical contact with the work piece on both sides of the joint. This presents two issues for this application:

1. To achieve an electrical contact with the winding it is necessary to remove the insulation from the back of the joint (compromising the winding insulation);
2. The joint has to be clamped directly between the electrodes during welding; (this is contrary to the second criteria, as previous layers of the winding stack will obstruct the site of the joint from one side) making spot welding inappropriate for this application.

4.3.4 Blind Spot Welding

A lack of access to the back of the joint can be overcome by performing blind spot welding. This process differs from standard spot welding as it only requires access to one side of the joint; however, the removal of winding insulation from the rear of the winding is still required, making this technique inappropriate also.

4.3.5 Clinching

Clinching forms connections between sheets of metal using pressure to plastically deform the sheets, locking them together. Potentially this could be performed on the full winding stack in one operation, removing the need for access to the rear of the individual windings. An issue with this is that the brittleness of the aluminium oxide would result in cracking in to the aluminium oxide layer during this process. This would produce short circuits between the winding layers, ruling out this technique.

4.3.6 Electrically conductive Epoxies/Tapes

Electrically conductive epoxies are produced by doping an epoxy with electrically conductive particles such as silver, nickel or copper. Electrically conductive tapes, similarly, are produced by applying a conductively doped adhesive to a conductive foil. Generally speaking, in both of these cases, the base adhesive prior to doping is not electrically conductive [109] and therefore, the adhesive composite has a relatively high resistance compared to the filler material, as conduction paths only exist within the adhesive where the filler forms continuous conductive chains. Consequently, joints formed in this way will have a higher resistance than the filler material.

4.3.7 Pressure Contacts

Pressure contacts are produced by applying an external force to the joint, compressing the contact surfaces and holding them together. In this case, space between the contact surfaces can be filled using a conductive filler material, such as a foil. As this filler is included only to act as a bridge between the joint surfaces, and not to provide adhesion, it does not need to be compromised by a less conductive adhesive (as is the case with conductive tape) resulting in a better joint. However, it is necessary to maintain the external holding force on the joint throughout the lifetime of the joint.

Due to the potential joint performance, pressure contacts were selected as the method to be used for joining the layers of the winding together to produce a winding stack in this work

4.4 Bulk thermal performance of winding stacks

To evaluate the thermal performance of the different winding insulation materials the thermal testing rig shown in Figure 4.5 was constructed. This test rig was used to evaluate the effective thermal conductivity through winding stacks insulated using different materials. This was achieved by stacking multiple winding layers together (in the configuration which would be used within an inductor) and then placing them into the rig in the position highlighted in Figure 4.5.

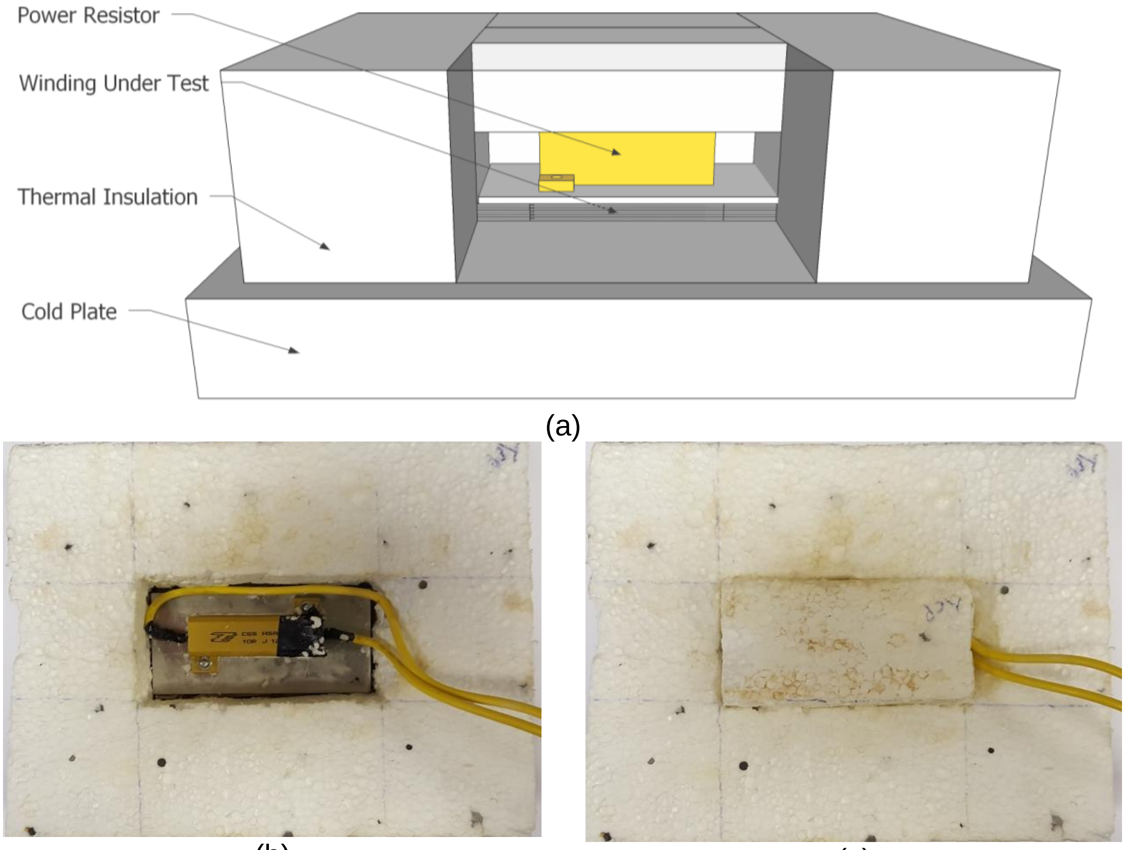

(a)

(b)

(c)

Figure 4.5 - Winding stack bulk thermal properties measurement rig. (a) – Diagram of structure; (b) – Rig (Top removed); (c) – Rig (assembled)

In this test rig the winding sample is placed between a cold plate and heating resistor. Thermal insulation made from expanded polystyrene was placed around the sample and heating resistor to ensure that all of the applied power passed through the winding stack under test, rather than into the surrounding environment.

By dissipating a known power within the power resistor and monitoring the temperature gradient across the winding stack (using k-type thermocouples) it is possible to calculate the bulk thermal conductivity of the winding stack being considered by rearranging the 1D heat flow equation (equation (4.3)) to obtain equation (4.4).

$$P = \frac{\Delta T k A}{l} \tag{4.3}$$

$$k = \frac{P l}{\Delta T k A} \tag{4.4}$$

Where:

P	Is the power dissipated with the resistor (W)
ΔT	Is the temperature gradient developed across the sample at steady state (°C)
k	Is the bulk thermal conductivity of the winding stack (W/m.K)
l	Is the height of the winding stack (m)
A	Is the cross sectional area of the winding stack (m^2)

For the purposes of this test three different winding / insulation configurations were tested:

- 25 μm kapton film insulation;
- 25 μm aluminium oxide insulation;
- 25 μm aluminium oxide with heat sink compound (HSC) applied between the layers.

The heat sink compound applied between the layers was HTS manufactured by Electrolube. It is based around a silicone oil, combined with metal oxide powder fillers to achieve a thermal conductivity of 0.9 W/m.K [107].

Each of these configurations was tested by applying a 10 W power dissipation to the power resistor while measuring the temperature gradient across the sample. The recorded temperature gradient during these experiments can be observed in Figure 4.6. Additionally, the steady state temperature values for each configuration are recorded in Table 4.4 along with the bulk thermal conductivity values for heat flow perpendicular to the winding stack.

When considering the time to reach steady state visible in Figure 4.6 it is interesting to note that the transient time varies inversely to the thermal conductivity of the winding insulation. Whilst there will be a small amount of variation between the thermal capacitances of the different samples, this will be relatively small. This is because the majority of the thermal capacity within the winding stack is provided by the aluminium windings themselves (which are 20 times thicker than the insulation layers separating the windings). The difference in transient times can be attributed to the differences in thermal resistance, as a higher thermal resistance will result in a longer rise time, owing to the slower rate at which the thermal capacity of the component can be heated up.

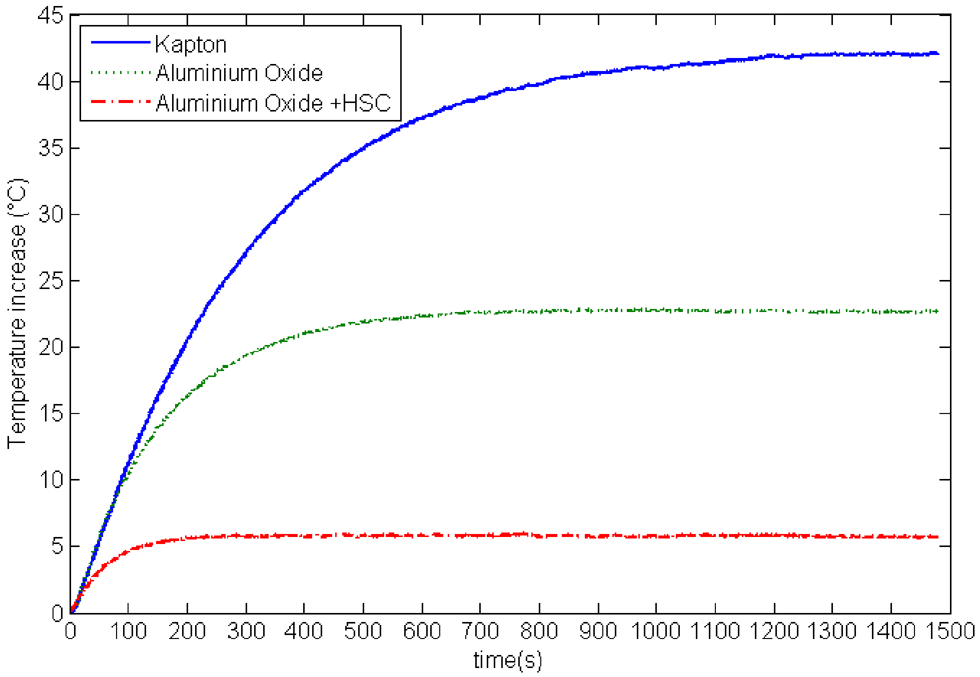

Figure 4.6 - Temperature difference measured across sample winding stacks with a 10 W power dissipation

Insulation	ΔT (K)	k (W/m.K)	% improvement
Kapton	42.1	0.38	0.0 %
Aluminium Oxide	22.8	0.70	84 %
Aluminium Oxide + Heat Sink Compound	5.7	2.80	637 %

Table 4.4 - Steady state winding temperatures and calculated bulk thermal conductivities

From the experimental data, the effects of changing the winding insulation material can be clearly observed. By replacing the kapton insulation with aluminium oxide the bulk thermal conductivity of the winding can be seen to increase by 84 % from 0.38 W/m.K to 0.70 W/m.K. The further improvement which can be achieved by including heat sink compound between the layers of the winding makes a strong case for its use, as its inclusion yields an improvement of over 600 % when compared to kapton. Based on this, it was decided that the manufactured prototype would incorporate aluminium oxide insulation and would include heat sink compound between the layers, as it is obvious from the test results that this configuration achieves the best thermal performance results.

4.5 Electrical performance of aluminium oxide

In considering the use of aluminium oxide as an insulation material there are two points which must be considered from an electrical perspective:

- The capacitance between two plates using the insulation;
- The breakdown voltage of the insulation.

To test these parameters the configuration shown in Figure 4.7 was utilised. In this configuration two insulated windings are clamped together using a plastic clamp which occupies the same footprint on the windings as the magnetic core. In these tests the configurations with and without heat sink compound were tested.

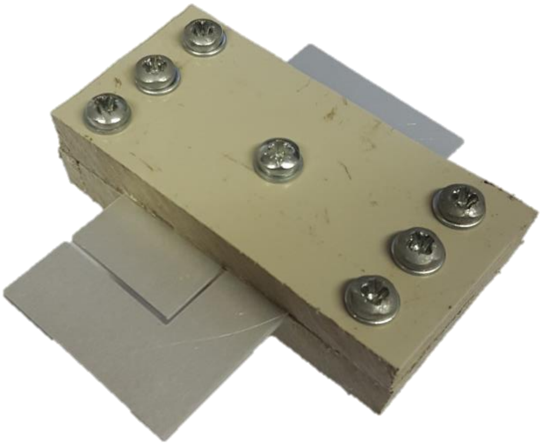

Figure 4.7 - Clamp configuration used for electrical testing of insulation

4.5.1 Capacitance measurement

To measure the interlayer capacitance the windings were arranged in the manner shown in Figure 4.7, after which the interlayer capacitance was measured using an LCR meter at 50 kHz. From the measurements shown in Table 4.5 it can be seen that the introduction of heat sink compound between the layers increase the capacitance slightly. This can be attributed to the fact that the heat sink compound has a higher permittivity than the air which it is displacing from between the windings. Both configurations exhibit a higher level of capacitance than the windings insulated with kapton; this is unsurprising as the relative permittivity is lower in kapton than aluminium oxide.

4.5.2 Breakdown voltage testing

To evaluate the breakdown voltage of the insulation two different methods were used.

Firstly the winding sample was connected in series with a resistor (included to limit the breakdown current) to a dc power supply. The voltage of the power supply was slowly increased from 0 V. During this time the current was monitored to determine the point at which breakdown occurred. The voltages at which this happened in both samples are shown in Table 4.5. It can be seen from this data that the breakdown voltage is higher when heat sink compound is included; again this can be attributed to the superior breakdown voltage of the heat sink compound (18 kV/mm) when compared to the air that it is displacing (3 kV/mm).

The second method of testing the insulation was to use a Fluke 1653B multifunction tester. This equipment can be used to test the performance of insulation at a fixed voltage of 50, 100, 250, 500 or 1000 V. Using this equipment the test voltage was increased until a range was selected at which the insulation failed. The voltage range at which failure was experienced for each sample is also included in Table 4.5.

From this, it can be concluded that the introduction of heat sink compound between the winding layers offers the advantage of an increased insulation breakdown voltage while only marginally impacting on the capacitance.

In both cases the breakdown voltage is in excess of 400 V. This should be sufficiently high as each insulation layer will only be subjected to the inter-turn voltage, and not the total inductor terminal voltage in a multi-turn design.

When kapton was subjected to these tests breakdown did not occur. This is predictable considering breakdown voltages quoted for kapton which are an order of magnitude higher than the values quoted for aluminium oxide.

	Plain	**HSC**	**Kapton**
Capacitance	2.2 nF	2.4 nF	0.7 nF
Breakdown voltage	420 V	582 V	-
Breakdown failure range	500 V	1000 V	-

Table 4.5 - Measured electrical properties of windings

4.6 Prototype inductor

From the results presented thus far it can be seen that aluminium oxide is suitable for use as an insulation material, both thermally and electrically. Based on this observation it was decided to construct an inductor which employed aluminium oxide insulated windings. This was done through the construction of the inductor shown in Figure 4.8, the specification of which is listed in Table 4.6. This inductor was constructed on a liquid cooled cold plate, which was cooled using water. Also visible in this photograph are three clamps: (from left to right) the first and second clamps are used to apply pressure to the windings, making contact between the layers; while the third clamp is used to hold the core halves together.

Core	E58/11/38 (In E-I configuration)
Air gap	0.5 mm (All legs)
Windings	Custom planar windings (Figure 4.2); aluminium oxide insulation; HSC between layer
Winding configuration	Stack composed of 10 layers, interlayer connections formed with pressure contacts
Inductance	52.5 µH
DC Resistance	26.7 mΩ
Saturation Current	35 A

Table 4.6 - Prototype inductor specification

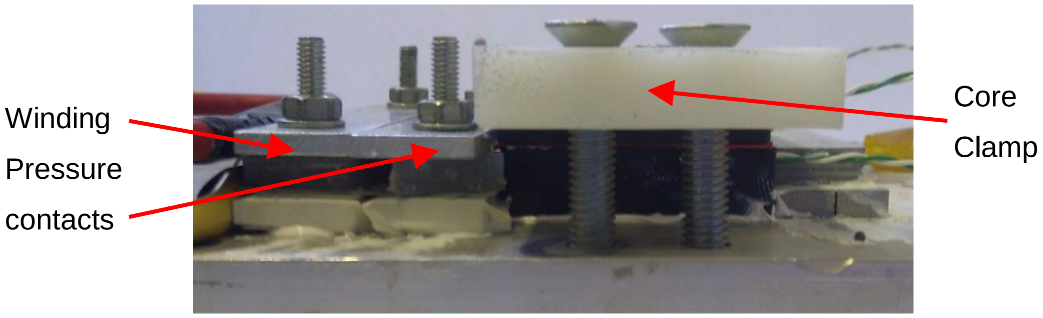

Figure 4.8 - Prototype aluminium oxide insulated inductor

The thermal performance of this inductor was evaluated by applying a 35.45 A dc current to the inductor until thermal steady state was achieved. During these tests, temperatures within the inductor were monitored using both k-type thermocouples and a thermal imaging camera. A thermal image of the prototype at steady state can be observed in Figure 4.9(b). From these tests the peak winding temperature was measured as 304.8 K; when the coolant temperature is taken into account (281 K) this equates to a temperature increase of 23.8 K. With a 35.45 A current being passed through the windings, this equates to a power dissipation of 33.55 W. Based on the bulk thermal conductivity values measured for the winding previously in section 4.4, a temperature increase of 19.1 K would be predicted. This shows reasonable agreement to the value measured here.

It may be noted that the test current is 0.45 A (1.3 %) higher than the quoted saturation current of the inductor. This was a result of the precision of the dc power supply used during this experiment. While this means that the inductor under test was operated slightly beyond the saturation point, it was not felt that this was an issue for this particular test, as the purpose of this particular test was to evaluate the thermal performance of the inductor and not evaluate its magnetic performance.

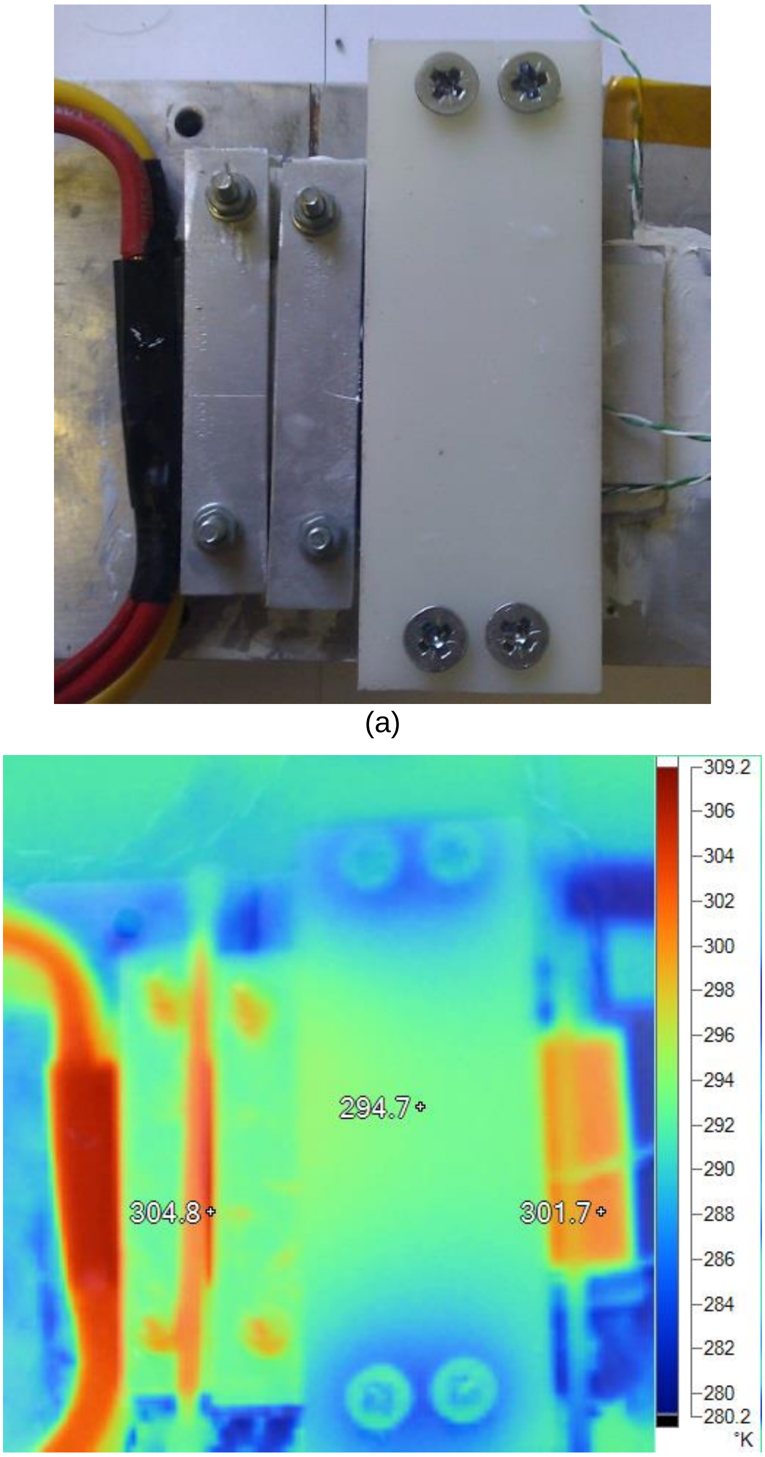
(a)

(b)

Figure 4.9 - Prototype inductor testing under dc excitation: (a) – Photograph of prototype; (b) – Thermal image of inductor at steady state (coolant temperature is 281 K)

4.7 FEA comparison of winding insulation thermal performance

To compare the performance of the constructed prototype inductor with those using other insulation materials, a 2D finite element model of the inductor was produced, this model is shown in Figure 4.10. In these simulations the bulk thermal conductivity values obtained from the tests performed previously were used in the regions which represent the windings. The finite element analysis results from these simulations can be seen in Figure 4.11; additionally the results of this simulation are summarised in Table 4.7. As would be suggested by the thermal conductivity values these results show that replacing the winding insulation with aluminium oxide has the potential to improve the thermal performance of the component, with the addition of heat sink compound offering further improvements beyond this. The simulation of the case which uses aluminium oxide and heat sink compound shows a good correlation with the results obtained through practical experimentation, with the simulation predicting a temperature rise of 23.7 K compared to the 23.8 K of the experiments presented in section 4.6. This result instils confidence that the FEA model is a fair representation of the manufactured prototype.

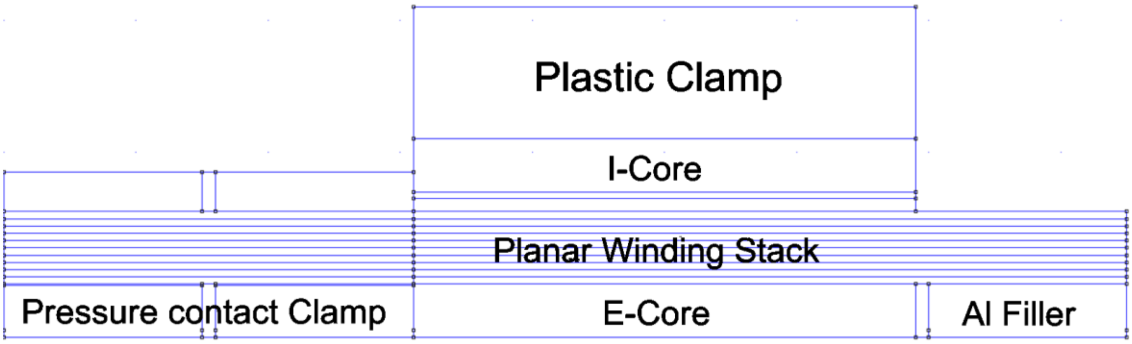

Figure 4.10 - 2D Finite element analysis model of inductor using planar windings

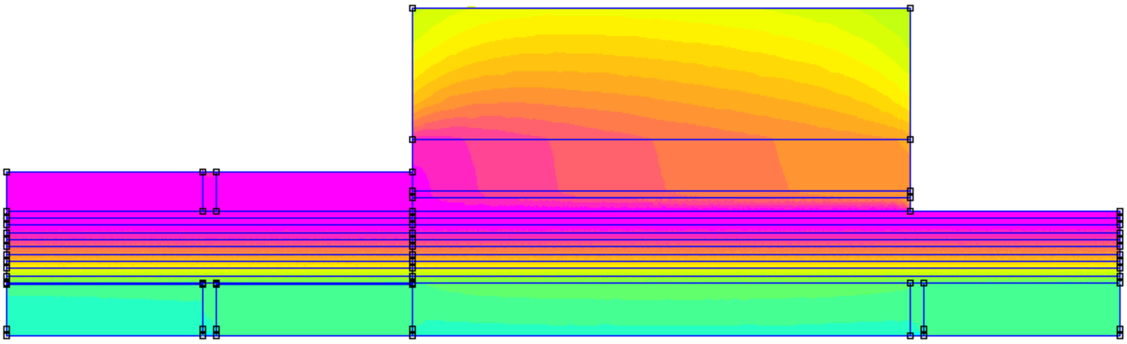

(a)

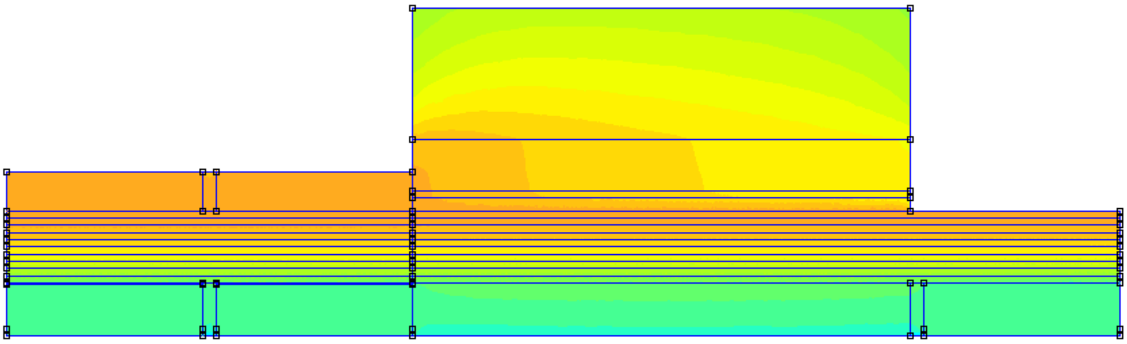

(b)

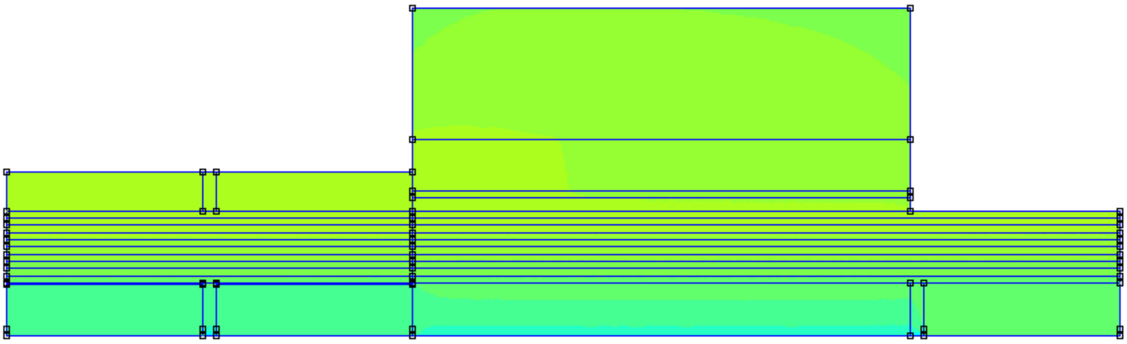

(c)

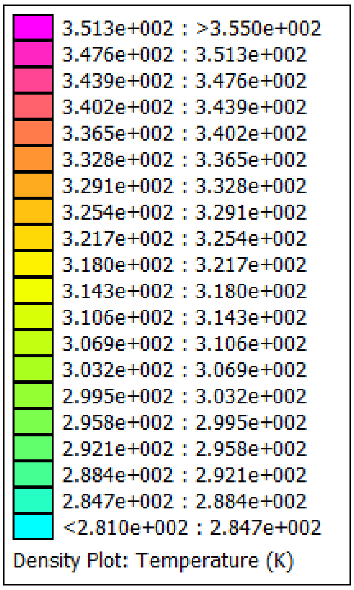

Figure 4.11 - Finite Element simulation results for different winding insulation materials (coolant temperature set to 281 K): (a) – Kapton insulation; (b) – Aluminium oxide insulation; (c) Aluminium oxide and heat sink compound insulation

Insulation	Temperature increase	% reduction (wrt kapton)
Kapton	73.2	0.0
Aluminium Oxide	49.8	32.0
Aluminium Oxide + HSC	23.7	67.6

Table 4.7 – Peak temperature increase predicted by finite element analysis and % reduction to temperature with respect to kapton

4.8 Conclusions

Aluminium oxide is a viable insulation solution for use in magnetic components in which the winding shape can be pre-formed prior to the anodisation process, as is the case in the planar winding structure discussed here. In such a case the thermal advantages result in improved heat removal from the component winding, reducing the operating temperature of the component or, in the case of a thermally limited component, allowing the current rating to be increase. It should be noted however that due to the brittle nature of the material it may be less suited to topologies in which it is necessary to form the aluminium after the anodisation process has been performed, since bending the oxide layer will result in cracking of the oxide layer, compromising its properties.

In this chapter, consideration has been given to the use of aluminium oxide in planar winding topologies for the purpose of improving the thermal performance of the windings. In the next chapter an alternative method of improving thermal transfer within inductors through the use of encapsulants will be explored. Here, particular consideration is given to the use of composite encapsulants. Composites are considered due to the fact that they offer greater improvement than standard encapsulants. To use a composite effectively it is necessary to be able to model its bulk thermal properties, this is the specific area which is addressed within chapter 5. The use of composites in practical applications is also explored in chapter 6.

Chapter 5

The use of composite materials to improve the thermal performance of encapsulant materials

In previous chapters the advantages of an improved thermal path within a component have been examined. Having discussed the use of novel winding insulation materials and manufacturing techniques, this chapter considers the further increases in thermal performance which can be obtained from the use of encapsulants. Encapsulant materials are commonly utilised in power electronic components with the aim of improving both the thermal and mechanical performance of the component. An issue of particular prevalence in wound components are the small pockets of trapped air between winding layers as a consequence of imperfect tessellation between the winding components; this is illustrated in Figure 5.1. If nothing is done to address this, these pockets of air behave as excellent thermal insulators, causing hotspots within the winding assembly and potentially limiting the maximum current rating of the component. To this end, an encapsulant material, possessing superior thermal properties to that of the trapped air can be used to displace the trapped air providing an improved thermal path and resulting in lower operating temperatures. An example of this can be seen in Figure 5.2. Here it can be seen that by displacing the air from within the winding assembly it is possible to reduce the peak operating temperature of the assembly considerably.

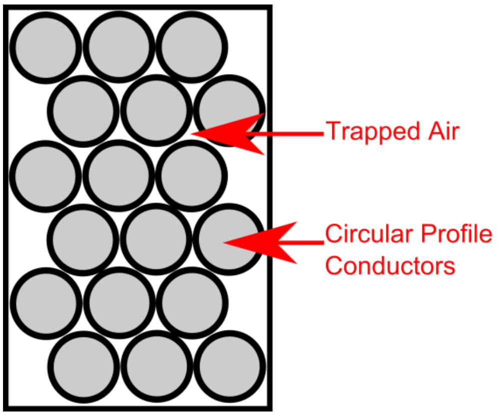

Figure 5.1 - Illustration of trapped air in a winding assembly

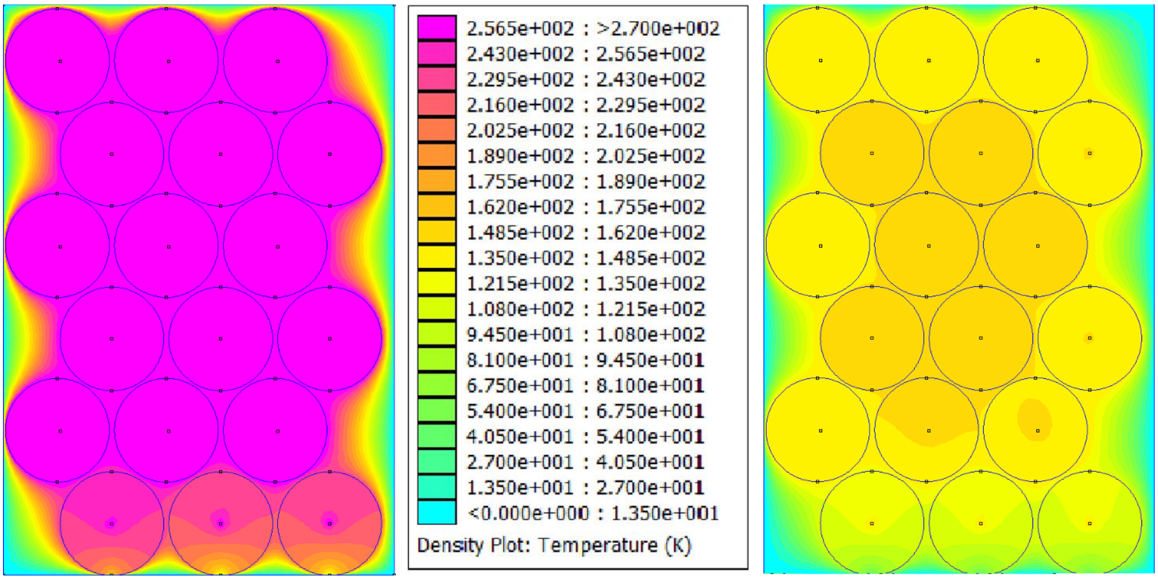

(a) (b)

Figure 5.2 - Illustration of effects of epoxy impregnation. (a) – windings in air; (b) – windings in epoxy (k = 1 W/m.K)

The thermal performance of potting compounds can be enhanced by combining them with thermally conductive filler particles, producing a composite material. While these composites present the opportunity to further improve the performance of the component, predicting their performance can prove challenging. When designing components it is not uncommon to utilise design tools such as Finite Element Analysis (FEA) to develop the design. Within these tools the inclusion of a composite material may prove challenging in that it is necessary to represent the filler particles within the model in some way. One such method of achieving this is to recreate the structure of the composite within the FEA model. For this method to produce valid results the structure included within the model must accurately reflect the reality of the composite. The filler used to make up the composite is likely to be composed of very small (of the order of100 μm), randomly distributed particles. This can make producing an accurate representation of it problematic. Assuming that the filler particle arrangement has been successfully replicated within the FEA model there is still an issue relating to solving the model, because a very small mesh must be to be used to mesh the fine particles. This greatly increases the processing time to solve the FEA models. This issue is of particular concern in cases where the transient performance of the component is of interest, as in such cases, it is necessary to solve the model at multiple time steps to capture the transient response, multiplying the effect of the increased processing time by the number of transient steps. This can be avoided by using an equivalent property to represent the composite material within the finite element model. Whilst this removes the need to recreate the structure of the composite accurately, it also introduces the requirement for the equivalent parameter to be determined prior to simulation. The approaches which can be used to accomplish this can be divided into three categories:

- Analytical;
- Numerical;
- Empirical.

The use of these approaches and a comparison of the results they generate will be explored now.

5.1 Analytical modelling of composite materials

Analytical models are derived for composite systems based on assumptions regarding the makeup and structure of the composite. The effectiveness of these models is highly dependent on the validity of these assumptions. This section will consider the workings of several analytical models drawn from literature and provide comparisons between them.

5.1.1 Series and Parallel models

The simplest of analytical models are the series and parallel models; these models are defined by the assumption that each constituent element of the composite is arranged into a discreet layer, as illustrated for a two phase system in Figure 5.3.

In the series model the layers are orientated perpendicular to the direction of power flow. Using this assumption, it is possible to derive an equation for the bulk properties of the composite based on the one-dimensional heat flow equation (equation (5.1)). When this is done for the arrangement shown in Figure 5.3(a) the resulting equation is equation (5.2). If the layers are arranged perpendicular to the direction of power flow the parallel model is produced; equation (5.3) shows the equation for calculating the bulk properties in this configuration.

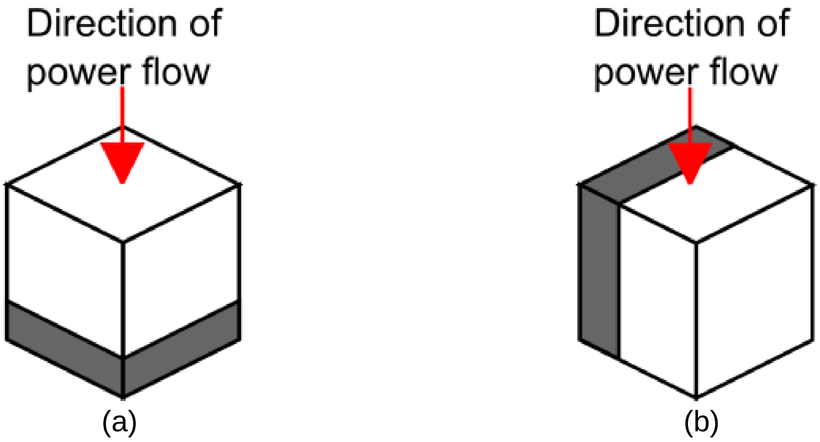

Figure 5.3 - Illustration of series and parallel models; (a) – series; (b) – parallel

$$R = \frac{L}{k\,A} \tag{5.1}$$

$$k_{series} = \frac{1}{\frac{1-\emptyset}{k_c} + \frac{\emptyset}{k_d}} \tag{5.2}$$

$$k_{parallel} = (1-\emptyset)\,k_c + \emptyset\,k_d \tag{5.3}$$

Where:

R	is the thermal resistance of a sample (K/W)
L	is the length of the sample along power flow axis (m)
k	is the thermal conductivity of sample material (W/m.K)
A	is the cross-sectional area of sample perpendicular to power flow (m^2)
Φ	is the volume fraction of filler material in sample
k_c, k_d	are the thermal conductivities of the continuous (epoxy) and discontinuous phases respectively (W/m.K).

Whilst the derivation of these models is simple, the assumed structure which they use is not representative of that found within a powder composite as in reality the two material phases will be mixed together and not in separate layers. To improve the accuracy of this model it is necessary to give more attention to the actual structure of the composite material.

5.1.2 Maxwell model

In an attempt to more accurately capture geometry of a composite material, Maxwell derived an equation for spherical particles within a medium [110]. This equation is expressed in equation (5.4). One key assumption of this model is that the composite is a dilute composite. (Here dilute is defined as a composite in which the particles are sufficiently well spaced so as to not influence each other, allowing them to be considered independently.) As a consequence of this assumption, this model is only truly valid for composites with a low filler concentration, as when filler concentration increases, the space between the particles decreases, violating the dilute assumption. Furthermore, as the filler concentration increases the particles tend to form agglomerates. This behaviour is not considered by this equation and consequently the thermal conductivity of the composite is underestimated in such cases. To address this, it is necessary to incorporate a mechanism into the model which allows for the consideration of the composite structure at all filler levels.

$$k_{Maxwell} = k_c \frac{2k_d + k_c + \emptyset(k_d - k_c)}{2k_d + k_c - 2\emptyset(k_d - k_c)} \tag{5.4}$$

5.1.3 Pal models

The Pal models are built around the assumption that if the thermal conductivity of a composite which has a filler concentration of *Φ* is known, then from this it should be possible to determine the thermal conductivity of a composite with a filler concentration of *Φ*+*dΦ*, and by extension it should be possible to determine the thermal conductivity of a composite of any given filler concentration. To achieve this, the model uses a technique called the differential effective mean approach (DEMA) [111]. The initial basis of this model is arrived at by integrating Maxwell's model and will be referred to as Pal1 (equation (5.5)). This model can be further enhanced through the inclusion of a maximum filler concentration parameter (Φ_{max}). Two different approaches to incorporating this parameter are considered by the author, both of which are included here as equations (5.6) and (5.7), and are referred to as Pal2 and Pal3 respectively. By including the Φ_{max} parameter it is possible for the model to reflect the effects of the filler powder producing agglomerates within the composite on the bulk thermal conductivity.

$$\left(\frac{k_{Pal1}}{k_c}\right)^{1/3} \left(\frac{k_d - k_c}{k_d - k_{Pal1}}\right) = \exp(\emptyset) \tag{5.5}$$

$$\left(\frac{k_{Pal2}}{k_c}\right)^{1/3} \left(\frac{k_d - k_c}{k_d - k_{Pal2}}\right) = \exp\left(\frac{\emptyset}{(1 - (\emptyset/\emptyset_{max})}\right) \tag{5.6}$$

$$\left(\frac{k_{Pal3}}{k_c}\right)^{1/3} \left(\frac{k_d - k_c}{k_d - k_{Pal3}}\right) = \left(1 - \frac{\emptyset}{\emptyset_{max}}\right)^{-\emptyset_{max}} \tag{5.7}$$

Where:

Φ_{max} is the maximum filler concentration

5.1.4 Lewis/Nielsen model

The method proposed by Lewis and Nielsen also incorporates a Φ_{max} parameter. In this instance a further parameter A_{LN} is also included to reflect the shape of the filler particles. Example values for A_{LN} for different filler shapes can be found in [112] and in the case of spherical particles the value of A_{LN} is 1.5. By incorporating this parameter it is possible for this model to not only consider the formation of agglomerates within the composite, but also account for the effect which varying the filler material shape may have on performance. This is not a major concern if the filler particles are spherical (or can be approximated as such as this is the assumption which most models make), however it does have advantages in other cases (for example if the filler is composed of long fibres).

$$k_{LewisNielsen} = k_c \frac{1 + A_{LN} B \emptyset}{1 - B\psi\phi} \tag{5.8}$$

$$B = \frac{k_d/k_c - 1}{k_d/k_c + A_{LN}} \tag{5.9}$$

$$\psi = 1 + \left(\frac{1 - \phi_{max}}{\phi_{max}{}^2}\right)\phi \tag{5.10}$$

Where:

A is a parameter determined by the shape of the filler particles

5.1.5 Comparison of models

Predictions from all of the analytical models discussed previously are shown plotted in Figure 5.4. The first observation which can be drawn from this figure is that the parallel model deviates substantially from all of the other models being considered. This can be attributed to how the model is derived, as in this model it is assumed that the high thermal conductivity filler material is arranged into a singular piece which reaches from the location of heat generation to the location of heat extraction, effectively producing a short circuit through the material. As the filler is actually a powder, and is not arranged in this way, this leads to a substantial overestimation of the material properties.

Secondly, it can be observed that the other models all yield relatively similar values for low filler concentrations; however deviations occur at higher fill factors. This can be explained by considering the structure of the composite material. At low concentrations there are few filler particles within the composite and consequently the formation rate of agglomerates is relatively low; all of the models are equipped to deal with such a scenario. In the case of higher filler concentrations, the chances of agglomerates forming are increased; therefore the models are differentiated by the manner in which this is dealt with. Models which do not account for such effects present a lower prediction for the thermal conductivity of the composite, (this is likely to be an underestimation), while more complete models which include provision for agglomerates give higher thermal conductivity predictions.

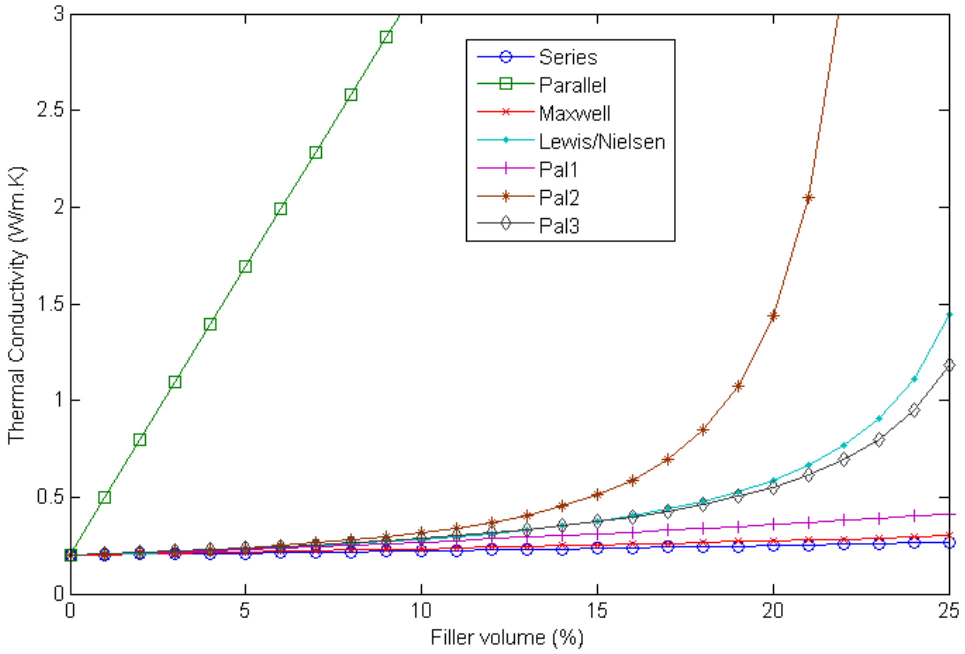

Figure 5.4 – Analytical models plotted with respect to filler concentration (k_c = 0.2 W/m.K; k_d = 30 W/m.K; A = 1.5; Φ_{max} = 0.28, where required)

5.2 Numerical modelling of composite materials

An alternative approach to the use of analytical models to analyse composites is the use of numerical methods. To employ this approach it is necessary to produce a model which represents the composite in a form which can be solved numerically. This is achieved through the use of a steady state thermal FEA simulation. As a starting point for this analysis a section of composite is divided into a series of blocks. Each of these blocks is then assigned the properties of either the potting compound, or the filler material, so as to achieve the desired filler volume. To solve this model, the bottom surface of the model is constrained to a fixed temperature and a fixed power is applied to the top surface; the bulk thermal conductivity can be determined from the average temperature on the top surface of the model using equation (5.1). An illustration of the configuration used in FEA is shown in Figure 5.5; in this instance the sample is shown divided into five pieces along its horizontal and vertical dimensions. In reality, the simulations which were run for the purpose of this work were divided into more pieces than this; however the principle is still the same. In Figure 5.6 the effect that grid size has on the FEA simulation results is shown. These results were obtained through the use of the Ansys FEA simulation package, using a 2D steady state thermal analysis. As the simulations are generated by randomly assigning the filler properties to the required number of cells to achieve the desired fill factor it is necessary to repeat the simulations a number of times to reduce the impact of a particular randomly generated configuration being a particularly good/poor example of the composite. To this end the data presented in Figure 5.6 shows 100 simulations for each filler concentration of interest. It is observable from this that dividing the sample up into a larger number of cells yields results which exhibit a tighter grouping between runs. This can be attributed to the fact that as the number of cells increases, the probability of producing an extreme configuration (good or bad) is decreased resulting in more consistent results.

A possible extension of this simulation is to consider the problem in 3D; this is formulated by replacing the square cells with cubes and adding a third dimension to the problem. Results of this simulation (also performed in Ansys, but employing 3D elements) are presented in Figure 5.7 along with the analytical results obtained from the Pal 3 model. It can be observed that the trend exhibited by the FEA simulation shows a steady linear increase in the thermal conductivity values, while Pal 3 shows an increase more exponential in shape. Additionally it is worth noting that the predictions obtained from the 3D model are higher than those seen in the 2D simulations of comparable filler volumes. Despite differing in curve shape the results obtained from the 3D model are of a comparable order of magnitude to the results obtained from the Pal 3 model.

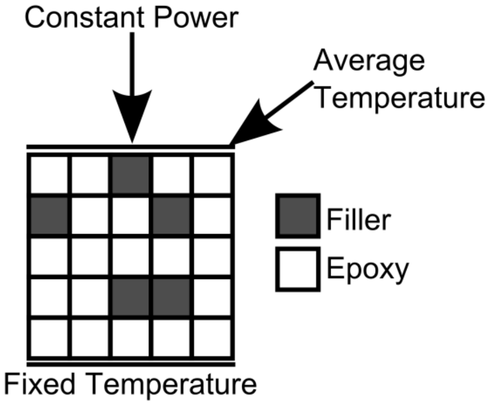

Figure 5.5 - Illustration of FEA configuration, shown with 20 % filler volume

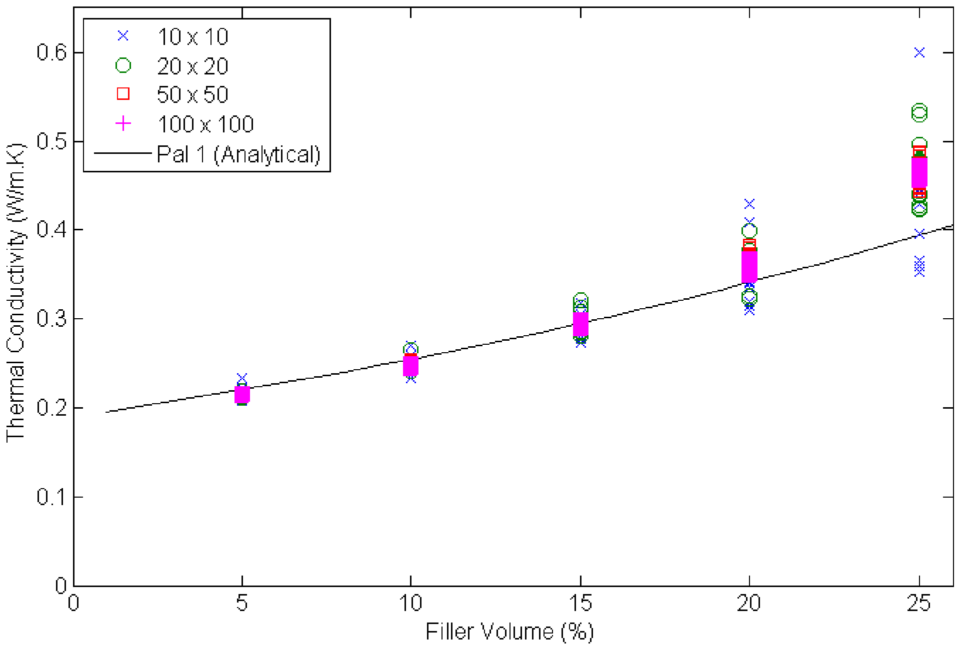

Figure 5.6 – 2D FEA composite thermal conductivity predictions (including effect of grid size)

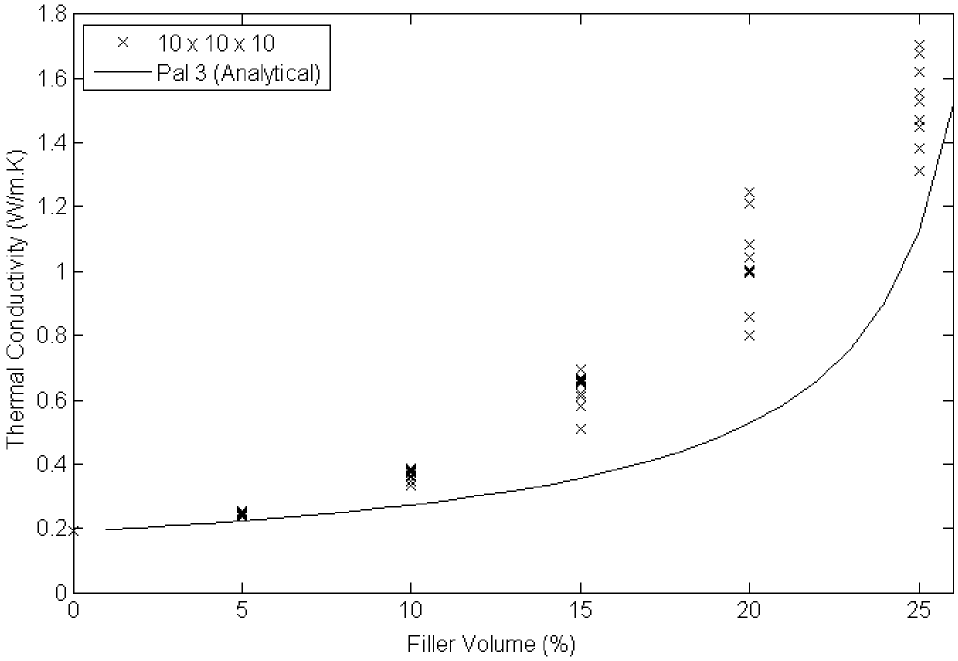

Figure 5.7 - 3D FEA composite thermal conductivity predictions

As the results obtained through these numerical methods are comparable to those obtained from analytical models there is little justification for the use of this method over analytical methods when the increased running time for the numerical methods is considered. The exception to this would be cases in which the filler is arranged in a very specific manner which would benefit from being replicated precisely in the model. In the application being considered, the filler is randomly arranged and so this is not the case.

5.3 Empirical modelling of composite materials

An alternative approach to using the methods described previously is the use of empirical models. These models contain parameters which can be tuned to represent the performance of manufactured composite samples. The drawback to this approach is that since these parameters are empirical, it is necessary to produce actual composite samples to determine them. Consequently, unlike the other methods described here, it is not possible to utilise these models during the initial design phases without first performing experimental work.

An example empirical model is the model proposed by Agari and Uno [113] (equation (5.11)); in this instance the empirical constants are C_1 and C_2. It will also be shown later in this chapter that it is also possible to utilise some of the analytical models discussed previously (for example those proposed by Pal and Lewis/Nielsen) in an empirical fashion. This is achieved by repurposing the material property values as empirical constants.

$$\log\left(k_{AgariUno}\right) = \phi\, \mathrm{C}_2 \log(k_d) + (1-\phi)\log(C_1 k_c) \tag{5.11}$$

Where:

C_1, C_2 are empirical constants determined from the composite

5.4 Production and evaluation of test samples

To determine the performance of the models discussed in this chapter, composite samples with varying concentrations of filler were manufactured. These composites were manufactured using an epoxy as the base material and aluminium oxide powder as a filler material.

5.4.1 Epoxy Properties

The epoxy which was selected to be used as the base material for the composite samples was ER1448 manufactured by electrolube. This epoxy was selected for its low viscosity, an important property, as a low viscosity material is easier to work with during the mixing process. The relevant properties of this epoxy are presented in Table 5.1.

Thermal Conductivity (W/m.K)	0.19
Density (g/cm^3)	1.10
Gel time (minutes)	25
Viscosity (mPa.s)	250
Dielectric Strength (kV/mm)	12
Temperature Range (°C)	-50 - 150

Table 5.1 - Material Properties of ER1448 Epoxy resin (Data from [114])

5.4.2 Filler Properties

The filler selected for this work is aluminium oxide powder. During the filler selection process the most important property considered was that the material was an electrical insulator. This is particularly important as the use of an electrical conductor introduces the risk of producing an electrically conductive epoxy, which could short circuit the component. The selection of aluminium oxide was made since it meets this requirement, while exhibiting a reasonably high level of thermal conductivity. The key properties of the aluminium oxide powder used in the production of the composite samples are shown in Table 5.2.

Thermal Conductivity (W/m.K)	16.6 – 36
Density (g/cm^3)	3.97
Poured Density (g/cm^3)	0.84
Tapped Density (g/cm^3)	1.11
Dielectric Strength (kV/mm)	9.1 – 17.7

Table 5.2 - Material Properties of aluminium oxide powder (Data from [106] and experimental work)

Two parameters which are included in Table 5.2 and which require further explanation are the pour density and tapped density of the powder. These are commonly employed metrics used to express the bulk density of powders. This is necessary due to the fact that in a powdered material the particles do not tessellate fully and consequently air is trapped between them. This makes the measured density of the powder appear to be lower than its theoretical chemical density. This measured density can be used to determine the maximum filler concentration which is achievable for a given powder. The more useful and meaningful of the two metrics will depend upon the manner in which the powder is being used.

5.4.2.1 Poured Density

The poured density is a measure of how well the powder particles pack together when they are not agitated; this is determined using the apparatus shown in Figure 5.8. To use this equipment the powder is poured through the funnel into the container below. It is important that the container is not disturbed during the pouring process as this will result in the powder particles being redistributed, resulting in a higher reported value for the poured density than is actually the case. When this container is full, the mass of the powder is weighed. Using this value and the known volume of the container the poured density of the powder can be calculated. In the case of the aluminium oxide powder used in this work, the poured density was measured as 0.84 g/cm^3; this represents 21.2 % of the theoretical density of the powder.

Figure 5.8 - Poured density measurement setup

5.4.2.2 Tapped density

The tapped density of a powder is a measure of how well the powder particles pack together when the powder is agitated. This value is higher than the poured density as the movement of the particles allows them to rearrange into a more efficient packing arrangement. Consequently, this packing factor may only be actually achievable within a composite if sufficient agitation is provided to the powder during the manufacturing process. The tapped density is determined using the equipment shown in Figure 5.9. Here, a known mass of powder is placed into a graduated measuring cylinder, the cylinder is then tapped on a solid surface repeatedly until the level of the powder reaches a stable value. Using the volume measurement from the measuring cylinder, combined with the known mass of the powder, the tapped density can then be calculated. In this case the tapped density was measured as 1.11 g/cm^3, which is 28.0 % of the theoretical density.

Figure 5.9 - Tapped density measurement setup

5.4.2.3 Powder physical properties

In addition to these tests the shape and size of the powder particles was also considered. Firstly the powder was examined under a microscope to observe the shape of the powder particles; an image captured from this can be seen in Figure 5.10. From this image it can be seen that although the particles are not precisely spherical, they can be approximated to be as such. It can also be observed that the particles vary in size between 20 μm and 160 μm.

Further to this, visual inspection the powder was also examined using particle size distribution equipment. This test was repeated three times to ensure that the powder was remaining in the same state throughout the test and was not forming agglomerates or breaking down during the tests; the outputs from these tests can be seen in Figure 5.11. It can be observed that the three runs show good agreement with each other, verifying the stability of the powder throughout the test. It can also be seen that 90 % of the particles are sized between 22.5 μm and 152.4 μm in size, with a minimum size of 0.85 μm and a maximum size of 219.4 μm. This shows good agreement with the microscope image.

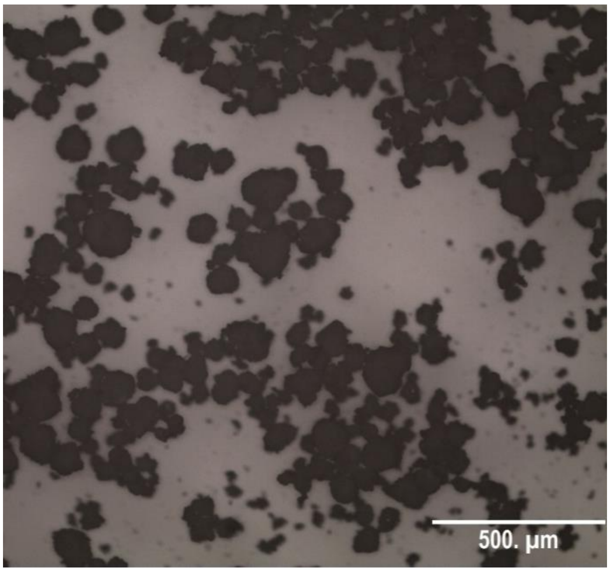

Figure 5.10 - Microscope image of filler powder particles

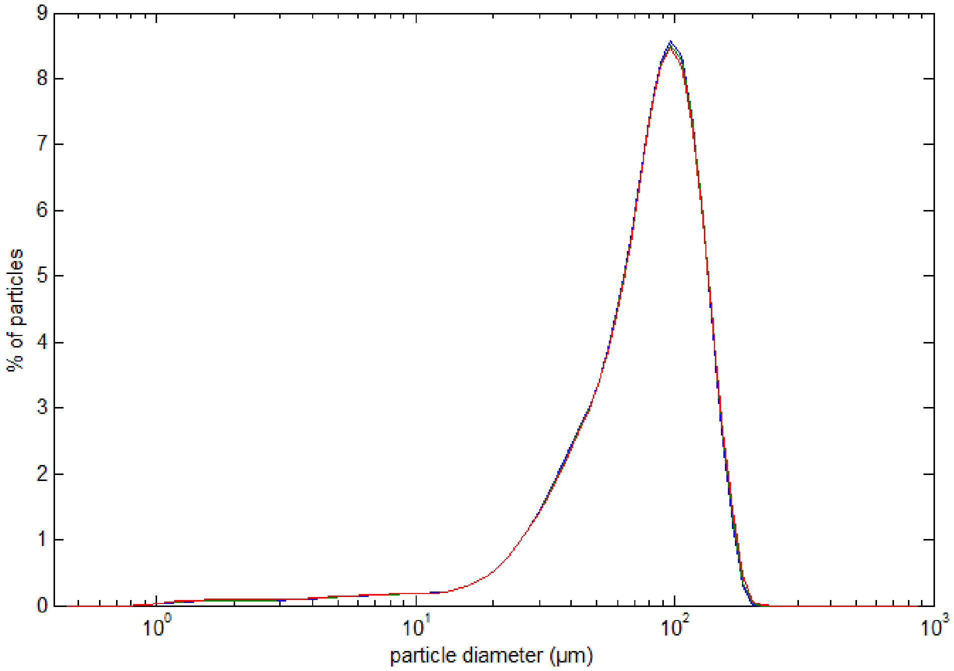

Figure 5.11 - Particle size distribution of filler material

5.4.3 Manufacturing methods

The production of the samples for this work employed three different methods. This was done to allow the different methods to be compared. Additionally as each method results in a different filler distribution, comparison of them also allows wider conclusions to be drawn on the effects of filler distribution within the composite materials.

5.4.3.1 Mixed method

The first method utilised in this work is referred to as the mixed method. In this method the constituent parts of the epoxy are combined together according to the manufacturer's instructions. The filler material (which has been pre-weighed and divided into appropriate quantities) is then incrementally added to the epoxy, during this time the epoxy is stirred. When all the filler is added, further stirring is performed until the resulting composite has a uniform constancy. This composite is then transferred to the mould and allowed to cure at room temperature.

5.4.3.2 Rotated method

Observation of samples produced using the mixed method show a visibly uneven filler distribution within the composite. This can be observed in Figure 5.13(a) as the distinct white band along the lower portion of the sample. In an attempt to alleviate this the rotated method was devised; this method employs the same mixing technique as that used to produce the mixed samples, however, the treatment of the sample during the curing time differs. In the case of the rotated samples after the composite has been placed within the mould, the mould is sealed and placed within the apparatus shown in Figure 5.12. This rig allows the samples to be rotated during the cure time to prevent the settling of the filler particles. Observation of Figure 5.13(b) demonstrates the success of this process, in which there is no visible formation of a filler layer towards the base of the sample.

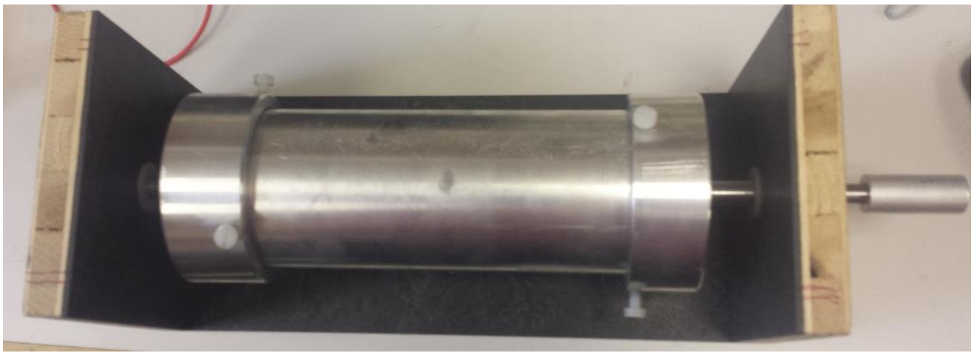

Figure 5.12 - Rig produced to rotate samples during cure time

5.4.3.3 Settled method

The third technique used to manufacture samples is referred to as the settled method. This production technique is designed to replicate the case in which all of the filler is in the lower portion of the sample. This allows highly non-uniform filler distributions to be considered. This is achieved by placing the filler material into the base of the mould, after which the epoxy is poured on top. As it is still liquid at this point the epoxy infiltrates into the filler layer. It can be seen from Figure 5.13(c) that the filler in the sample produced by this method is much less uniformly distributed, with the white filler band in this image appearing in a far more pronounced way.


(a) (b) (c)

Figure 5.13 – Side view of samples produced using the three described methods each with 5 % filler concentration (by volume): (a) – Mixed; (b) – Rotated; (c) – Settled

5.4.3.4 Sample production

All of the samples which were manufactured had a base size of 40 mm x 40 mm. Samples were produced by all three methods with a thickness of 40 mm. Further to this, samples with a thickness of 20 mm; 10 mm and 5 mm were also manufactured using the mixed and settled methods. For each size a range of filler concentrations from 0 % to 23 % (by volume) in increments of 5 % were produced. The limit of 23 % is imposed by the bulk density of the powder. While it is possible to exceed the limits imposed by the poured density of the powder (21.2 %) the tapped density (28 %) is not reached. This is due to the level of agitation of the filler required to achieve this packing density: in the case of the mixed method, the mixing action is not sufficient to achieve this level of packing. It should be noted that when the filler is added to the epoxy, the viscosity of the composite is considerably higher than the base epoxy, making the agitation harder and also making it more difficult to work with practically. In the settled method, packing the filler into the mould more tightly is possible; however this then inhibits the ability of the epoxy to penetrate into the filler layer fully.

5.4.4 Thermal conductivity testing

To evaluate the bulk thermal conductivity of the samples the experimental setup illustrated in Figure 5.14 was used. This configuration operates by placing the sample under test between a heat sink and a power resistor. All of the other surfaces of the sample are thermally insulated using polystyrene. When this rig is in operation, a known power is dissipated within the resistor and the temperature gradient developed across the sample is measured using thermocouples. From this temperature gradient and the known power dissipated within the power resistor, the thermal resistance of the composite sample can be determined using equation (5.12), which is obtained by rearranging equation (5.1). This assumes that all of the power dissipated within the power resistor passes through the sample under test. To account for the fact that a small amount of power will escape through the insulation the setup was calibrated using data obtained by testing a sample of polypropylene with the same dimensions as the sample under test. Polypropylene was selected due to its known properties, in addition to having a thermal conductivity value which is of the same order of magnitude as the samples being tested. Prior to testing the samples a thin layer of heat sink compound was applied to the top and bottom surfaces to reduce the impact of the contact surface roughness.

In the case of the cubic samples, testing was performed in all three axes; in the case of thinner samples, testing was only performed in the x-axis. An illustration of the axis definitions with respect to the samples can be seen in Figure 5.15.

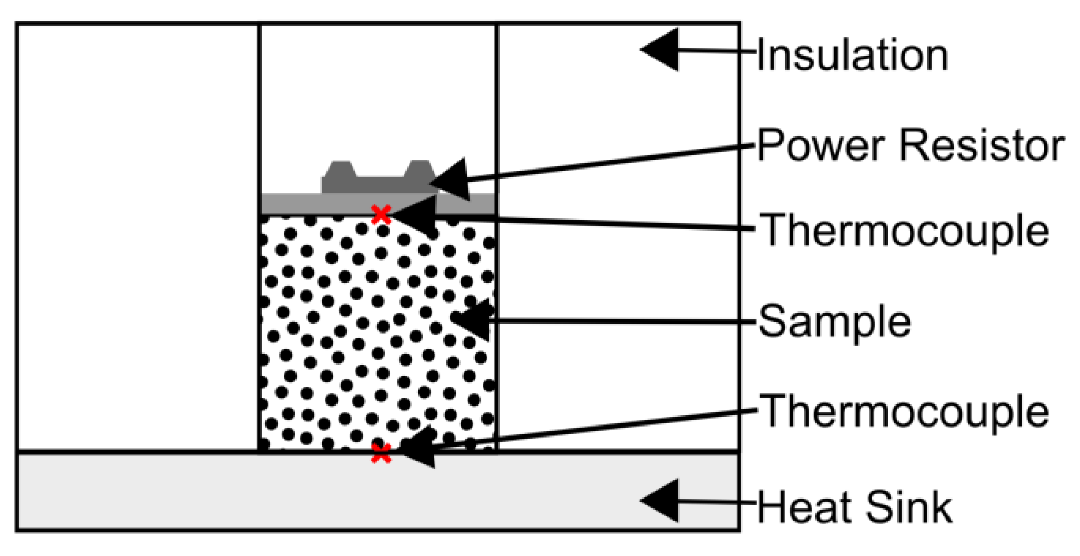

(a)

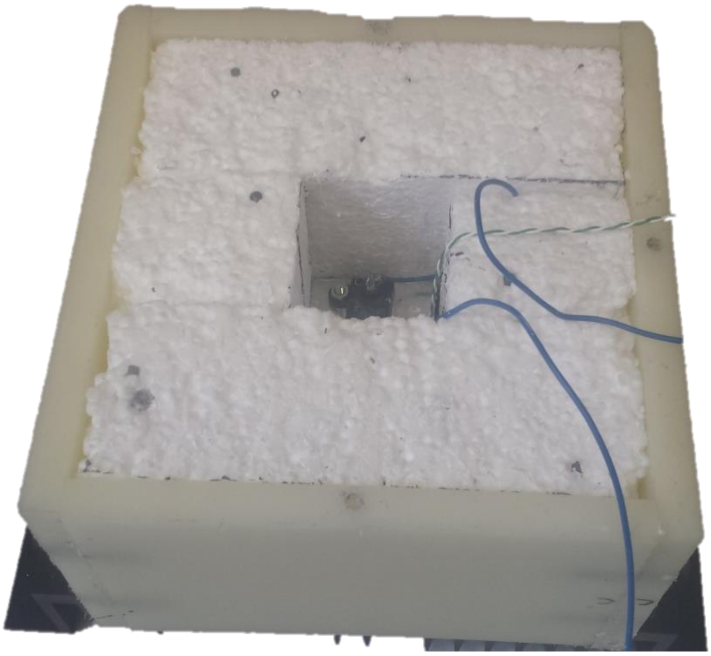

(b)

Figure 5.14 – (a) diagram of test rig used to determine bulk thermal conductivity of samples; (b) – photograph of rig (Top insulation removed)

$$k = \frac{LP}{TA} \tag{5.12}$$

Where:

k	is the bulk thermal conductivity of the sample (W/m.K)
L	is the length of the thermal path (the height of the sample) (m)
P	is the power dissipated within the resistor (W)
T	is the temperature gradient across the sample under test (K)
A	Is the cross sectional area of the sample under test (m^2)

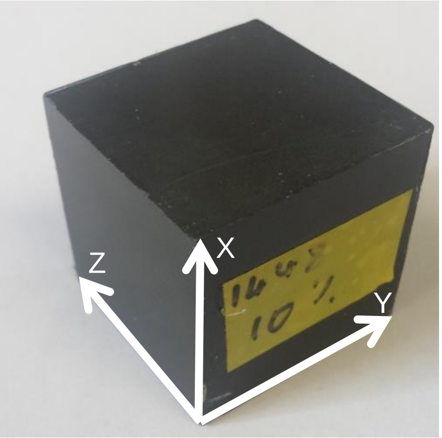

Figure 5.15 - Definition of axes with respect to sample

5.4.5 Experimental results

All of the manufactured samples were characterised using the procedure outlined in section 5.4.4. A summary of the measured bulk thermal conductivities can be seen in Figure 5.16.

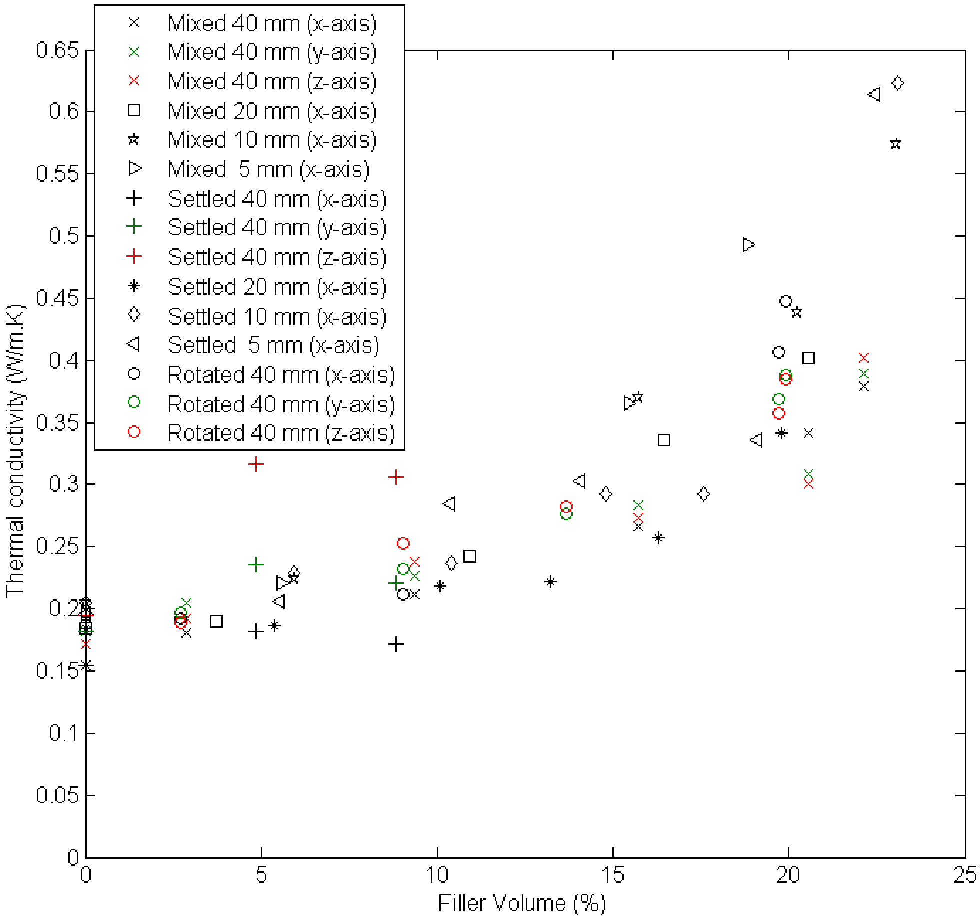

Figure 5.16 - Thermal conductivity of all manufactured samples

Considering the data shown in Figure 5.16 it can be seen that the experimental results exhibit slight differences in filler concentrations. This is because the filler concentrations were calculated based on the density of the manufactured samples after curing had occurred. This is achieved using equation (5.14), which is obtained by rearranging equation (5.13).

$$D = \emptyset D_d + (1 - \emptyset) D_c \qquad \textbf{(5.13)}$$

$$\emptyset = \frac{D - D_c}{D_d - D_c} \qquad \textbf{(5.14)}$$

Where:

ϕ	is the filler volume
D	is the density of the composite (g/cm^3)
D_c	is the density of the continuous phase (Epoxy) (g/cm^3)
D_d	is the density of the discontinuous phase (Filler) (g/cm^3)

When considering these results it is helpful to consider them in two separate groups. The first group contains the samples which were produced by mixing the epoxy and filler prior to placing it into the mould (*Mixed* and *Rotated*); the second group contains the samples in which the epoxy was added to the filler which was already within the mould (*Settled*).

Figure 5.17 and Figure 5.18 show the experimental results divided in this manner. Also included in these figures are the analytical models described earlier in this chapter. For the purposes of models which require a maximum filler concentration the value measured during the tapped density tests is used (28 %). While it would have been possible to use the maximum value which was achieved when producing the composites, the determination of this value is more difficult due to the fact that composites have to be manufactured to identify this value. Furthermore, the use of a lower value for the maximum filler concentration value increases the predicted thermal conductivity values generated by the models. It can be observed from Figure 5.17 and Figure 5.18 that this would make the prediction from the models which employ this parameter worse.

For the filler shape property required by the Lewis/Nielsen model the value for spheres is used (1.5). From these figures it can be observed that none of the analytical models fully capture the performance of the composite samples over the full range of filler levels.

Looking at the experimental results it can be observed that the data can be divided into three categories: 10% (dilute fill); 10% to 20% (intermediate fill) and 20%+ (fully filled). In dilute samples the filler loading level is sufficiently low that the filler has only a small effect on the thermal conductivity of the overall composite. This means that the particle arrangement is largely unimportant and the effects of manufacturing on filler distribution can generally be ignored.

Samples with filler levels in the intermediate range show a more apparent variation by manufacturing method; this can be attributed to the differing levels of uneven filler distribution. When using composites in this filler range it is important that the effects of the manufacturing method are considered, since the assumption of a homogeneous sample has the potential to over predict the thermal performance of the composite. In this range of filler values, the rotated samples exhibit a higher thermal conductivity than the mixed samples and the mixed samples exhibit a higher thermal conductivity than their settled counterparts. As has already been stated, the rotated samples visibly have the most uniform filler distribution. From this it can be inferred that the mixed samples are closer to homogenous than the settled samples and although filler settling can be observed in both cases, the settling in the mixed samples is not as complete as in the settled samples; hence the improved performance.

In the fully filled samples it is possible to assume that the filler distribution is homogenous, regardless of the manufacturing technique employed. This is because these samples approach the maximum fill level, therefore, the filler is distributed throughout the whole sample and settling cannot occur regardless of manufacturing method.

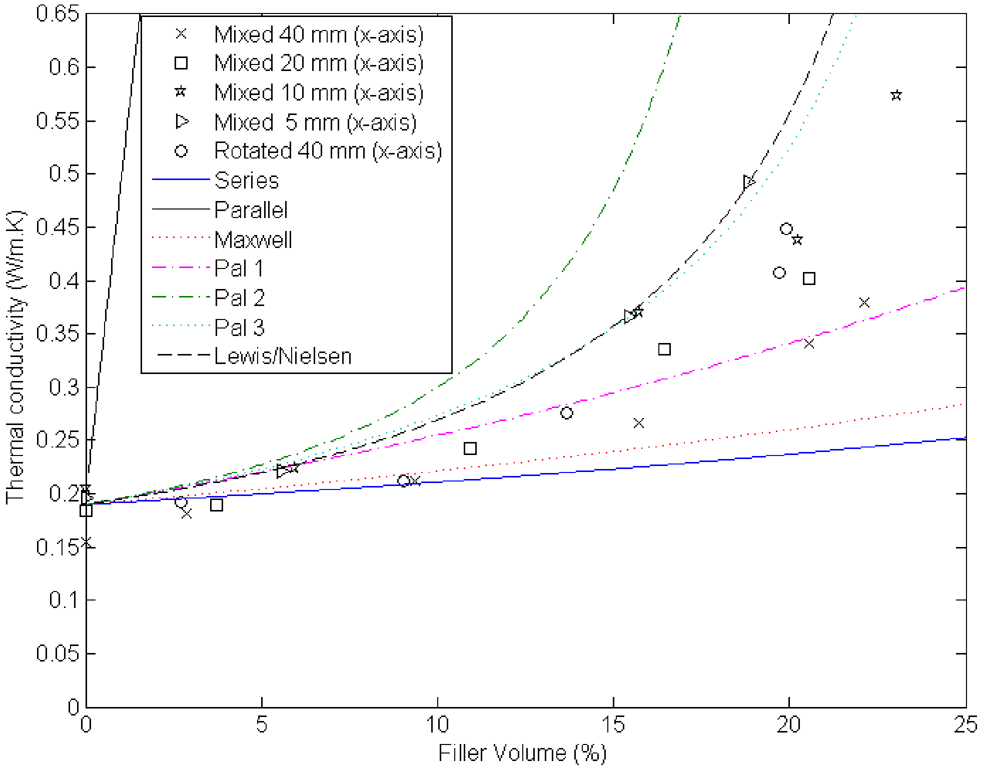

Figure 5.17 - Mixed and Rotated experimental results with analytical models

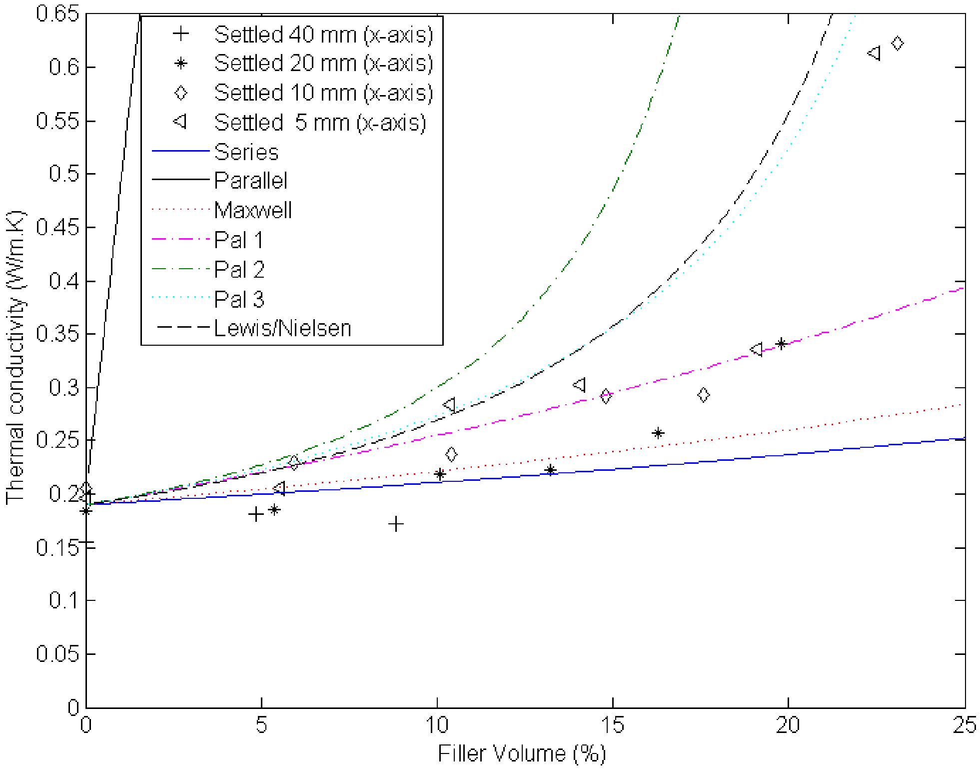

Figure 5.18 - Settled experimental results with analytical models

5.5 Empirical use of analytical models

It has been shown in the previous section that analytical models do not fully capture the experimental data over the full range of filler values. As was mentioned when discussing empirical models it is possible to utilise some analytical models in an empirical fashion. This is achieved by adjusting the parameters used to represent the material properties in an empirical manner. Of the analytical model considered here Pal 2, Pal 3 and the Lewis/Nielsen models are suitable to be used in this way. The use of analytical models which have been tuned empirically is demonstrated in Figure 5.19 and Figure 5.20. The tuning parameters used in these models are listed in Table 5.3. In the case of the mixed/rotated samples, a reasonable approximation of the experimental data is achieved here. It should be noted that the settled samples are overestimated by the model during the intermediate filler range. This is due to the fact that the model still assumes an even filler distribution, despite its use in an empirical manner.

Pal 2	Φ_{max} = 0.8070	
Pal 3	Φ_{max} = 0.4452	
Lewis/Nielsen	Φ_{max} = 0.3531	A = 1.4459
Agari/Uno	C_1 = 0.8767	C_2 = 0.8066

Table 5.3 - Analytical model tuning parameters

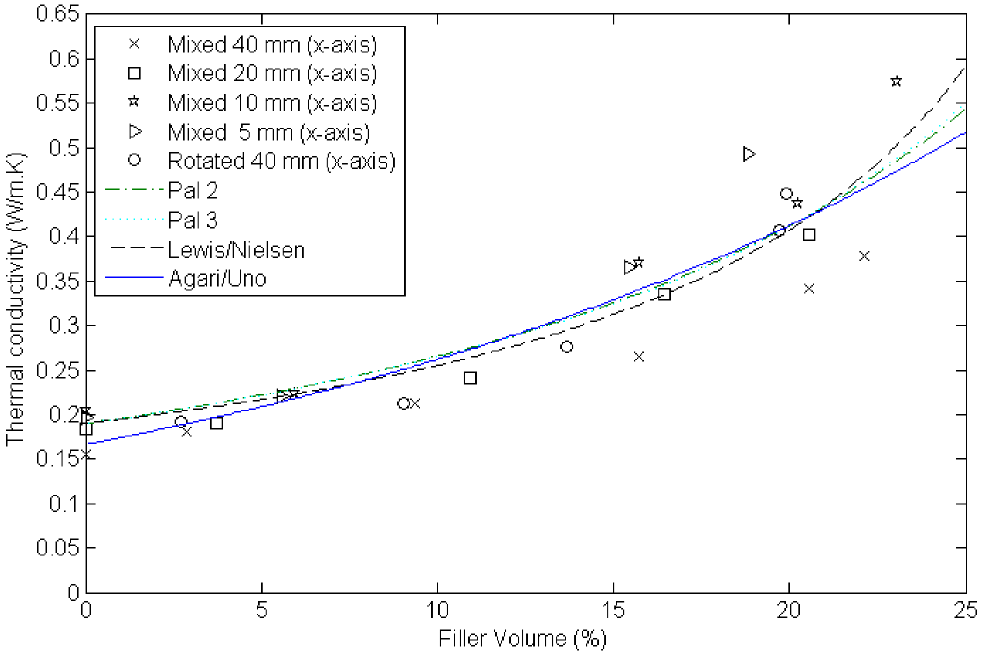

Figure 5.19 - Mixed and Rotated experimental results with empirically fitted models

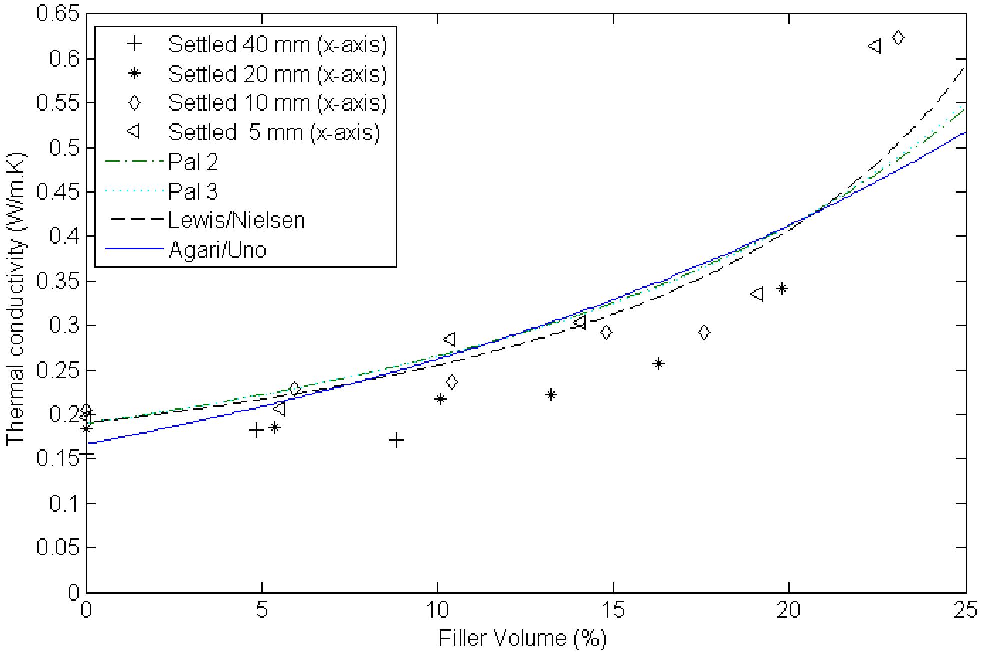

Figure 5.20 – Settled experimental results with empirically fitted models

5.6 Conclusions

In this chapter analytical, numerical and empirical methods have been considered as methods of modelling composite materials. The first conclusion which can be drawn from this is that, generally speaking, the use of numerical methods does not offer any advantage over the existing analytical models. It does however, carry a significant time penalty when compared to these models and so is less appropriate for general use.

It has also been shown that models which include more details about the composite structure yield predictions which are more accurate than those based on assumptions. By extension, empirical models that use data from real samples produce better predictions than standalone analytical models. However, as this accuracy is obtained through the production of samples, this approach may not be suitable for the design phases.

It has been shown in this chapter that substituting encapsulants for composite encapsulants offers the potential to improve the thermal conductivity of the encapsulants. A variety of methods of modelling encapsulant composites have also been discussed, with their performance being compared to experimental results obtained from the production of composite samples. In the next chapter, consideration is given to cases where composites are used in more realistic assemblies that consist of an inductor in addition to the composite encapsulation under consideration. In this way it is possible to examine the accuracy of the models discussed here when considered in a more practical configuration.

Chapter 6

Composite encapsulant potted inductors

In the previous chapters, consideration has been given to improvements in component thermal performance through the use of alternative winding insulations. Additionally, methods of modelling the bulk thermal conductivity of encapsulant composites have also been considered in the previous chapter. In this chapter, work is done to further expand on this by using a composite to encapsulate a prototype inductor. For the purpose of comparison, an inductor of identical construction potted using standard, unfilled epoxy is also manufactured.

The performance of the two prototypes is compared, with finite element analysis (FEA) being used to evaluate their performance. The FEA model is also used to evaluate the accuracy of performance predictions made using the values obtained from the analytical models discussed in the previous chapter (which contain errors in the prediction of the bulk composite properties) to represent the bulk thermal conductivity of the composite.

The novelty in this chapter is in the discovery that the temperature predictions obtained from the FEA model do not vary linearly with respect to the value used for the thermal conductivity in the encapsulant region. This leads to conclusions regarding the required accuracy to which the bulk composite properties need to be known to achieve a desired prediction accuracy of 10 % for the overall model performance.

6.1 Inductor Specification

To evaluate the performance of a composite encapsulant in a realistic application, it was necessary to produce an inductor which was suitable for encapsulation. For this purpose an inductor for a 2 kW interleaved boost convertor was designed. The specification of this inductor is listed in Table 6.1; a photograph of one of the prototypes can also be seen prior to potting in Figure 6.1.

Core	E42/21/20, N97 ferrite core (In E-E configuration)	
Air gap	0.94 mm (All legs)	
Windings	Copper litz wire (19 strands of 0.4 mm wire)	
Winding configuration	21 turns (arranged in 2 layers)	
Inductance	99.6 µH	
Saturation Current	20 A	
Encapsulant	ER1448 Epoxy	
Encapsulant filler	N/A	20 % (by volume) aluminium oxide powder

Table 6.1 – Specification of prototype potted inductors

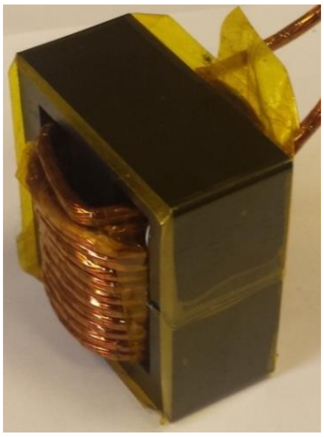

Figure 6.1 - Prototype inductor (Prior to potting)

6.2 Encapsulation of prototypes

Under atmospheric conditions, prior to potting, the component is surrounded with air. Consequently, when the potting compound is added to the mould it is necessary for said air to escape through the potting compound. Additionally, a further source of trapped air is air which is mixed into the epoxy during the mixing process which will also contribute to voiding. To prevent the formation of voids, it is necessary for the trapped air to reach the top surface of the epoxy and for the resulting bubble to burst, releasing the air. Performing the potting process in a reduced pressure environment addresses these issues in two different ways. Firstly, by removing most of the air from around the component prior to adding the potting compound, it does not become entrapped around the component. Secondly, due to the reduced air pressure in the chamber, any trapped air bubbles will grow in size (due to the difference in pressure between the chamber and the trapped air), increasing their buoyancy and aiding escape.

To prevent the entrapment of air within the encapsulant material it was decided that the potting process should be performed under vacuum. The equipment employed to achieve this can be seen in Figure 6.2. Here the component to be potted is placed within a mould which is then placed within the vacuum chamber. The reservoir that holds the encapsulant to be used during the potting process is positioned above the vacuum chamber and is connected to a valve external to the chamber. This is in turn connected to a feed-through into the chamber and finally, to the mould through two connection points. Multiple connections are employed to ensure that the mould fills evenly and to ensure that the mould can still be filled if one of the connections becomes blocked.

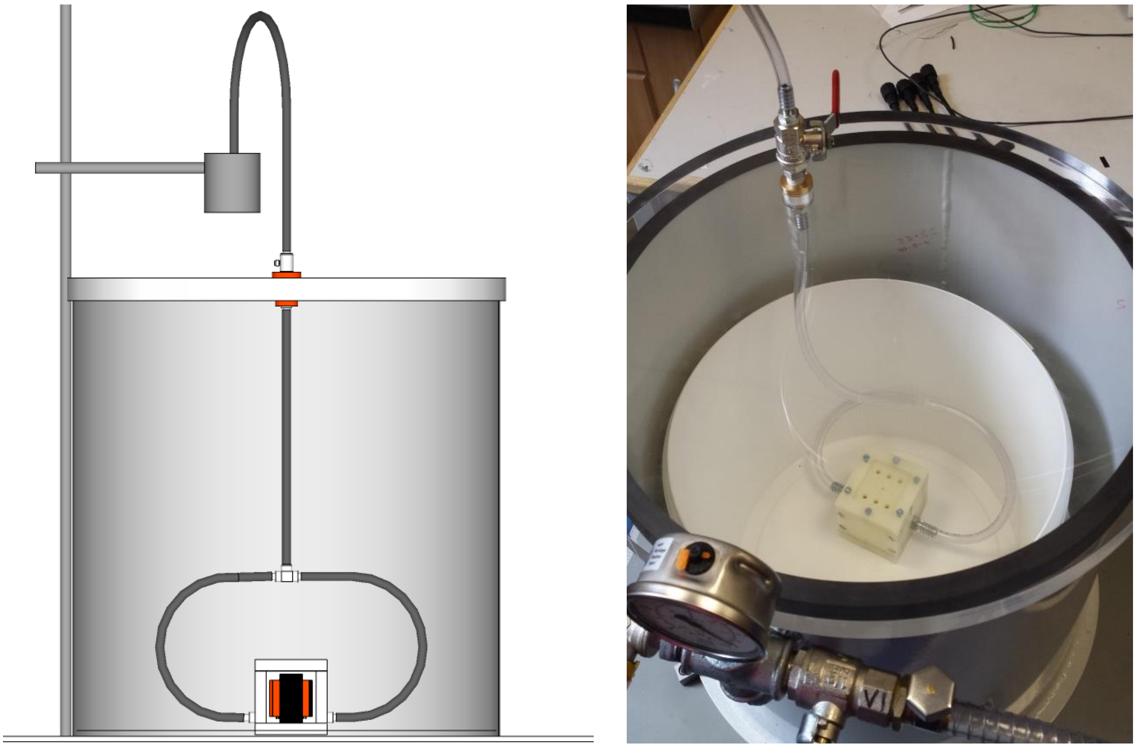
(a) (b)

Figure 6.2 - Vacuum potting equipment used for potting components: (a) – cross section view of vacuum chamber; (b) – Photograph of vacuum chamber prior to potting process

When potting a component using this configuration the pressure is reduced considerably within the chamber (~20 mbar) compared to environmental pressure using a vacuum pump. In this state, when the valve connected to the potting compound reservoir is opened, the low pressure within the chamber causes the epoxy to be pulled in, filling the mould. When the mould has been filled the epoxy valve is closed, resealing the chamber. During this process air bubbles can be observed escaping from the top of the mould. The chamber is kept under vacuum until bubbles are no longer observed, at which point the chamber is returned to atmospheric pressure. The removal of air from the assembly during the potting process is important as air bubbles within the liquid epoxy will be trapped as it solidifies, resulting in voids in the encapsulation, compromising the thermal performance of component.

Using the vacuum equipment two prototype inductors were produced, both of which were manufactured using the same epoxy and aluminium oxide filler discussed in the previous chapter. The first of these inductors was potted using standard epoxy; the second used the same epoxy but also included 20 % (by volume) aluminium oxide filler. This was mixed together using the method referred to in the previous chapter as the ‘mixed’ method. These potted prototypes can be observed in Figure 6.3. As both prototype inductors were structurally the same, this allows the enhancement achieved by using the composite encapsulant to be considered in isolation, while utilising the composite in a realistic application.

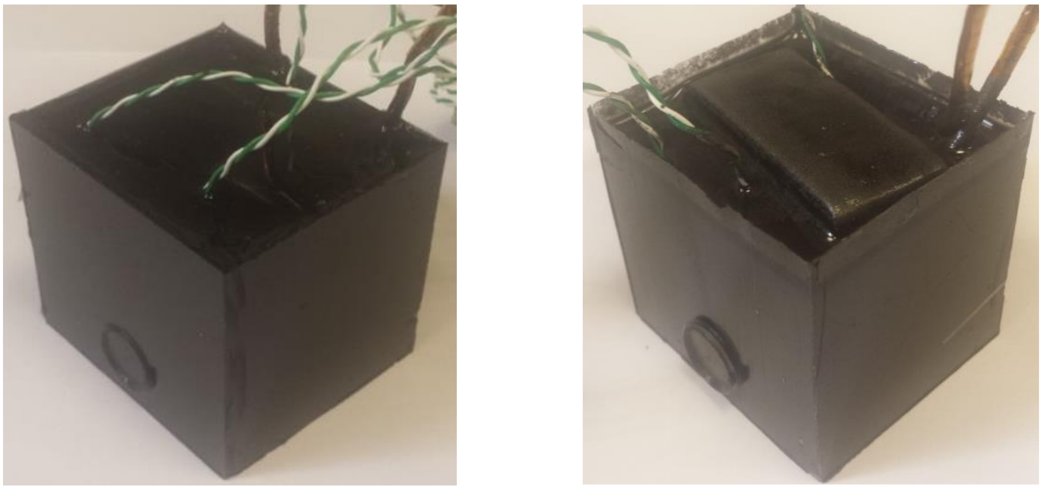

(a) (b)

Figure 6.3 - Potted prototype inductors: (a) – potted using standard epoxy; (b) – potted using 20 % filler composite

6.3 Testing methods

Prior to the encapsulation of the prototypes three k-type thermocouples were mounted to the inductor to allow the monitoring of temperatures inside the epoxy. These thermocouples were mounted:

1. On the core centre leg, close to the air gap between the two core halves
2. On the inside of the winding, mounted half way up
3. On the outside of the winding, mounted halfway up

Locations 1 and 2 were chosen as simulation showed that these would be the hottest areas within the assembly. This was important so as to ensure that the epoxy was not compromised by operating it above its rated temperature. Location 3 was chosen to allow the temperature gradient across the windings to be observed.

6.3.1 DC Excitation

To evaluate the thermal performance of the prototype inductors, each was subjected to a fixed dc excitation by connecting the winding of each inductor to a dc power supply. The power delivered to the component was kept constant by adjusting the output voltage of the supply to maintain a constant level of power. During this time the temperature rise within the inductor was monitored using the embedded thermocouples. In each case the experiment was performed for as long as necessary for the component under test to reach thermal steady state. This experiment was repeated for each of the prototypes at a range of powers to permit the evaluation of the components over a wide range of loads. As this work was concerned with the modelling of the potting compound it was decided that the use of ac excitation would add complexity to the simulation (as it would be necessary to calculate the frequency effects on the component), without contributing anything more to the findings. As a result, only the much simpler dc excitation was considered here.

6.4 Results

The steady state temperature exhibited by the prototype inductors are shown in Figure 6.4. From this data it can be observed that the inductor potted with an epoxy composite exhibits a marked improvement in thermal performance over the sample potted using standard epoxy. Over the experimental range an average reduction of 38 % is observed in the temperature rise. This demonstrates that the addition of thermally conductive filler is advantageous to thermal performance.

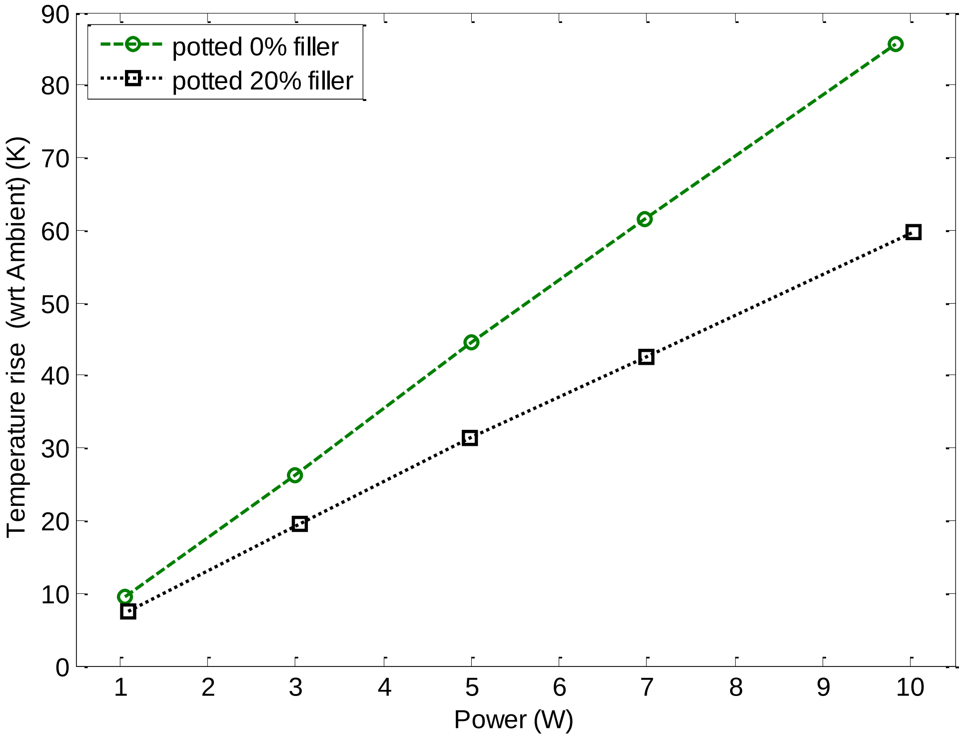

Figure 6.4 - Prototype temperature rise at steady state (with respect to ambient) under dc excitation

6.5 Finite Element Analysis of Inductor

To determine the thermal conductivity value of the composite material used to encapsulate the filled inductor, a 3D finite element model of the potted inductor was produced. To calibrate this model, the experimental data obtained for the inductor encapsulated using standard epoxy was used (as thermal conductivity of the epoxy was known). The geometry used for the FEA can be seen in Figure 6.5. The solutions from this simulation can be seen in Figure 6.6 . A summary of the values obtained from this simulation is presented in Table 6.2. It can be seen from the values shown in this table that this model exhibits good correlation to the experimentally obtained values with errors between the measured and predicted temperatures being within 1 K of each other.

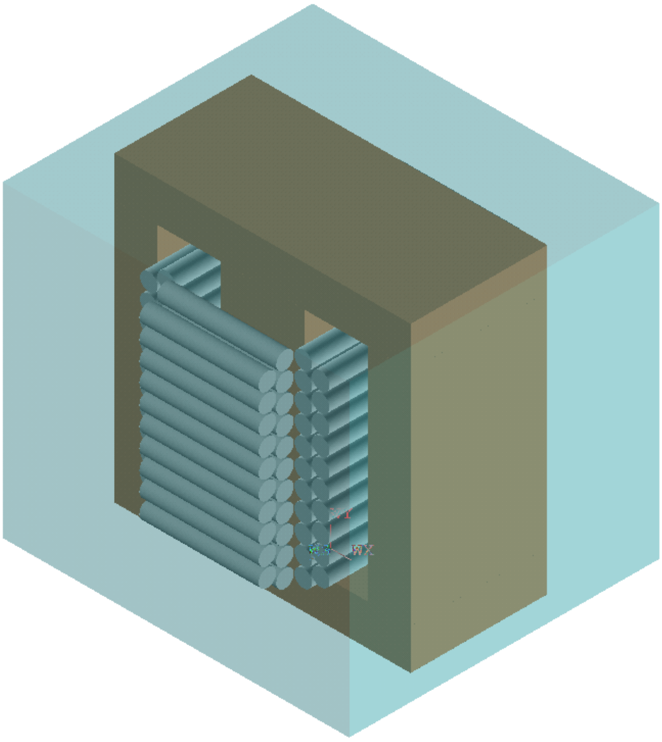

Figure 6.5 - Finite element model of prototype potted inductor

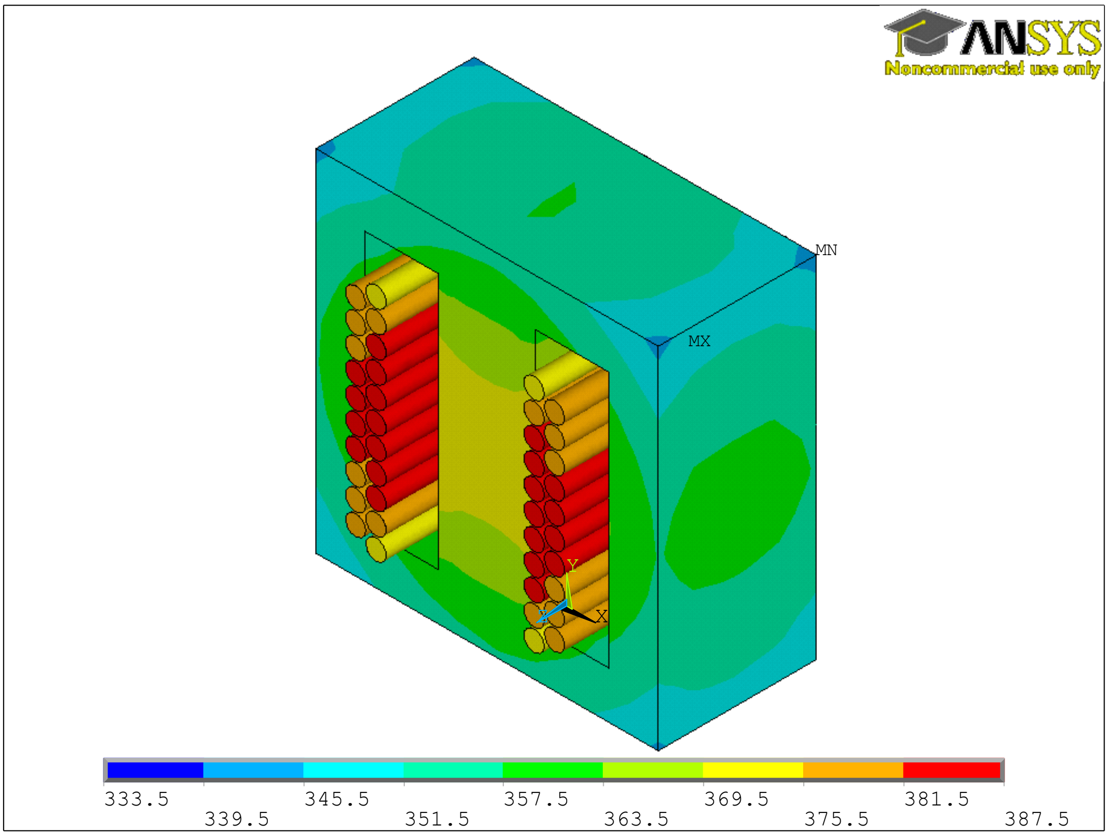

Figure 6.6 - Finite element simulation of unfilled encapsulated inductor (ambient temperature = 300 K, 10 W power dissipated in windings)

	Windings	**Core**
Measured	85.7 K	67.2 K
FEA	85.7 K	66.6 K
Difference	0.0	0.6
% error	0 %	0.9 %

Table 6.2- Comparison of experimental results and finite element temperature rise predictions for sample 1 under a 10 W excitation

Using this model it is possible to determine the bulk thermal conductivity of the encapsulant composite used in the composite potted sample. This is achieved by adjusting the thermal conductivity values of the region in the models which represent the encapsulant until the temperatures predicted for the windings and core correspond to the experimental results obtained for the inductor. From this a thermal conductivity value of 0.43 W/m.K was obtained, this value falls within the range obtained by the production of composite samples in section 5.4.5. The simulation results of the model in this configuration can be observed in Figure 6.7. A comparison of the measured and simulated results can be seen in Table 6.3; again a good agreement between the two results can be observed.

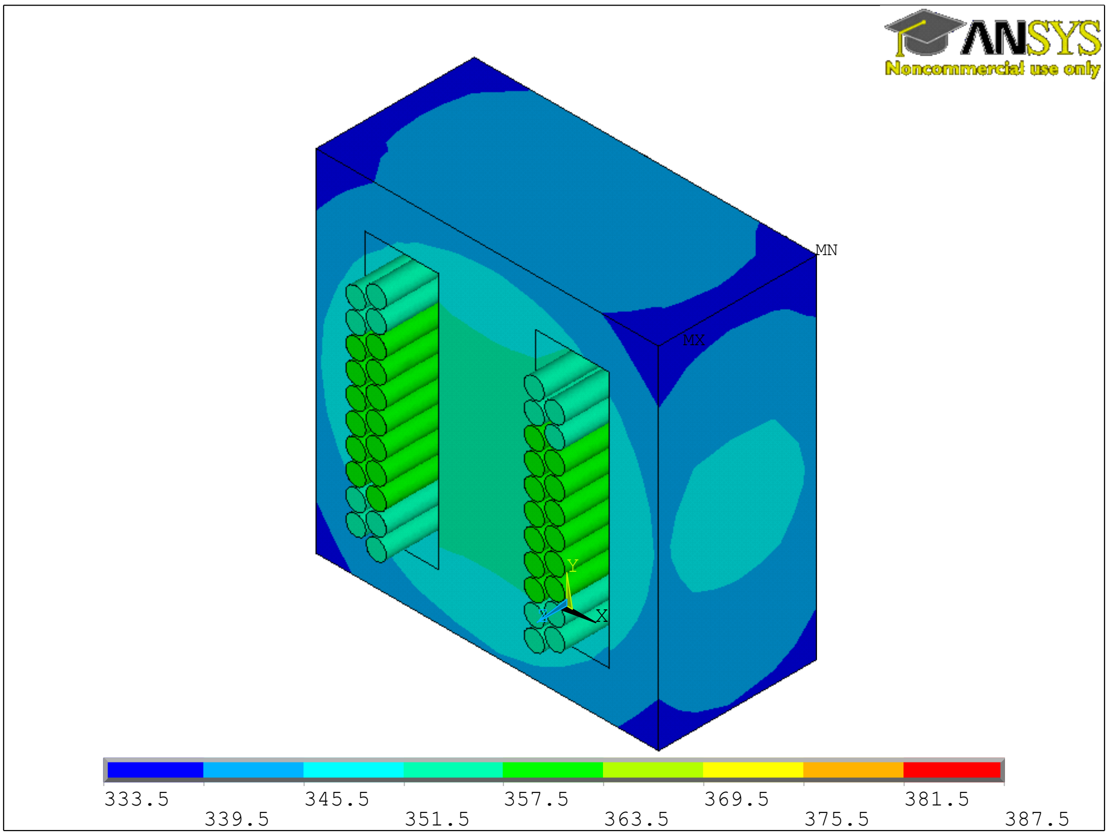

Figure 6.7 - Finite element simulation of filled encapsulated inductor (ambient temperature = 300 K, 10 W power dissipated in windings)

	Windings	Core
Measured	59.7 K	52.1 K
FEA	60.2 K	52.7 K
Difference	0.5	0.6
% error	0.8 %	1.1 %

Table 6.3 - Comparison of experimental results and finite element temperature rise predictions for filled inductor under a 10 W excitation

6.5.1 Composite Thermal Conductivity Sensitivity Study

Using the previously described FEA model, it is interesting to consider how variation in the bulk thermal conductivity value used to represent the encapsulant regions impacts on the predicted operating temperature of the component. To evaluate this the model was simulated with a range of thermal conductivity values for the encapsulant region from 0.1 W/m.K up to 2 W/m.K. The temperature predictions obtained from these simulations can be seen in Figure 6.8. From this it can be observed that the operating temperature is highly non-linear with respect to the thermal conductivity of the region. That is to say, as the thermal conductivity value of the encapsulant region increases, the overall thermal resistance of the component becomes desensitised to the encapsulant thermal conductivity value, and so increasing the conductivity further has little effect, and the other thermal resistances within the component have a much larger influence on the final component temperature. This leads to two important observations:

- While it may be possible to increase the thermal conductivity of the composite beyond the levels shown in this figure, it is a process of diminishing returns.
- Due to the non-linear nature of the temperature increase curve, it is possible that the use of a thermal conductivity value which contains errors may not be as inaccurate as would be suggested by considering the magnitude of this error in isolation.

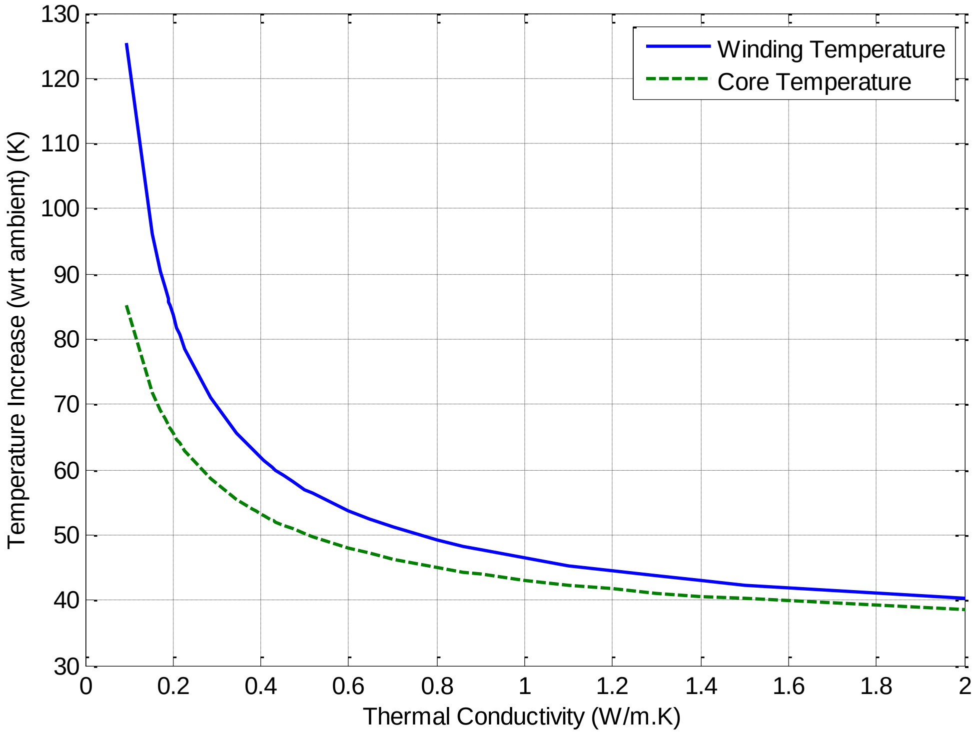

Figure 6.8 – Simulated temperature rise of inductor with respect to composite bulk thermal conductivity

6.5.2 Use of analytical models in FEA

Based on the findings in the previous section, it is reasonable to consider the accuracy of simulations that use the values predicted by analytical models.

Listed in Table 6.4 are the thermal conductivity values for a composite composed epoxy and 20 % (by volume) aluminium oxide obtained from the analytical models. Additionally, the values obtained from the composite samples produced in the previous chapter are also included. To evaluate which of these values are suitable for predicting the performance of the component, the FEA model used previously in this chapter is used with the values from Table 6.4 representing the composite region. The temperature increases predicted by this method are also included in the table.

Model	**Bulk Thermal Conductivity**		**FEA Predicted Winding Temperature (K)**
	(W/m.K)	**% variation from Experimental**	
Experimental	**0.4300**	**0.0 %**	**60.2**
Series	0.2371	-44.9 %	77.1
Maxwell	0.2604	-39.4 %	73.9
Pal 1	0.3400	-20.9 %	65.8
Pal 2	1.3740	+219.5 %	43.2
Pal 3	0.5261	+22.3 %	56.0
Lewis / Nielsen	0.5574	+29.7 %	54.9
Minimum Composite Sample	0.3360	-21.9 %	66.2
Maximum Composite Sample	0.4481	+4.2 %	59.3

Table 6.4 – Summary of values predicted by analytical models for a 20 % filler concentration (k_c = 0.19; k_d = 30; ϕ_{max} = 0.28; A = 1.5) (Models from [110, 111, 112]; composite sample data from [3])

The points listed in Table 6.4 are also plotted on the graph shown in Figure 6.9, alongside the winding temperature predictions from Figure 6.8. This figure also includes horizontal lines which denote the percentage error from the reference value. Here the reference value is defined as the value obtained during the experimental tests.

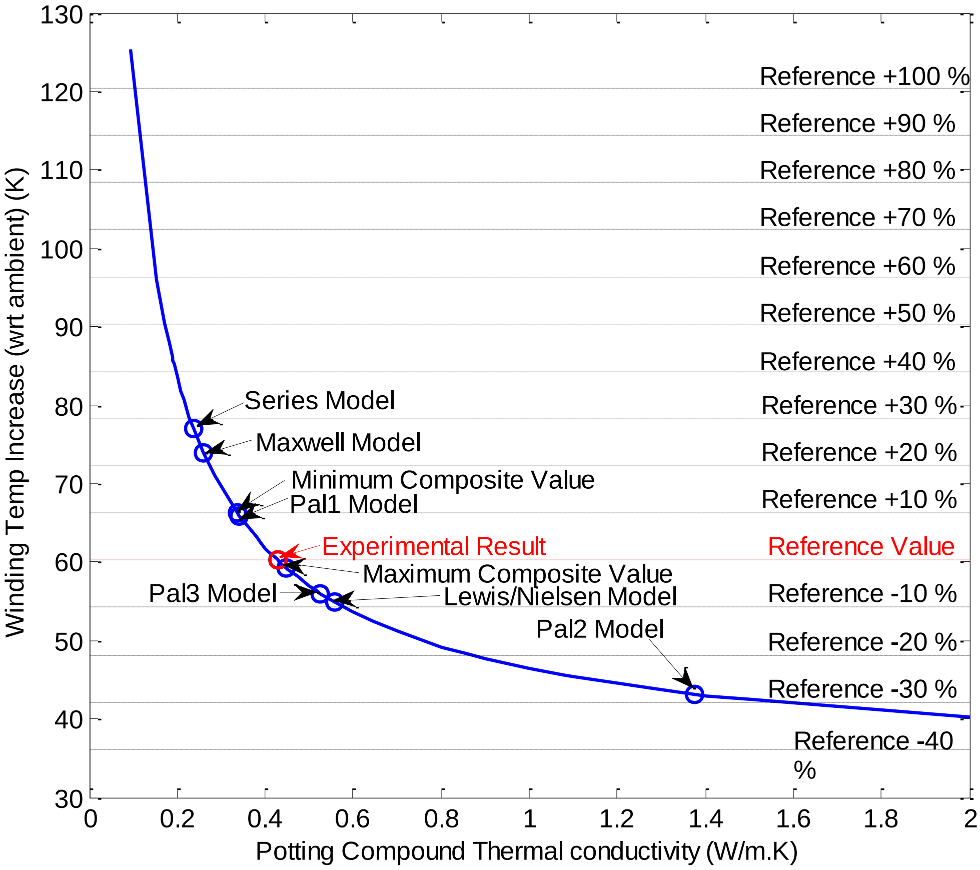

Figure 6.9 - Temperature predictions from FEA model with analytical bulk thermal conductivity values indicated

From Figure 6.9 it can be clearly seen that three of the analytical models and both of the composite samples yield temperature predictions which are within 10 % of the experimental result. The models which meet this criterion are:

- Pal 1 (+9.3 % error)
- Pal 3 (-7.0 % error)
- Lewis/Nielsen (-8.8 % error)

The temperature prediction errors shown for these models are considerably less than the errors present within the bulk thermal conductivity values (-20.9 %; +22.3 % and +29.6 % respectively). This shows that although the analytical model predictions of the thermal conductivity all contain considerable error, the use of any of the values given by these methods in an FEA model of the full system, will yield results that are within 10 % of the experimental result. This level of accuracy is sufficient for the purpose of creating an initial design of a component without necessitating the production of samples of the composite or manufacturing multiple different prototypes.

6.6 Designing inductors using analytical composite values

To determine if it is indeed possible to design an inductor and predict its operating temperature using the values obtained from the previously highlighted analytical models, another prototype inductor was designed and produced. This inductor was developed for use as a buck/boost inductor within a 1.5 kW battery charger and the specification for it is listed in Table 6.5.

Core	ETD 59, 3F3 ferrite core (In E-E configuration)
Air gap	0.95 mm (All legs)
Windings	Copper litz wire (19 strands of 0.4 mm wire)
Winding configuration	34 turns (arranged in 3 layers)
Inductance	409 μH
Saturation Current	15 A
Encapsulant	ER1448 Epoxy
Encapsulant filler	20 % (By volume) Aluminium oxide powder

Table 6.5 – Specification of verification prototype inductor

6.6.1 Evaluating the use of analytical models

To evaluate the effectiveness of using analytical models to determine the bulk thermal conductivity of composites within FEA during the design of a component. To achieve this a new prototype inductor was designed and constructed. During the design phase, the FEA model pictured in Figure 6.10 was employed. This model was solved a number of times, each time using the bulk conductivity value from an analytical model to represent the thermal conductivity of the encapsulant region. The results of this simulation can be seen in Figure 6.11.

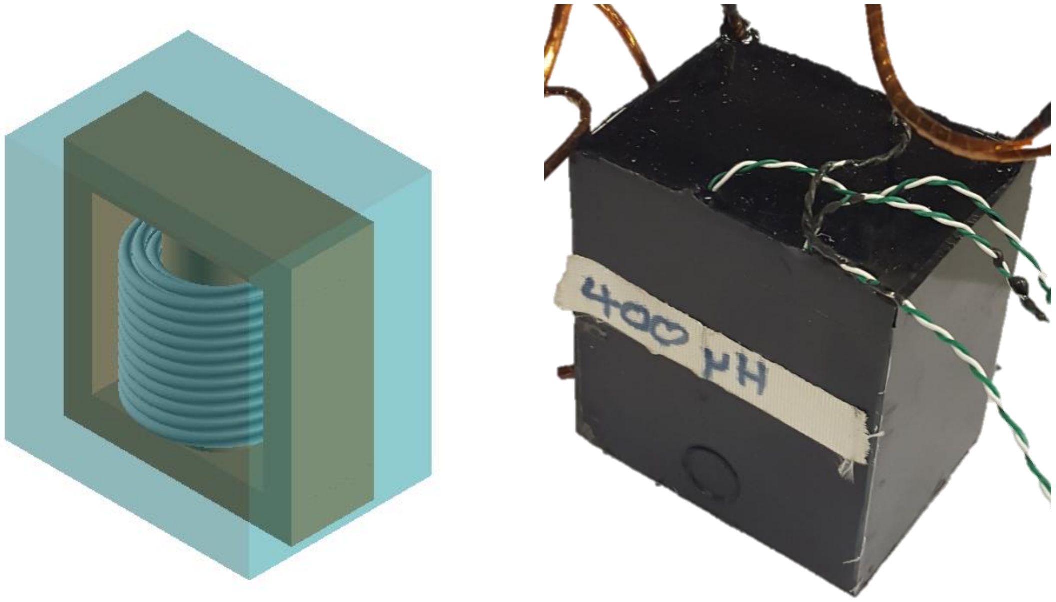

(a) (b)

Figure 6.10 – (a) - FEA model used to model thermal performance of section inductor; (b) – Photograph if prototype inductor

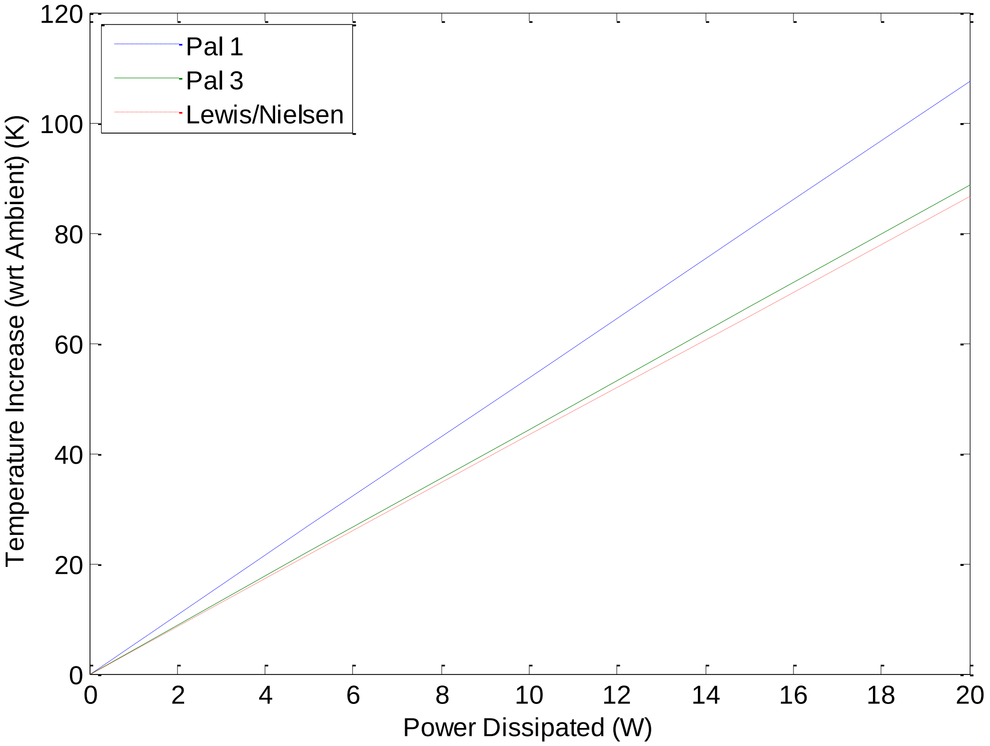

Figure 6.11 - Simulated temperature for prototype inductor using analytical values to represent composite region

For these analytical models to be considered as a viable method for the modelling of the composite region thermal resistance, the results obtained experimentally for the prototype inductor must fall within the boundaries defined by these models. To establish if this is the case, a prototype was constructed and potted using the same techniques as the previously discussed prototypes.

6.6.2 Prototype evaluation

Testing of this new prototype was performed using the same dc testing methodology which was described previously in this chapter. In this case test points of 5 W; 10 W; 15 W; and 20 W dissipation within the windings were evaluated. The steady state temperature increase from each of these tests can be observed in Figure 6.12. From this figure it can be seen that experimental results fall within the boundaries predicted by using analytical models. This validates the concept of using these models to predict boundaries within which the temperature of the inductor potted using composite encapsulant will fall.

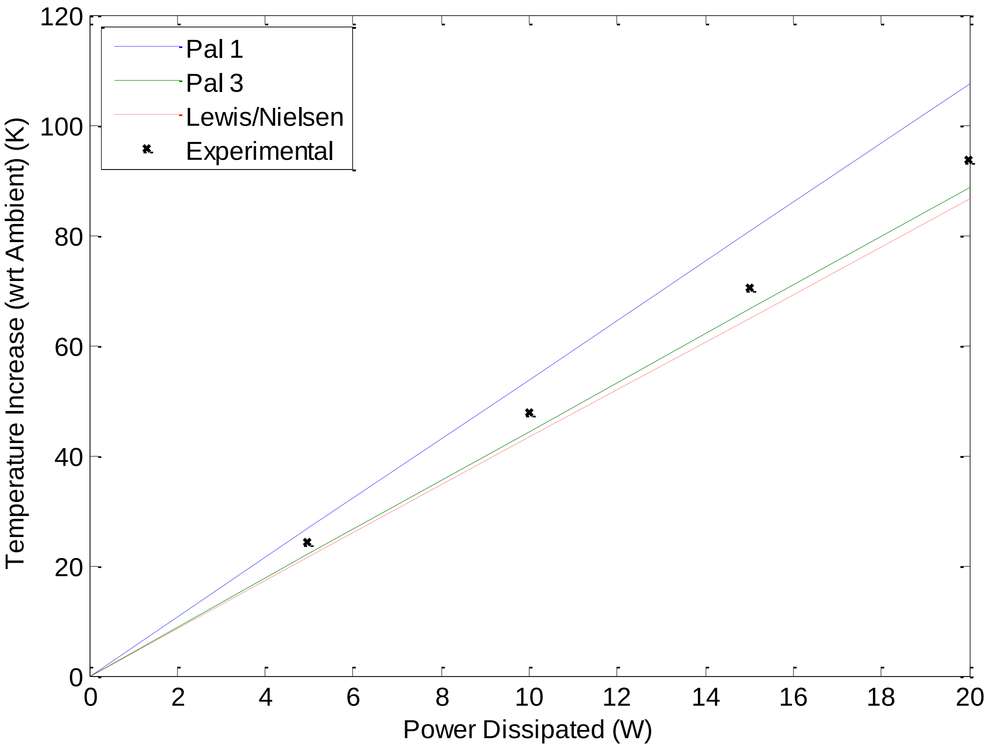

Figure 6.12 - Experimental results for dc testing of prototype inductor; also included are the temperature predictions using analytical models and FEA

6.6.3 Manufacturing consistency

Another factor which can be considered with respect to the use of composite encapsulants is the consistency of the composite being produced. To consider this, simulation was performed using the bulk thermal conductivity value determined experimentally for the previous inductor (0.43 W/m.K). The results of this simulation can be seen in Figure 6.13. Here it can be seen that the experimental results show good correlation with the results of this simulation. The most significant discrepancies occur during the higher power test, with the simulation slightly over predicting the temperature increase. This can be attributed to the fact that within the FEA model, convection is modelled as a linear parameter. In reality it is nonlinear, with convection coefficients being a function of the temperature differential between the heat source and the cooling air [62]. Based on this good correlation between results, it is reasonable to conclude that the method used to manufacture the composite material is constant between manufacturing batches.

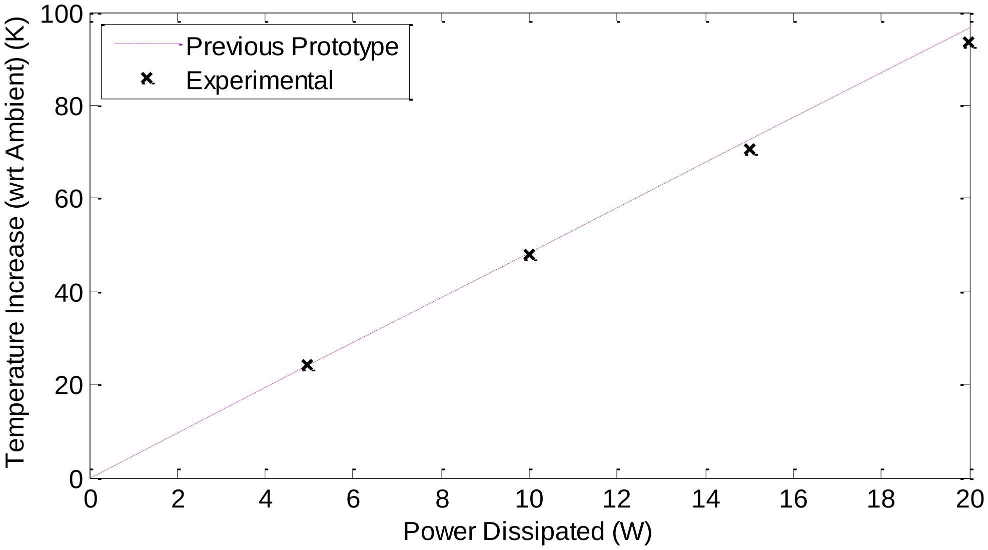

Figure 6.13 - Comparison of experimental results to simulations using previously determined thermal conductivity values

6.7 Conclusions

From the work presented here several conclusions can be drawn. Firstly, several of the analytical models yield results for the thermal resistance of the encapsulant that are potentially accurate enough to achieve suitable FEA results. This is despite the fact that analytical models produce a wide range of predictions for the bulk thermal conductivity of a composite. These models are referred to in this chapter as Pal1 [111]; Pal3 [111]; and Lewis/Nielsen [112]. Although these models have a deviation of up to 30 % from the experimentally determined bulk thermal conductivity value, it was found that due to the nonlinear relationship between encapsulant thermal conductivity and operating temperature, an error of less than 10 % was achieved when predicting the component operating temperature using FEA. Consequently, it is possible to design an inductor using these analytical values to predict the boundaries of the operating temperature.

The practicality of this is demonstrated by determining the range of the temperatures in which a second inductor topology will operate, prior to the construction of the component. This is supported by experimental measurements obtained from the second prototype inductor topology. The experimental results obtained from this inductor also demonstrate that the manufacturing technique utilised in this work provides consistent properties. This was demonstrated using the bulk thermal conductivity value from the first prototype topology within the second prototype inductor finite element model. In this case a strong correlation between the simulated and experimental results can be observed.

In this chapter analytical models suitable for generating simulated temperature bounds using FEA have been identified. This allows the operating temperature of an inductor to be predicted during the design phase, without the production of prototypes. The next chapter will serve to draw conclusions from the thesis as a whole and suggest future directions in which the work could be continued.

Chapter 7

Conclusions and future direction of work

7.1 Conclusions

This thesis presents a range of methods by which the power density of an inductor can be improved. This is achieved through the consideration of several different techniques.

Firstly, in chapter 3 the use of alternative winding materials is considered, with focus being given to a comparison of copper and aluminium. Here it is found that in some topologies, aluminium will exhibit a lower ac resistance than copper for some frequencies. This exchange therefore results in an inductor which is lighter and cheaper than the copper equivalent, with a lower ac resistance at some frequencies. Additionally, it was found that due to frequency effects, for an even wider range of frequencies, the difference in resistance between aluminium and copper is considerably lower than the dc ratio. In such cases, the resulting inductor will still weigh less when constructed with aluminium, resulting in a potential increase power density in terms of kW/kg.

The use of aluminium oxide as an insulation material in planar components was explored in chapter 4 [1, 2]. A planar topology was selected for this work so as to not have to bend the aluminium windings after the anodisation process had been performed, as this would lead to cracks forming in the oxide layer. The thermal advantages of using aluminium oxide instead of a conventionally used plastic (e.g. kapton) were explored and a marked improvement in thermal performance was observed when aluminium oxide was used. Further improvements were made to this by including heat sink compound between the layers, enhancing the thermal transfer through the component considerably. This technique has the potential to improve power density in inductors in two ways. If a component is thermally limited, by utilising this thermally improved solution, the current handling of the inductor can be increased. Alternatively, it may be possible to reduce the size of the inductor by employing this technique, improving the power density in this way.

In chapters 5 and 6 consideration has been given to the use of composite materials to improve the performance of encapsulants [3, 4]. The initial findings of this work verify that the addition of fillers does improve the thermal performance of the encapsulant. In this way, it is possible to improve the power density through the same mechanisms described in the previous paragraph. An issue which arises when using a composite material is representing it within design tools (*e.g.* FEA) therefore potential methods of achieving this were explored. These methods included analytical models, numerical methods and empirical models. From this it was concluded that it is difficult to accurately calculate the thermal conductivity for all composite production cases. To evaluate the effect of this error, simulation was performed to predict the temperatures of prototype potted inductors. From this analysis several of the analytical models were determined to be sufficiently accurate to obtain FEA predictions with an accuracy within 10 % of the experimental results. While this finding does not directly impact the power density of the manufactured components it does potentially allow the designer to reduce the level of over engineering required when designing components using composites. This, in turn, potentially allows the size of components to be reduced.

A prototype which incorporated all of these ideas into a single solution was not produced. This is because the advantages to be gained through the encapsulation of planar inductors is considerably less than that for encapsulating conventional wire wound inductors, due to the close fitting nature of the planar windings. Consequently it was felt that such a prototype would not effectively showcase the advantages which can be gained through potting components.

7.2 Future work

Using this thesis as a starting point there are a range of possible directions which this work could be taken in, these will now be proposed for each of the major areas of this thesis.

7.2.1 Use of aluminium as a winding material

This work has presented cases in which aluminium windings exhibit superior resistive performance to copper windings at a range of frequencies. An additional line of enquiry would be to consider the use of other alloys of copper or aluminium as winding materials. It is believed that similar effects to those discussed in this work will be observable for alloys which have different electrical conductivities, permitting a possible tuning of the losses through careful selection of the alloy used.

7.2.2 Anodised aluminium insulation

This work studies the use of anodic aluminium oxide as a potential winding insulation material and concludes that it is potentially viable. Further work could be performed to optimise the anodisation process so as to achieve improvements in the insulation properties of the anodic coating.

In this research a planar topology was selected since it allowed the shape of the winding to be formed prior to anodisation, removing the need to form the winding afterwards which results in cracking of the oxide layer. An extension of this work would be to produce a winding formed from uninsulated aluminium wire which would then be anodised to add the insulation. To make this approach feasible and ensure short circuits did not occur between the turns it may be necessary to employ some kind of spacer. It is important that the selected material for this purpose did not impede the anodisation process. It would also be important to ensure that a winding produced in this way did not trap any of the acid used during the anodisation process because this could be potentially hazardous.

7.2.3 Encapsulant composites

In modelling the performance of encapsulant materials a range of suitable models were considered. To extend this work further consideration could be given to alternative manufacturing methods, potentially allowing the packing factor to achieve levels which exceed the natural maximum packing factor. This may be potentially possible by modifying the method referred to within chapter 5 as the settled method, by applying force to the filler matrix prior to the application of epoxy. It would be interesting to see if this can be successfully achieved when an inductor is placed at the heart of the filler matrix. Additionally it would be interesting to observe how well the epoxy impregnates into the newly formed compressed filler matrix. In using this method it would be important to ensure that a high quality of impregnation was achieved as failure to do so would result in an encapsulant which performed worse, despite the increased filler concentration.

Another consideration which may be of interest regarding this work is the use of moulds which are contoured to conform more closely to the inductor. This would potentially improve the thermal transfer within the component by reducing the amount of epoxy which heat flux has to travel through to reach the heat extraction surfaces. In addition to this, due to the reduced quantity of epoxy used this would also increase the power density of the component and decrease materials cost. It is possible however, that the reduced materials cost will be offset by the increased production costs of the more complex mould required to achieve this.

Chapter 8

References

[1] D. Hewitt, D. Stone and M. Foster, “An investigation into the feasibility of using aluminium oxide to insulate aluminium planar windings,” in *iPower2*, Warwick, 2012.

[2] D. Hewitt, D. Stone and M. Foster, “Design of thermally integrated planar inductors utilising aluminium oxide as a winding insulation material,” in *PCIM Europe*, Nuremberg, Germany, 2013.

[3] D. Hewitt, D. Stone and M. Foster, “An experimental evaluation of thermally conductive filler loaded encapsulant composites,” in *Power Electronics, Machines and Drives (PEMD 2014), 7th IET International Conference on*, Manchester, 2014.

[4] D. Hewitt, D. Stone and M. Foster, “Modelling the enhancement to the thermal performance of encapsulants using thermally conductive filler materials,” in *PCIM Asia*, Shanghai, 2015.

[5] B. Whitaker, A. Barkley, Z. Cole, B. Passmore, D. Martin, T. McNutt and A. Lostetter, “A High-Density, High-Efficiency, Isolated On-Board Vehicle Battery Charger Utilizing Silicon Carbide Power Devices,” *Power Electronics, IEEE Transactions on,* vol. 29, no. 5, pp. 2606 - 2617, 2014.

[6] B. Whitaker, A. Barkley, Z. Cole, B. Passmore, T. McNutt and A. Lostetter, “High-frequency AC-DC conversion with a silicon carbide power module to achieve high-efficiency and greatly improved power density,” in *Power Electronics for Distributed Generation Systems (PEDG)*, Rogers, AR , 2013.

[7] Ferroxcube, “3F3 Material specification,” 2008 9 1. [Online]. Available: http://www.ferroxcube.com/FerroxcubeCorporateReception/datasheet/3f3.pdf. [Accessed 18 6 2015].

[8] A. V. d. Bossche and V. Valchev, Inductors and Transformers for power electronics, CRC Press, 2005.

[9] M. Albach, T. Durbaum and A. Brockmeyer, “Calculating core losses in transformers for arbitrary magnetizing currents a comparison of different approaches,” *Power Electronics Specialists Conference, 1996. PESC '96 Record., 27th Annual IEEE , vol.2, no., pp.1463-1468 vol.2, 23-27 Jun 1996.*

[10] M. Sippola and R. Sepponen, “Accurate prediction of high-frequency power-transformer losses and Temperature rise,” *Power Electronics, IEEE Transactions on , vol.17, no.5, pp. 835- 847, Sep 2002.*

[11] C. Sullivan, J. Harris and E. Herbert, “Core loss predictions for general PWM waveforms from a simplified set of measured data,” *Applied Power Electronics Conference and Exposition (APEC), 2010 Twenty-Fifth Annual IEEE , vol., no., pp.1048-1055, 21-25 Feb. 2010.*

[12] K. Venkatachalam, C. Sullivan, T. Abdallah and H. Tacca, “Accurate prediction of ferrite core loss with nonsinusoidal waveforms using only Steinmetz parameters,” *Computers in Power Electronics, 2002. Proceedings. 2002 IEEE Workshop on , vol., no., pp. 36- 41, 3-4 June 2002.*

[13] J. Muhlethaler, J. Biela, J. Kolar and A. Ecklebe, “Core Losses Under the DC Bias Condition Based on Steinmetz Parameters,” *Power Electronics, IEEE Transactions on,* vol. 27, no. 2, pp. 953-963, 2012.

[14] Y. Chen and P. Pillay, “An improved formula for lamination core loss calculations in machines operating with high frequency and high flux density excitation,” in *Industry Applications Conference,*, Pittsburgh, 2002.

[15] R. Wrobel, A. Mlot and P. Mellor, “Contribution of End-Winding Proximity Losses to Temperature Variation in Electromagnetic Devices,” *Industrial Electronics, IEEE Transactions on ,* vol. 59, no. 2, pp. 848 - 857, 2012.

[16] M. Mu, Q. Li, D. Gilham, F. Lee and K. Ngo, “New Core Loss Measurement Method for High-Frequency Magnetic Materials,” *Power Electronics, IEEE Transactions on,* vol. 29, no. 8, pp. 4374-4381, 2014.

[17] N. Mohan, First course on power electronics and drives, Minneapolis: MNPERE, 2003.

[18] P. Bardell, Magnetic materials in the electrical industry, Macdonald and Co. (Publishers) ltd.: London, 1955.

[19] C. W. T. McLyman, Transformer and Inductor Design Handbook (3rd edition), Marcel Decker Inc., 2004.

[20] M. Rylko, B. Lyons, K. Hartnett, J. Hayes and M. Egan, “Magnetic material comparisons for high-current gapped and gapless foil wound inductors in high frequency dc-dc converters,” *Power Electronics and Motion Control Conference, 2008. EPE-PEMC 2008.13th , vol., no., pp.1249-1256, 1-3 Sept. 2008.*

[21] Magnetics, “A Critical Comparison of Ferrites with Other Magnetic Materials,” Magnetics, Butler, PA, 2000.

[22] A. Jack, B. Mecrow, P. Dickinson, D. Stephenson, J. Burdess, N. Fawcett and J. Evans, “Permanent-magnet machines with powdered iron cores and prepressed windings,” *Industry Applications, IEEE Transactions on,* vol. 36, no. 4, pp. 1077-1084, 2000.

[23] J. Widmer, C. Spargo, G. Atkinson and B. Mecrow, “Solar Plane Propulsion Motors With Precompressed Aluminum Stator Windings,” *Energy Conversion, IEEE Transactions on,* vol. 29, no. 3, pp. 681-688, 2014.

[24] T. E. Salem, D. P. Urciuoli, V. Lubomirsky and G. K. Ovrebo, “Design Considerations for High Power Inductors in DC-DC Converters,” in *Applied Power Electronics Conference, APEC 2007 - Twenty Second Annual IEEE*, Anaheim, CA, USA , 2007.

[25] D. A. Smith, “Folded foil transformer construction”. USA Patent 6,087,922, 11 7 2000.

[26] F. Sarvar, N. Poole and P. Witting, “Pcb glass-fibre laminates: Thermal conductivity measurements and their effect on simulation,” *Journal of Electronic Materials,* vol. 19, no. 12, pp. 1345-1350, 1990.

[27] DuPont, “DuPont Kapton HN - polyimide film - Technical Data Sheet,” [Online]. Available: http://www.dupont.com/content/dam/assets/products-and-services/membranes-films/assets/DEC-Kapton-HN-datasheet.pdf. [Accessed 16 3 2015].

[28] K. Ngo, R. Alley and A. J. Yerman, “Fabrication method for a winding assembly with a large number of planar layers,” *Power Electronics, IEEE Transactions on,* vol. 8, no. 1, pp. 55-61, 1993.

[29] E. de Jong, E. de Jong, B. Ferreira and P. Bauer, “Toward the Next Level of PCB Usage in Power Electronic Converters,” *Power Electronics, IEEE Transactions on,* vol. 23, no. 6, pp. 3151-3163, 2008.

[30] M. Gerber, J. Ferreira, I. Hofsajer and N. Seliger, “A high-density heat-sink-mounted inductor for automotive applications,” *Industry Applications, IEEE Transactions on,* vol. 40, no. 4, pp. 1031-1038, 2004.

[31] C. Quinn, K. Rinne, T. O'Donnell, M. Duffy and C. Mathuna, “A review of planar magnetic techniques and technologies,” in *Applied Power Electronics Conference and Exposition, 2001. APEC 2001. Sixteenth Annual IEEE* , Anaheim, CA , 2001.

[32] London Metal Exchange, [Online]. Available: https://www.lme.com/. [Accessed 1 6 2015].

[33] Bullion Rates, [Online]. Available: http://www.bullion-rates.com/silver.htm. [Accessed 1 6 2015].

[34] C. J. Smithells, E. A. Brandes and G. B. Brook, Smithells metals reference book (7th Edition), Oxford: Butterworth-Heinemann, 1992.

[35] J. Olivares-Galván, F. de León, P. Georgilakis and R. Escarela-Pérez, “Selection of copper against aluminium windings for distribution transformers,” *Electric Power Applications, IET,* vol. 4, no. 6, pp. 474-485, 2010.

[36] W. W. Orr, “Aluminum and its future in power transformers,” *Electrical Engineering,* vol. 78, no. 7, p. 737, 1959.

[37] E. Tipton, “Experiences With the Use of Aluminum in Windings for Dry-Type Power Transformers,” *Power Apparatus and Systems, Part III. Transactions of the American Institute of Electrical Engineers ,* vol. 74, no. 3, pp. 1201 - 1204, 1955.

[38] National Electrical Manufacturers Association , “NEMA MG 1-2014 (Motors and generators),” National Electrical Manufacturers Association , Virginia, 2014.

[39] International Electrotechnical Commission, “IEC 60317-0-1:2013 (Specifications for particular types of winding wires - Part 0-1: General requirements - Enamelled round copper wire),” International Electrotechnical Commission, 2013.

[40] S. Babicz, S. Ait-Amar Djennad and G. Velu, “Preliminary study of using anodized aluminum strip for electrical motor windings,,” in *Electrical Insulation and Dielectric Phenomena (CEIDP)*, Des Moines, IA , 2014.

[41] “Aluminum strips reduce size of transformer windings,” *Electrical Engineering ,* vol. 74, no. 11, pp. 1024-1025, 1955.

[42] N. Mohan, T. Undeland and W. Robbins, Power Electronics : Converters, Applications and Design, Wiley, 2003.

[43] P. Dowell, “Effects of eddy currents in transformer windings,” *Electrical Engineers, Proceedings of the Institution of,* vol. 113, no. 8, pp. 1387-1394, 1966.

[44] J. Ferreira, “Improved analytical modeling of conductive losses in magnetic components,” *Power Electronics, IEEE Transactions on,* vol. 9, no. 1, pp. 127-131, 1994.

[45] A. Loth and F. Lee, “Two-dimensional skin effect in power foils for high-frequency applications,” *Magnetics, IEEE Transactions on,* vol. 31, no. 2, pp. 1003-1006, 1995.

[46] N. Kutkut, “A simple technique to evaluate winding losses including two-dimensional edge effects,” *Power Electronics, IEEE Transactions on ,* vol. 13, no. 5, pp. 950-958, 1998.

[47] P. Wallmeier, “Improved analytical modeling of conductive losses in gapped high-frequency inductors,” *Industry Applications, IEEE Transactions on,* vol. 37, no. 4, pp. 1045-1054, 2001.

[48] M. Albach and H. Rossmanith, “The influence of air gap size and winding position on the proximity losses in high frequency transformers,” in *Power Electronics Specialists Conference, 2001. PESC. 2001 IEEE 32nd Annual (Volume:3)* , Vancouver, BC , 2001.

[49] W. Roshen, “Fringing Field Formulas and Winding Loss Due to an Air Gap,” *Magnetics, IEEE Transactions on,* vol. 43, no. 8, pp. 3387-3394, 2007.

[50] X. Nan and C. Sullivan, “Simplified high-accuracy calculation of eddy-current loss in round-wire windings,” in *Power Electronics Specialists Conference, 2004.*

PESC 04. 2004 IEEE 35th Annual (Volume:2) , 2004.

[51] J. Ferreira, “Analytical computation of AC resistance of round and rectangular litz wire windings,” *Electric Power Applications, IEE Proceedings B,* vol. 139, no. 1, pp. 21-25, 1992.

[52] D. Nath, “Indian Experience with Aluminum Busbars,Links,and Cable Terminations for Use on Low-Voltage Systems up to 1000 v,” *Components, Hybrids, and Manufacturing Technology, IEEE Transactions on,* vol. 9, no. 1, pp. 30 - 34 , 1986 .

[53] J. Aronstein, “Evaluation of a Setscrew Connector for Aluminum Wire,” in *Electrical contacts - 2007, the 53rd ieee holm conference on* , Pittsburgh, PA , 2007.

[54] J. Aronstein, “Analysis of field failures of aluminum-copper pigtail splices made with twist-on connectors,” in *Electrical Contacts, 1999. Proceedings of the Forty-Fifth IEEE Holm Conference on*, Pittsburgh, PA, USA , 1999.

[55] M. Weigl, A. Grimm and M. Schmidt, “Laser-welded connections for high-power electronics in mobile systems,” in *Electric Drives Production Conference (EDPC), 2011 1st International* , Nuremberg, 2011.

[56] J. Tsujino and T. Ueoka, “Ultrasonic butt welding of aluminium, anticorrosive aluminium and copper plate specimens,” in *Ultrasonics Symposium, 1988. Proceedings., IEEE*, Chicago, IL , 1988.

[57] V. Manjubhargavi, P. Chakravarthy, P. Venugopal and D. Achar, “Influence of Rubbing Profile on Friction Welding of Pre-Strained Aluminum to Copper,” in *Emerging Trends in Engineering and Technology (ICETET), 2009 2nd International Conference on* , Nagpur, 2009.

[58] W. Bonwitt, “An Experimental Investigation of the Electrical Performance of Bolted Aluminurm-to-Copper Connections,” *American Institute of Electrical Engineers, Transactions of the,* vol. 67, no. 2, pp. 1208-1219, 1948.

[59] N. Bond, “Electrical Transition Interfaces at Aluminum Terminations,” *Components, Hybrids, and Manufacturing Technology, IEEE Transactions on,* vol. 2, no. 1, pp. 37-40, 1979.

[60] M. Braunovic, “Evaluation of different platings for aluminum-to-copper connections,” *Components, Hybrids, and Manufacturing Technology, IEEE Transactions on,* vol. 15, no. 2, pp. 204-215, 1992.

[61] L. Dixon, “Magnetics design for switching power supplies,” Texas Instruments.

[62] J. Lienhard and J. Lienhard, A heat transfer textbook (fourth edition), Phlogiston Press, 2011.

[63] S. Anandan and V. Ramalingam, “Thermal management of electronics: A review of literature,,” *Thermal Science,* vol. 12, no. 2, pp. 5-26, 2008.

[64] E. Snelling, Soft Ferrites (1st edition), Iliffe Books Ltd, 1969.

[65] N. Goel, A. Bhattacharya, J. Cervantes, R. Mongia, S. Machiroutu, H.-L. Lin, Y.-C. Huang, K.-C. Fan, B.-L. Denq, C.-H. Liu, C.-H. Lin, C.-W. Tien and J.-H. Pan, “Technical Review of Characterization Methods for Thermal Interface Materials (TIM),” in *Thermal and Thermomechanical Phenomena in Electronic Systems, 2008. ITHERM 2008. 11th Intersociety Conference on* , Orlando, FL , 2008.

[66] A. Aranyosi, L. Bolle and H. Buyse, “Compact air-cooled heat sinks for power packages,” in *Semiconductor Thermal Measurement and Management Symposium, 1997. SEMI-THERM XIII., Thirteenth Annual IEEE* , Austin, TX , 1997.

[67] E. Amoiralis, M. Tsili, A. Kladas and A. Souflaris, “Distribution transformer cooling system improvement by innovative tank panel geometries,” *Dielectrics and Electrical Insulation, IEEE Transactions on,* vol. 19, no. 3, pp. 1021 -1028, 2012.

[68] Q. Wenjuan, Z. Jiming, H. Guiqing, Z. Jibin and X. Yongxiang, “Thermal analysis of underwater oil-filled BLDC motor,” in *Electrical Machines and Systems (ICEMS), 2011 International Conference on*, Beijing, 2011.

[69] J. Zou, W. Qi, Y. Xu, F. Xu, Y. Li and J. Li, “Design of Deep Sea Oil-Filled Brushless DC Motors Considering the High Pressure Effect,” *Magnetics, IEEE Transactions on,* vol. 48, no. 11, pp. 4220 - 4223, 2012.

[70] G. Enzensberger, E. Spycher and J. Scheibengraf, “Converter series, using oil immersed cooling, for main line locomotives,” in *Power Electronics and*

Applications, 1993., Fifth European Conference on, Brighton, 1993.

[71] H. Zhang, D. Pinjala and P. Teo, “Thermal management of high power dissipation electronic packages from air cooling to liquid cooling,” in *Electronics Packaging Technology, 2003 5th Conference (EPTC 2003)* , 2003.

[72] W. Nakayama, O. Suzuki and Y. Hara, “Thermal management of electronic and electrical devices in automobile environment,” in *Vehicle Power and Propulsion Conference, 2009. VPPC '09. IEEE* , Dearborn, MI , 2009.

[73] D. Price, “A review of selected thermal management solutions for military electronic systems,” *Components and Packaging Technologies, IEEE Transactions on,* vol. 26, no. 1, pp. 26-39, 2003.

[74] C. Glynn, T. S. O'Donovan and D. B. Murray, “Jet Impingement Cooling,” in *9th UK National Heat Transfer Conference*, Manchester, 2005.

[75] R. Skuriat and C. Johnson, “Direct substrate cooling of power electronics,” in *Power Electronics and Applications, 2009. EPE '09. 13th European Conference on*, Barcelona, 2009.

[76] I. Mudawar, D. Bharathan, K. Kelly and S. Naramanchi, “Two-phase spray cooling of hybrid vehicle electronics,” *Components and Packaging Technologies, IEEE Transactions on,* vol. 32, no. 2, pp. 501-512, 2009.

[77] S. Lee, S. Chu, C. Choi and Y. Jaluria, “Performance characteristics of vapor chambers with boiling enhanced multi-wick structures,” in *Semiconductor Thermal Measurement and Management Symposium, 2007. SEMI-THERM 2007. Twenty Third Annual IEEE* , San Jose, CA , 2007.

[78] M. Gerber, J. Ferreira, I. Hofsajer and N. Seliger, “High temperature, high power density packaging for automotive applications,” in *Power Electronics Specialist Conference, 2003. PESC '03. 2003 IEEE 34th Annual*, 2003.

[79] R. Wrobel, N. McNeill and P. Mellor, “Performance analysis and thermal modelling of a high-energy-density prebiased inductor,” *Industrial Electronics, IEEE Transactions on,* vol. 57, no. 1, pp. 201-208, 2010.

[80] F. Bryan and A. Forsyth, “A power dense DC-DC converter for a small electric vehicle,” in *Power Electronics, Machines and Drives (PEMD 2012), 6th IET*

International Conference on , vol., no., pp.1-6, Bristol, 2012.

[81] R. Wrobel and P. Mellor, “Thermal Design of High-Energy-Density Wound Components,” *Industrial Electronics, IEEE Transactions on,* vol. 58, no. 9, pp. 4096-4104, 2011.

[82] W. Liu, J. Dirker and J. v. Wyk, “Power density improvement in integrated electromagnetic passive modules with embedded heat extractors,” *Power Electronics, IEEE Transactions on,* vol. 23, no. 6, pp. 3142-3150, 2008.

[83] M. Yovanovich, “Four decades of research on thermal contact, gap, and joint resistance in microelectronics,” *Components and Packaging Technologies, IEEE Transactions on,* vol. 28, no. 2, pp. 182-206, 2005.

[84] Dow Corning, “Silicone grease solutions for your thermal interface needs,” [Online]. Available: https://www.dowcorning.com/content/publishedlit/11-1712-01.pdf. [Accessed 1 5 2015].

[85] Bergquist, “Gap pad comparison table,” [Online]. Available: http://www.bergquistcompany.com/thermal_materials/graph_pdfs/GPComparison_Web_Table.pdf. [Accessed 1 5 2015].

[86] Aavid Thermalloy, “Thermal Adhesives,” [Online]. Available: http://www.aavid.com/product-group/interface/adhesive. [Accessed 1 5 2015].

[87] J. Wilson, “Thermal Conductivity of solder,” 8 2006. [Online]. Available: http://www.electronics-cooling.com/2006/08/thermal-conductivity-of-solders/. [Accessed 1 5 2015].

[88] Heraeus, “Industrial Sintering Process,” [Online]. Available: http://heraeus-contactmaterials.com/media/webmedia_local/media/downloads/documents_am/broschures/HERAEUS_BESI_IndustrialSinteringProcess_Brochure_2013.pdf. [Accessed 1 5 2015].

[89] J. Holmes, D. Stone, M. Foster and A. Skinner, “Evaluation of thermally efficient mounting techniques for ferrite cores,” in *IPEC, 2010 Conference Proceedings* , Singapore, 2010.

[90] L. Weicheng, “The Void-free Reflow Soldering of BGA with Vacuum,” in *Electronic Packaging Technology, 2007. ICEPT 2007. 8th International*

Conference on , Shanghai, 2007.

[91] H. Schwarzbauer and R. Kuhnert, “Novel large area joining technique for improved power device performance,” *Industry Applications, IEEE Transactions,* vol. 27, no. 1, pp. 93 - 95, 1991.

[92] M. Knoerr and A. Schletz, “Power semiconductor joining through sintering of silver nanoparticles: Evaluation of influence of parameters time, temperature and pressure on density, strength and reliability,” in *Integrated Power Electronics Systems (CIPS), 2010 6th International Conference on*, Nuremberg, 2010.

[93] J. Holmes, M. Foster and D. Stone, “System-wide temperature estimation for IMS based power electronics circuits,” in *Power Electronics and Drive Systems, 2009. PEDS 2009. International Conference on*, Taipei, 2009.

[94] J. Holmes, D. Stone and M. Foster, “Device temperature projection technique for IMS based systems,” in *Power Electronics, Machines and Drives (PEMD 2010), 5th IET International Conference on* , Brighton, UK , 2010.

[95] G. Kamath, “An electrical circuit based 3-D thermal model of a fan cooled 600µH, 80A inductor for a plasma cutting power supply,” in *Applied Power Electronics Conference and Exposition, 2008. APEC 2008. Twenty-Third Annual IEEE* , Austin, TX , 2008.

[96] R. Wrobel, N. McNeill and P. Mellor, “Design of a high-temperature pre-biased line choke for power electronics applications,” in *Power Electronics Specialists Conference, 2008. PESC 2008. IEEE* , Rhodes, 2008.

[97] R. Wrobel, N. McNeill and P. Mellor, “Thermal analysis of a high energy density pre-biased choke,” in *Electrical Machines, 2008. ICEM 2008. 18th International Conference on* , Vilamoura, 2008.

[98] R. Wrobel and P. Mellor, “A General Cuboidal Element for Three-Dimensional Thermal Modelling,” *Magnetics, IEEE Transactions on ,* vol. 46, no. 8, pp. 3197-3200, 2010.

[99] N. Simpson, R. Wrobel and P. Mellor, “A General Arc-Segment Element for Three-Dimensional Thermal Modeling,” *Magnetics, IEEE Transactions on,* vol. 50, no. 2, pp. 265-268, 2014.

[100] N. Simpson, R. Wrobel and P. Mellor, “Estimation of Equivalent Thermal Parameters of Impregnated Electrical Windings,” *Industry Applications, IEEE Transactions on,* vol. PP, no. 99, p. 1, 2013.

[101] C. Sullivan, “Aluminum Windings and Other Strategies for High-Frequency Magnetics Design in an Era of High Copper and Energy Costs,” *Power Electronics, IEEE Transactions on,* vol. 23, no. 4, pp. 2044-2051, 2008.

[102] D. Zimmanck and C. Sullivan, “Efficient calculation of winding-loss resistance matrices for magnetic components,” in *Control and Modeling for Power Electronics (COMPEL), 2010 IEEE 12th Workshop on*, Boulder, CO , 2010.

[103] R. Wrobel, D. Salt, N. Simpson and P. Mellor, “Comparative study of copper and aluminium conductors - future cost effective PM machines,” in *Power Electronics, Machines and Drives (PEMD 2014), 7th IET International Conference on*, Manchester, UK, 2014.

[104] D. Murthy-Bellur and M. Kazimierczuk, “Winding losses caused by harmonics in high-frequency flyback transformers for pulse-width modulated dc-dc converters in discontinuous conduction mode,” *Power Electronics, IET,* vol. 3, no. 5, pp. 804-817, 2010.

[105] Y. Han, G. Cheung, A. Li, C. Sullivan and D. Perreault, “Evaluation of Magnetic Materials for Very High Frequency Power Applications,” *Power Electronics, IEEE Transactions on,* vol. 27, no. 1, pp. 425-435, 2012.

[106] W. Gitzen, Alumina as a ceramic material, American Ceramic Society, 1970.

[107] Electrolube, “Silicone Heat Transfer Compound,” 2003. [Online]. Available: http://www.electrolube.com/core/components/products/tds/044/HTS.pdf. [Accessed 15 3 17].

[108] “Military specification, Anodic coatings, for aluminum and aluminum alloys (MIL-A-8625F),” 2003.

[109] Y. Li and C. Wong, “Recent advances of conductive adhesives as a lead-free alternative in electronic packaging: Materials, processing, reliability and applications,” *Materials Science and Engineering: R: Reports,* vol. 51, no. 1-3, pp. 1-35, 2006.

[110] J. Maxwell, “A Treatise on Electricity and Magnetism” 3rd Edition, New York : Dover, 1954.

[111] R. Pal, “New models for thermal conductivity of particulate composites,” *Journal of reinforced plastics and composites,* vol. 26, no. 7, pp. 643-651, 2007.

[112] L. Nielsen, “The Thermal and Electrical Conductivity of Two-Phase Systems,” *Industrial & Engineering Chemistry Fundamentals ,* vol. 13, no. 1, pp. 17-20, 1974.

[113] I. H. Tavman, “Thermal and mechanical properties of aluminum powder-filled high-density polyethylene composites,” *Journal of Applied Polymer Science,* vol. 62, no. 12, pp. 2161-2167, 1996.

[114] Electrolube, “Encapsulation resins Technical data sheet ER1448 Epoxy Resin,” Electrolube, 2014.

[115] S. Krishnan, S. V. Garimella and S. Kang, “A novel hybrid heat sink using phase change materials for transient thermal management of electronics,” in *Thermal and Thermomechanical Phenomena in Electronic Systems, 2004. ITHERM '04. The Ninth Intersociety Conference on*, 2004.